Life Cycle Assessment (LCA) of Future Perovskite Tandem Solar Cells

Abeer Ali Khan
Student ID: 4773024

Master thesis submitted in partial fullfillment of the requirements for the Degree of Master of Science in Renewable Energy Engineering and Management

First Examiner: **Prof. Dr. Carsten Agert**

Second Examiner: **Jun.-Prof. Dr. Stefan Pauliuk**

Scientific Supervisor: **Juan Camilo Gomez Trillos**

Oldenburg, Germany

25th of September 2020

UNI FREIBURG

DLR Deutsches Zentrum für Luft- und Raumfahrt
German Aerospace Center
Institute of Networked Energy Systems

REM M.Sc. Renewable Energy Engineering and Management
Faculty of Environment and Natural Resources

Statutory Declaration

I, Abeer Ali Khan, herewith confirm that the submitted master thesis is my own independent work and that I only used sources and resources listed therein and I have not made use of any inadmissible help from any other third party. In particular, I have clearly identified matter from other works, cited verbatim or paraphrased, as such.

The submitted thesis or parts thereof have not been presented at any institution or higher education for the examination procedure.

23.09.2020, Oldenburg — Abeer

Date, Place — Signature

Acknowledgements

I could never start with thanking anyone but my beautiful family, for their constant support in all the adventures I undertake. I stand in awe of your faith in me, especially on the days when I had none in myself.

A special thanks to Prof. Dr. Carsten Agert for giving me the opportunity to be part of the German Aerospace Center - Institute of Networked Energy Systems and being the evaluator of this thesis.

I gratefully acknowledge the full support and guidance of the department of Energy Systems Analysis of this institution and I would like to thank Dr. Urte Brand and Dr. Thomas Vogt for facilitating this brilliant environment of learning.

I would like to express my sincere gratitude to my scientific supervisor, Juan Camilo Gomez Trillos, for his continuous support and patience. He continually conveyed a spirit of adventure in regard to research and an excitement in regard to teaching which made this thesis possible.

In addition, a thank you to Jun.-Prof. Dr. Stefan Pauliuk of the Albert Ludwigs University of Freiburg, who introduced me to Life Cycle Assessments and whose bold words had a far lasting effect in me.

To Amran Al-Ashouri of the Helmholtz Zentrum Berlin, whose insights helped me throughout my research. Furthermore, I humbly extend my thanks to all concerned persons who cooperated with me in this regard.

Last but not least, I express my heartfelt gratitude towards my close friends for keeping the sun shining in my life throughout every storm.

Abstract

The photovoltaic (PV) technology has become a key technology to decrease the dependence on finite fossil fuels and imports, and simultaneously reduce greenhouse gas emissions to fight climate change. Among the PV technologies, solar panels of the perovskite/Si tandem architecture have shown high potential. The prospects of conducting a Life Cycle Assessment (LCA) at low technology readiness levels (TRL) has gained immense interest for its potential to accelerate development of emerging technologies with improved environmental performances. Therefore, a cradle-to-gate and a cradle-to-grave LCA was conducted for the two terminal, monolithic, single-heterojunction perovskite/Si tandem solar cells. The stoichiometry observed for the perovskite layer of this solar cell was $Cs_{0.05}$-$(FA_{0.77}MA_{0.23})_{0.95}Pb(I_{0.77}Br_{0.23})_3$ and the solar cell showed an overall power conversion efficiency of 29.15%.

Comprehensive life cycle inventories (LCIs) were developed for all the components required for efficient functioning of the modules at all life cycle stages. However, till date no universally employed recycling process is available for waste PV installations. Consequently, the end of life (EoL) stage of the developed perovskite/Si tandems was also focused to reveal the environmental impact of the two EoL scenarios developed in this study, (i) recycling and (ii) combination of residual landfill (91%) and incineration (9%). The impact categories included in the ReCiPe 2016, 1.1 impact assessment method and the cumulative energy demand (CED) were calculated for per square meter of tandem surface area and subsequently, for per kWh of electricity produced. Furthermore, the results of the Energy Payback Time (EPBT) and the CO_2 eq. emission of this panel were compared with existing PV technologies and other energy technologies. The results, along with the sensitivity analysis, indicated that future research efforts should be directed towards improving the device lifetime, and reducing energy-intensive operations and precious metal consumption in order to develop a more benign environmental profile for this technology.

List of Contents

List of Figures

List of Tables

List of Abbreviations

ALD:	Atomic Layer Deposition
a-Si:	Amorphous Silicon
a-Si:H:	Hydrogenated Amorphous Silicon
BOS:	Balance of System
CAGR:	Compound Annual Growth Rate
CED:	Cumulative Energy Demand
CdTe:	Cadmium Telluride
CIGS:	Copper Indium Gallium (di) Selenide
CIS:	Copper Indium Diselenide
c-Si:	Crystalline Silicon
CSS:	Close Space Sublimation
CZTS/Si:	Tandem Copper Zinc Tin Sulfide– Crystalline Silicon
CZ process:	Czochralski Process
DC:	Direct Current
DMF:	Dimethyl formamide
DMSO:	Dimethyl sulfoxide
DR:	Degradation Rate
DSSC:	Dye-Sensitized Solar Cell
EF:	Environmental Flows
EGS:	Electronic Grade Silicon
EoL:	End of Life
EPBT:	Energy Payback Time
ETL:	Electron Transport Layer
eV:	Electron-Volt
EVA:	Ethyl Vinyl Acetate
EROI:	Energy Return on Energy Invested
FA:	Formamidinium-ion
FAI:	Formamidinium Iodide
FTO:	Fluorine Doped Tin Oxide
FU:	Functional Unit
FZ:	Float Zone Process
GaAs:	Gallium Arsenide
GHG:	Greenhouse Gas
GW:	Gigawatt
GWP:	Global Warming Potential
HTL:	Hole Transport Layer
HZB:	Helmholtz Zentrum Berlin
IEA:	International Energy Agency
IPCC:	International Panel for Climate Change
IRENA:	International Renewable Energy Agency
ISO:	International Organisation for Standardisation
ITO:	Indium Tin Oxide

IZO:	Indium Zinc Oxide
kWh:	Kilowatt-Hour
MA:	Methylammonium Ion
MGS:	Metallurgical Grade Silicon
MJ:	Multijunction
MWp:	Megawatt Peak
nc-SiO_x:H:	Hydrogenated Nano-Crystalline Silicon Oxide
LCA:	Life Cycle Assessment
LCI:	Life Cycle Inventory
LCIA:	Life Cycle Impact Assessment
LHE:	Light Harvesting Efficiency
OPV:	Organic Photovoltaic
PCE:	Power Conversion Efficiency
PECVD:	Plasma-Enhanced Chemical Vapor Deposition
PERC:	Passivated Emitter and Rear Cell
Perovskite/Si:	Tandem Perovskite Solar Cell – Crystalline Silicon
p-Si:	Poly (Multi) Crystalline Silicon
PR:	Performance Ratio
PV:	Photovoltaic
PVD:	Physical Vapour Deposition
QDPV:	Quantum Dot Photovoltaics
RF:	Radio Frequency
SDG:	Sustainable Development Goals
SHJ:	Silicon Heterojunction
SQ:	Shockley-Queisser limit
TCO:	Transparent Conducting Layer
TRL:	Technology Readiness Level
VTD:	Vapour Transport Deposition
WEEE:	Waste Electrical & Electronic Equipment

Chapter 1 Introduction

In the year 2015, 195 countries have signed the Paris Agreement at the COP21; an effort to limit global temperature rise below 2°C (UNFCCC 2015). To realize this goal, the agreement considers the use of technological solutions as a potential method. In addition, the United Nations adopted the Sustainable Development Goals (SDG) of which, SDG 7 comprises of three key targets: ensure affordable, reliable and universal access to modern energy services; increase the share of renewable energy in the global energy mix substantially; and finally, double the global rate of improvement in energy efficiency (UN 2015). In order to reach these targets, strategic energy transition from fossil fuels to low-carbon solutions is rather important, as energy-related carbon dioxide (CO_2) emissions represent two-thirds of all greenhouse gases (GHG) (Gielen, Boshell et al. 2019). Predictions, highly unreliable by nature, typically suggest that the time for a new energy technology to develop from first market uptake to majority market share could be half a century (Gielen, Boshell et al. 2019). However the Covid-19 pandemic has set in motion the historical lowest in global energy investment, plunging spending in every major sector from fossil fuels to renewables, resulting in an estimate of only 1% increase in global renewable energy use in 2020 (IEA 2020).

1.1 Renewable Energy and Climate Protection

In June 2018, the European Union has adjusted its 2030 binding target to 32% reduction of GHG emission while Germany aims to do so by 80% within 2050 through an accelerated uptake of renewables (Gielen, Boshell et al. 2019). Therefore, the supply of energy must be decarbonized by using low-carbon technologies which could be solved by renewable energies, replacing the current carbon-intensive energy infrastructure (Change 2014). While fossil fuel-generated electricity accounts for CO_2 emissions between 400 g and 1000 g CO_2 eq/kWh (Chowdhury, Rahman et al. 2020), the CO_2 emission from silicon-based solar panels ranged from 18 g to 180 g CO_2 eq/kWh (Schlömer, Bruckner et al. 2014). Consequently, expansion of global combined renewable power capacity by 50%, equivalent to 1200 GW, is expected between 2019 and 2024 whereof 60% is accounted for solar PV (IEA 2020).

Solar PV was the world's leading source of generation of additional power in 2017 (Lunardi 2019). According to the International Renewable Energy Agency scenario, a cumulative solar photovoltaic installed capacity of 2,840 GW and 8,519 GW could be expected globally for 2030 and 2050, respectively, implying an eighteen times higher total installed capacity in 2050 than in 2018 (IRENA 2019). However, because of the limited energy conversion efficiency and high system cost compared to

non-renewable energy sources, this technology is not the most widely used primary electrical energy source.

1.2 Perspectives of Photovoltaic Technologies

Crystalline silicon represents 90% of the global photovoltaics (PV) (Liu, Sofia et al. 2020); and its use in photovoltaics has benefited from the developments in the semiconductor industry. However, its use in single junctions poses physical limits in terms of power conversion efficiency, known as the Shockley-Queisser limit (SQ). The SQ of the ideal commercial photovoltaic (PV) cells, predominantly based on crystalline silicon single-junction solar cells, is limited to an efficiency of 33% due to intrinsic losses such as inability to absorb below-bandgap photons, band edge thermalization and radiative recombination (Boriskina and Chen 2014). As revealed by the detailed balance calculations, the SQ of the serial connected tandem solar cells can exceed 40% if an ideal material combination is selected for the top and bottom solar cell (Hossain, Qarony et al. 2019). For instance, with an efficiency of 29.1%, perovskite/silicon (Si) tandem solar cells have become prime candidates for next-generation solar cells because of its high power conversion efficiency and minimal additional cost (NREL 2020). The advantage of such tandem solar cells is their efficiency in absorbing a wider range of the solar spectrum by stacking p–n junctions with a higher band-gap on top of those with a lower bandgap (Todorov, Gunawan et al. 2016). For instance, two terminal a-Si based tandem solar cells use a top cell with a higher band gap than silicon so that a voltage that is approximately twice what silicon would generate can be generated as the top cell absorbs the higher energy photons (Lunardi 2019). This is what makes tandem solar cells of exciting prospects.

1.3 Environmental Impacts of Solar Photovoltaic Technologies

Climate change, resource depletion, and ecotoxicity are among the most concerning environmental challenges that need to be addressed. In this regard, photovoltaic technologies are associated with clean electricity production and negligible amounts of emissions are produced during its operation. However, significant greenhouse gases are emitted from it during the production of the raw materials and the non renewable energy used in the manufacturing processes of its different components, transportation and installation among others. Besides, record-high power conversion efficiencies have been achieved as the lead halide perovskite proves to be more stable when compared to other metal or low lead perovskite solar cells (Ono, Qi et al. 2018). But environmental impacts from the use of toxic metals, such as lead, in the perovskite dye and the disposal methods of perovskite solar cells cause great concerns. Lead pollution can cause long-term environmental damage because of its high toxicity and long dissipation time. Often remaining undetected and symptomless in the human body, lead results in learning disabilities, behavioural problems, malformed bones, slow growth, seizures, coma, and

even death (Zhang, Hao et al. 2018). Even though silicon solar panels contain trace amounts of lead in the glass that encases the cells' active components, it is not soluble while that in perovskite compounds readily dissolve in water and exposes the lead to the environment (Zhang, Hao et al. 2018). Organic methylammonium used for preparing the precursors for perovskite deposition results in high marine eutrophication impact (Celik, Song et al. 2016). Although studies can show that the environmental impacts from the manufacturing processes of perovskite solar cells were lower than that of mono-Si solar cell, the overall environmental impacts per unit electricity generated by perovskite solar cell tandems were higher than all commercial PV technologies (Celik, Song et al. 2016). For these reasons, photovoltaic technologies cannot be considered neutral regarding greenhouse gas emissions and toxicity. Beside greenhouse gas emissions, various other environmental impacts in other categories can be caused during the life cycle of a photovoltaic cell (Gomez Trillos 2018). All these environmental impacts are needed to be accounted and analysed holistically and mitigated for a sustainable development of the technology.

1.4 Motivation

The motivation of this thesis comes from the need of a comprehensive environmental impact assessment to be conducted on the perovskite/Si tandem solar cells, in order to describe the effects of this technology throughout its life cycle and to guide research efforts towards tandem designs with minimum environmental impacts. A suitable methodology that assesses the environmental impacts through the inputs and outputs associated with all the stages of a product's life cycle, considering raw material extraction, materials processing, manufacture, distribution, use, repair and maintenance, and end of life is the life cycle assessment (LCA) (Standardization 2006). From such an assessment, environmental impacts associated with different life cycle stages over a considered lifetime can be evaluated. Every LCA study is unique and the depth of detail of each depends on their respective goal and scope definition which requires a higher selection requirement in order to conduct a harmonised comparison among LCAs. Nevertheless, an LCA can ensure an environmentally sustainable development of the technology by locating impact hotspots.

Furthermore, by the middle of this century, large volumes of decommissioned waste photovoltaic modules can be expected (Kadro and Hagfeldt 2017). The worldwide solar PV waste is anticipated to reach between 4%-14% of the total generation capacity by 2030 and rise to over 80% (around 78 million tonnes) by 2050, assuming an average panel lifetime of 25 years, making PV a burning environmental issue in the next decades (Chowdhury, Rahman et al. 2020). Consequently, the management of panels and other hazardous waste at end of life (EoL) stage becomes rather important, which motivates this LCA study to explore potential EoL scenarios for possibilities of value generation from the waste solar cell tandems.

1.5 Research Questions and Challenges

The objective of this research is to analyse the environmental impacts of perovskite/Si tandem solar cells and compare the results with that of different photovoltaic module technologies through the LCA method, with the aid of the LCA software of Brightway2. The research questions to be answered are:

1. Which are the critical environmental impacts of the investigated perovskite/Si tandem technology in different life cycle stages?
2. How is the environmental performance of the investigated perovskite/Si tandem technology compared to other commercial photovoltaic technologies?
3. Which are the critical environmental impacts of different end of life scenarios?
4. What is the effect of software selection on the impact assessment results?
5. How do the environmental impacts change with the operational lifetime, conversion efficiency, irradiance, degradation rate and performance ratio as a basis (sensitivity analysis)?
6. What is the uncertainty of the obtained results (uncertainty analysis)?

The most common background data for LCA studies related to energy generation is the ecoinvent database (Wernet, Bauer et al. 2016), which has been used in this thesis to assess the environmental impact results from the life cycle processes of perovskite/Si tandem solar modules. In order to perform a detailed LCA and achieve realistic results, a significant amount of high-quality inventory data is necessary to build a model as close as possible to reality. But the greatest challenge for all LCA practitioners is the availability of relevant and recent data, especially for rapidly evolving technologies like the investigated perovskite/Si tandem solar cell. Most of these values are from laboratory experiments which fail to portray realistic results for industrial mass production. In cases when the inventory was considered old and did not account for the most recent developments, values had to be estimated. These assumptions are based on available publications and personal communication with experts or project partners. The uncertainties related to the data required and the assumption made throughout this work might limit the precision of the final results.

1.6 Outline and Structure of Thesis

Following this introductory chapter, the second chapter gives an overview of the photovoltaic technologies and a detailed description of the different life cycle stages and characteristics of the investigated perovskite/Si tandem solar cell.

The third chapter consists of a literature review that focuses on the LCA studies made on Perovskite/Si tandem solar technology. LCA studies on EoL scenarios are also reviewed in this chapter.

The fourth chapter initiates with a detailed description of the methodology used in this LCA study, which is according to ISO 14040/14044. After an overview of the software Brightway 2 for LCA, this chapter defines the goal and scope of the study, the inventory analysis and the impact assessment methods. Furthermore, interpretation methods of these results can also be found in this chapter.

Chapter five discusses and compares that result with other technologies obtained from the existing literature. Furthermore, this chapter includes important comparisons that show the effect of different softwares on the LCIA results. Finally, chapter six concludes the thesis with suggestions for future research work.

Chapter 2 Photovoltaic Technologies

Initially developed for application in space, the solar PV technologies are now being used ubiquitously where electricity is required. This technology has proved to be one of the most promising and mature technologies for generating renewable energy. It produces direct current (DC) electrical power from semiconductor materials when photons illuminate them, which is measured in Watts (W). An electric current flow is generated as the photons of the solar irradiance fall on the free electrons of the PV cell and mobilizes them (Abdelhady, Abd-Elhady et al. 2017). This technology can produce energy only while the photovoltaic cells are being illuminated (Lunardi 2019) and more input of solar energy to the PV cell results in more electrical output from them (Abdelhady, Abd-Elhady et al. 2017). However, only photons with a specific energy level, i.e. the band gap energy; the energy difference between the top of the valence band (outer electron) and the bottom of the conduction band (free electron flow), can free the electron and allow a flow of current.

This chapter will provide an overview of the historical development of photovoltaic cells, followed by a classification of the photovoltaic technologies. It further contains the status of photovoltaic market and a brief description of investigated perovskite/Si tandem solar cells regarding the manufacture, efficiency, lifetime and end of life along with others.

2.1 History

Like the discovery of penicillin, the discovery of the photovoltaic effect happened rather coincidentally in 1839, when French physicist, Alexandre Edmond Becquerel, discovered that conductance rises with illumination in his work focused on the behaviour of solids in electrolytes. The photovoltaic effect is a physical phenomenon allowing light-electricity conversion. This paved the way to the development of photovoltaics. Discovery of basic phenomena and properties of PV materials took place between the years 1839-1899. Adams and Day observed the same effect in solid selenium in 1877 while later, in 1883, Fritz developed the first thin-selenium PV cell which had an efficiency of approximately 1% (Lunardi 2019).

The theoretical explanation of the photovoltaic effect and development of the first solar cells occurred between the years 1900 to 1949. Albert Einstein was awarded a Nobel Prize in 1921 for his comprehensive theoretical work about the photoelectric effect which he conducted in 1904. In 1918 Jan Czochralski discovered a method for monocrystalline silicon production which paved the way to construction of the first silicon monocrystalline solar cell in 1941, which had an efficiency of approximately 6%.

During the years 1950 to 1969, there was an accelerated development of PV technology for intensive space research. Bell Laboratories published the results of the solar cell operation

with 6 % efficiency in 1954. At this time, the traditional primary market for PV was small-scale such as telephone repeaters which needed tens of Watts. The following year, the preparation of satellite energy supply by solar cells began. In 1960, Hoffman Electronics introduced yet another solar cell with 14 % efficiency and in 1963, Sharp Corporation developed the first usable photovoltaic module from silicon solar cells. Fields with photovoltaic modules of 242W and 470W were set up in Japan and United States of America in 1964 and 1965 respectively. By 1966, an astronomical observatory was tracked in Earth's orbit which had 1 kW peak power photovoltaic field.

From 1970 to 1979, establishment of several large photovoltaic companies, such as Solar Power Corporation, gradually began to lower the cost of the technology. In 1977, the world production of photovoltaic modules exceeded 500 kW. NASA LeRC set up the first system ever to satisfy the demands of the entire village, used for water pumping and power supply of 15 households, by a 3.5 kW PV system.

By the end of the 70's, concern about the environment increased, making the study of PV modules and research about renewable sources of energy ever more significant. This accelerated the development of first large utility-scale photovoltaic systems, such as ARCO solar. This company was the first to produce PV modules with over 1 MWp production output, breaking the historical records. In 1985, highly efficient, more than 20% efficiency, silicon solar cells were constructed by researchers at the University of New South Wales in Australia. The following year, ARCO Solar introduced the first commercial thin film PV module, a module that used different materials and technology.

In 1990's, several large-scale solar cell producers set up and the use of PV technology increased. During this time, significant research interest developed in thin film cells because of their flexibility and lower cost compared to silicon cells. From 2000's, multi MW utility-scale PV power plants, such as Sharp and Kyocera, were well in operation. Many large systems, up to 5 MW, were built in Germany in the year 2004 because of the renewable energy act or EEG (*Erneuerbare-Energien-Gesetz*). In 2009, perovskite cells made of lead, iodide and methylammonium were first developed with an efficiency of 3-4% which doubled after 2 years by optimizing the perovskite coating conditions (Park, Quan et al. 2016). As the thin-film cells were low in efficiency when compared with Si solar cells, at present only a few companies manufacture thin-film solar cells that represent a PV market share of below 10% (Lunardi 2019). By 2016, perovskite solar-cell efficiencies rose to 20% and were commercially competitive with silicon PV cells (Carbeck 2016).

2.2 Limitations of PV Technology

Among all the benefits of PV technology, the most important is that solar energy is a truly renewable and cost free energy source. But there are some limitations which prevent this technology to reach grid parity without subsidies. The first major limitation of silicon PV cells is that, while there is no shortage of silicon in the form of silicon dioxide (quartz), it is rarely found in nature in the pure, elemental state that is needed. Tremendous amounts of energy are consumed to purify the required materials to their elemental state. For instance, manufacturers melt silicon dioxide at 1500–2000 degrees Celsius in an electrode arc furnace and this energy needed to run such furnaces sets a fundamental lower limit on the production cost of silicon PV cells and further adds emissions of greenhouse gases from their manufacture (Carbeck 2016). Besides, emisions from end of life of PV technology and use of scarce and toxic elements also add to the environmental profile.

The second major limitation of conventional PV technology is their power conversion efficiency. The power conversion efficiency is limited by: (i) the losses due to thermalization of charge carriers generated by absorption of the photons with the energies above the bandgap of the PV material, (ii) the losses caused by the PV cell inability to use the photons with the energies below the bandgap, (iii) the losses caused by recombination of the light generated charge carriers and (iv) technical, such as low absorption efficiency of the PV material, which can be overcome by the proper design of the PV cell (Boriskina and Chen 2014). Besides, the efficiency is also physically constrained by the Shockley-Queisser limit which, for single junctions is approximately 33% for an irradiance of 962.5W/m2 under the Air Mass 1.5 solar spectrum. Multiple junctions with different band gaps to convert photons of different energy can overcome this limit. Additionally the optical properties of materials used in the cells and the electronic characteristics of the cell also affect the performance (Gray 2011).

The third limitation of silicon PV cells is their rigidity and weight. Silicon PV cells work best when they are flat and housed in large, heavy panels which makes large-scale installations very expensive. This limitation can be eliminated by the thin film and PV tandem technologies (Carbeck 2016).

Furthermore, PV technologies are weather dependent; although solar energy can still be collected during cloudy and rainy days, the efficiency drops (Premalatha and Rahim 2017). Unless used right away, solar energy storage in batteries can incur further costs (Luque and Hegedus 2011).

2.3 Market Status

Solar power attracted the largest share of new investments in renewable energies, followed by wind power, for the ninth year in a row (Jäger-Waldau 2019). Photovoltaics is a fast growing market. Between the years 2010 to 2019, the Compound Annual Growth Rate (CAGR) of cumulative PV installations was 32%. China and Taiwan, followed by Malaysia, held the lead PV module production in 2017 with a share of 70%, followed by Rest of Asia-Pacific & Central Asia (ROAP/CA) with 14.8%, while Europe contributed with a share of 3.1% (compared to 4% in 2016) and USA/CAN contributed 3.7% (Jäger-Waldau 2019, ISE 2020). Total cumulative PV installations in Europe and China in 2019 amounted to 24% (compared to 25% in 2018) and 36% (same value as the year before) respectively.

In 2019, with about 1.7 million PV systems installed, Germany accounted for about 49 GWp (8%) of the cumulative PV capacity installed worldwide, 635 GWp, including the newly installed capacity of approximately 4 GWp. This covered 8.2% of Germany's gross electricity demand in 2019 (ISE 2020).

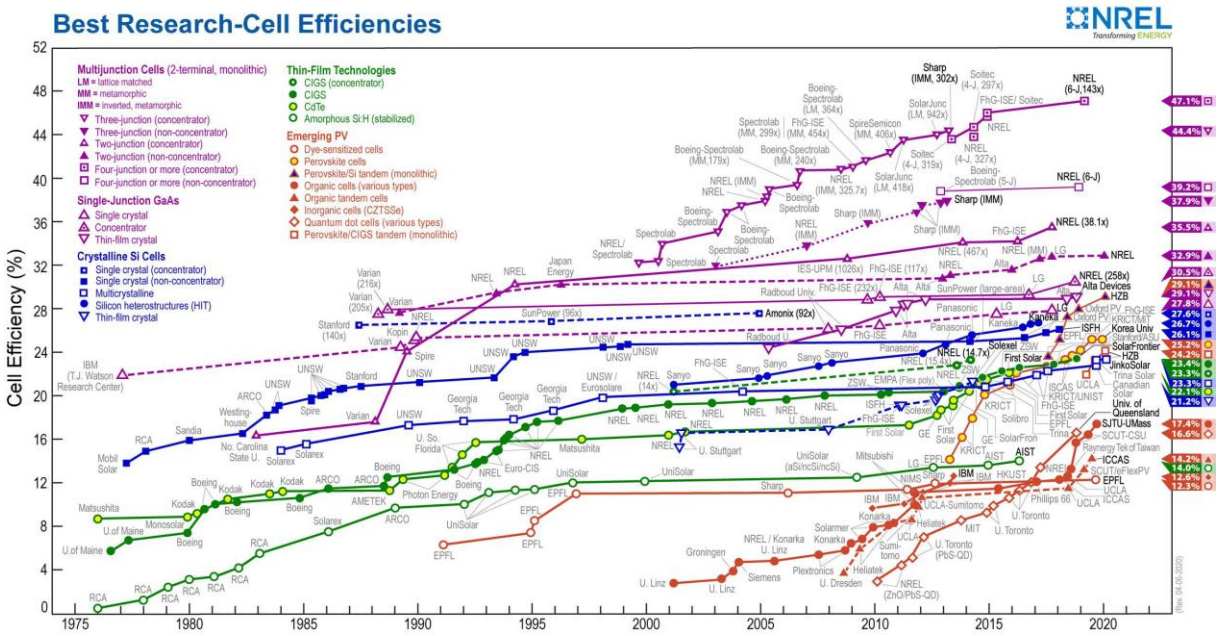

Figure: 1. Best research-cell efficiencies chart compiled by NRE (NREL 2020)

As stated in the photovoltaics report 2020 of Fraunhofer Institute for Solar Energy Systems, in 2017, Si-wafer based PV technology and multi-crystalline technology accounted for about 95% and 62% (compared to 70% in 2016), respectively, of the total production Department of Economic and Social Affairs (ISE 2020). Market shifts have been noticed from subsidy driven to competitive pricing models. A commercial production of perovskite technology is not yet established, but is attempted by the companies such as China's Wonder Solar and Microquanta Semiconductor, Toshiba and Panasonic in Japan, Poland's Saule Technologies, U.S. startup Energy Materials Corp, Solar-Tectic, Dyesol and Oxford photovoltaics (Extance

2019). Oxford PV has demonstrated perovskite/silicon tandems that reach lab efficiencies up to 28%, while those produced by Helmholtz Zentrum Berlin (HZB) show 29.1% lab efficiency, outperforming both perovskite and silicon single-junction devices. As is depicted in Figure 1, efficiency for current commercial technologies was recorded since 1976 which increases progressively towards today's values. Currently, the combination of perovskite and silicon technologies is considered the most promising and fastest route to market for perovskites and are expected to appear in mass production as early as 2021 (2020).

2.4 Classification

PV technologies, currently, can be classified in two categories: (1) wafer-based and (2) thin film cells. The wafer based PV technology can be categorized primarily into three technologies: (i) Crystalline Silicon (c-Si), (ii) Gallium Arsenide (GaAs) and (iii) III-V multijunction (MJ). Of these categories, approximately 90% of present global manufacturing capacity is occupied by the most mature of all PV technologies, the crystalline Silicon (c-Si) (Zendehdel, Nia et al. 2020). Furthermore, the thin film cells technology can be divided into six types primarily, namely: (i) Amorphous-Si technology, (ii) Cadmium telluride technology, (iii) Chalcogenide technologies, (iv) Dye-sensitised technology, (v) Organic photovoltaics technology and lastly, (vi) Organic-inorganic halide perovskite technology. The copper zinc tin sulfide (CTZS) and colloidal quantum dot photovoltaics (QDPV) technology shown in the *figure* 2 are included in future developments in the latter part of this chapter.

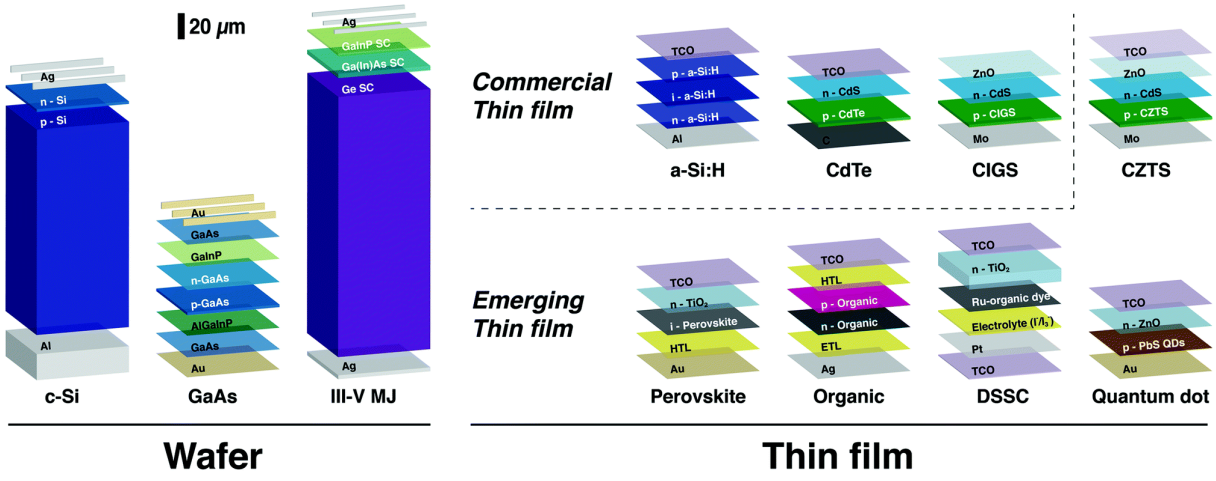

Figure: 2 Classification of PV technology (Jean, Brown et al. 2015)

2.4.1 Wafer Technology

The present PV technologies could be classified in two categories: (1) wafer-based cells and (2) thin film cells. The wafer-based cells are fabricated on semiconducting wafers which

can be used without an additional substrate. The modules are typically covered with glass and encapsulation material for improving the mechanical stability and protection whereas thin film cells are semiconducting layers deposited onto different substrates like plastic, glass or metal, which are later encapsulated for weather protection (Zendehdel, Nia et al. 2020).

For tandem cells, thin-film technologies have become attractive for using on top of a silicon base cell because of the possibility of a higher band gap. Besides, this technology is developed and therefore, has potentially low cost, more flexible geometries and requires relatively small quantities of material (Lunardi 2019). Although recently developed, some believe that implementation of tandem cells on an industrial scale is possible through perovskite and crystalline silicon (c-Si). Nevertheless, the potential for perovskites to enter the global PV market is challenged by their performance, stability and scalability (Ono, Qi et al. 2018). In addition, the power conversion efficiency of perovskite is a challenge currently being addressed, the focus of the field is gradually shifting also towards improving the device lifetime (Assadi, Bakhoda et al. 2018).

2.4.2 Thin Film Technology

Approximately 10% of the global PV module market is based on thin semiconducting films at present (Zendehdel, Nia et al. 2020). In 2016 a-Si, Cadmium telluride and CIGS had a production rate of 0.5 GWp, 3.1 GWp and 1.3 GWp respectively with decreasing production of the first and an increasing production of the latter two technologies (Gomez, 2018). Three thin film PV technologies were developed to commercial phase in 2019 which are hydrogenated amorphous silicon (a-Si:H), cadmium telluride (CdTe) and copper indium gallium diselenide (CIGS). A key advantage of these commercial thin film technologies that can affect results of the LCA is the use of less precursor material.

2.4.2.1 Amorphous-Si Technology

The hydrogenated amorphous silicon (a-Si:H), with a band gap of 1.7–1.8 eV, allows higher absorption compared to c-Si with 1.12 eV. Although larger, this band gap is not well matched to the solar spectrum resulting in poor efficiency (Zendehdel, Nia et al. 2020). Such a thin film PV is typically fabricated at relatively low substrate temperatures of 150–300°C by plasma-enhanced chemical vapor deposition (PECVD). A 300 nm film of a-Si:H can absorb approximately 90% of above band gap photons in a single pass which results in lightweight and flexible solar cells and panels. This makes the technology well suited for small scale and low-power applications. But properties such as light induced degradation (the Staebler-Wronski effect) and low average efficiency (6% or less) of a-Si PV module, compared to mature thin film technologies, has led to decreasing market interest (Aberle 2009).

2.4.2.2 Cadmium Telluride Technology

Cadmium telluride (CdTe) is the leading thin-film PV in the present global market. This technology represented approximately 5% of the PV world market share in 2019 (Lunardi 2019). Properties such as direct band gap of 1.45 eV and strong solar spectrum absorption make it a favorable semiconductor for solar energy harvesting (Zendehdel, Nia et al. 2020). Although relatively high processing temperatures (400–600 °C) are required, the two polycrystalline semiconductor materials, cadmium and telluride, are chemically very stable and are relatively easy to deposit stoichiometrically. The deposition methods for these semiconductor films typically include: Physical Vapour Deposition (PVD), Vapour Transport Deposition (VTD), Close Space Sublimation (CSS) and Sputter Deposition. Fabrication of such CdTe PV modules occurs in the superstrate configuration and charge carrier separation takes place through a heterojunction (Aberle 2009). The layers consist of a Transparent Conducting Layer (TCO), a cadmium sulfide (CdS) layer, a CdTe layer and a contact layer.

CdTe has record efficiencies of 22.1% for the lab-scale cells and efficiencies of the commercial module continue to improve steadily (NREL 2020). The CdTe modules provided by First Solar® promises a linear performance during 25 years, with a decrease of efficiency between 98% and 86%. The degradation rate for such modules can be higher than 1% per year. On the other hand, this company ensures recovery of 95% of semiconductor material and 90% of glass through its own collection and recycling program (Gomez Trillos 2018).

The main technical problem that reduces the long-term stability of such cells is the relatively light doping of the CdTe back contact layer (Lunardi 2019). Although this technology employs high throughput deposition processes and the lowest module costs of any PV technology on the market, the toxicity of elemental cadmium and the scarcity of tellurium remain the main concerns that have motivated research on alternative material systems (Zendehdel, Nia et al. 2020).

2.4.2.3 Chalcogenide Technologies

The chalcogenide technologies such as Copper Indium Diselenide (CIS) and Copper Indium Gallium Diselenide (CIGS) modules are both fabricated similarly in the substrate configuration, i.e. from back to front. Depending on the choice of substrate, a transparent supporting material is not necessary for such a module, giving flexibility (Aberle 2009). Because of its availability, cost effectiveness and the enhancement of the doping concentration in the CIS absorber layer, soda-lime glass is usually considered the standard substrate. The main challenge in CIS technology is the complexity of the 5-

element system CIS absorber layer, that constraints the realisation of uniform film properties across large-area substrates using high-throughput equipment (Aberle 2009).

Copper indium diselenide has a band gap of 1.0 eV and the band gap increases when gallium is added to replace indium in the ratio of Ga/(In+Ga) 0.2-0.3 (Shafarman, Siebentritt et al. 2011). Copper indium gallium diselenide (CIGS) is a semiconductor composite with a band gap of 1.1–1.2 eV (Zendehdel, Nia et al. 2020). Main materials required for CIGS are copper, indium, selenium and also a considerable amount of sodium.

Key technological challenges for this technology can be listed as: (1) high variability in film stoichiometry and physical properties, (2) limited knowledge of the grain boundaries activity, (3) low open-circuit voltage due to structural and electronic inhomogeneity and (4) engineering of higher-band gap alloys to enable multijunction devices (Zendehdel, Nia et al. 2020).

The CIGS thin film technology of the manufacturer Solar Frontier maintains 90% of nominal power for 10 years and 80% for another 25 years, with a degradation rate of approximately 0.5% a year. Such CIGS modules contain 89% glass, 7% of aluminium and 4% polymers, containing a very small amount of semiconductor material, which are separated through a laser process followed by a chemical treatment (Gomez Trillos 2018).

Active materials used as light absorbers in commercial thin-film PV technologies can absorb the sun light 10–100 times more efficiently than silicon (Zendehdel, Nia et al. 2020). Issues that hinder large-scale deployment are use of cadmium and the scarce element indium. Estimates predict that all known reserves of indium would be sufficient for the production of only a few GWp of CIS or CIGS PV modules (Aberle 2009). In order to avoid the use of indium, copper zinc tin sulfide/Si (CZTS/Si) tandem cells are expected to be of increasing interest. Although CZTS has lower efficiency than CIGS, it is very similar to CIGS in optoelectronic and crystallographic properties and methods of fabrication.

2.4.2.4 Dye-Sensitised Technology

The dye-sensitized solar cells (DSSCs) have arisen as a technically and economically credible alternative to the p-n junction PV technology which produces a photoelectrochemical effect when dye molecules and wide band gap semiconductor electrodes are incorporated (Lunardi 2019). The four key parameters for this technology are: working electrode, sensitizer (dye), redox-mediator (electrolyte), and counter electrodes. It is an assembly of working electrode soaked with a sensitizer or a dye and

sealed to the counter electrode soaked with a thin layer of electrolyte. Hot melt tape prevents the leakage of the electrolyte for this technology.
The efficiency of ZnO-single crystal dye-sensitized solar cells was very poor, as only 1% of the incident light could be absorbed by the monolayer of dye molecules. Afterwards, the efficiency was improved by optimizing the porosity of the electrode made up of fine oxide powder, so that the absorption of dye over electrode could be enhanced which would subsequently increase the light harvesting efficiency (LHE) (Sharma, Sharma et al. 2018). DSSCs with nanoporous titanium dioxide (TiO2) electrodes with a roughness factor of ca.1000, showed efficiency of 7% in 1991, while the current efficiency of DSSC technology is 12.3% (NREL 2020).

Key challenges of DSSCs include limited long-term stability under illumination and high temperatures, low absorption in the near-infrared, and low open-circuit voltages created from interfacial recombination. Moreover, due to the energy mismatch between the oxidized dye and an electrolyte, a significant amount of energy loss of the oxidized dye occurs during the process of regeneration (Sharma, Sharma et al. 2018). Although the manufacturing process for DSSC solar cells is simple, low-cost, and uses environmentally friendly materials, stability and performance limits the commercialization of this technology.

2.4.2.5 Organic Photovoltaics Technology

After almost 45 years of research and development, the efficiency of organic photovoltaic (OPV) technology has increased from 0.001% in 1975 to 17.4% in 2020 (NREL 2020). Flow of excitons (neutral pairs of electrons/holes), formed in OPV materials when a photon is absorbed, creates electricity.

An organic photovoltaic device is composed of layers such as the metal layer, the transparent substrate layer, the TCO layer and glass layer. The substrate is composed of glass, polyester or some other transparent materials, while the TCO can be indium tin oxide (ITO). Carbon nanotubes (CNTs) are increasingly used as the transparent conductive layer instead of transparent conductive oxides. A protective layer is placed between the active layer and the anode, as the elements of the anode may diffuse into the active layer and cause device degradation due to the formation of charge trap centers (Abdulrazzaq, Saini et al. 2013). A standard example of such a protective layer can be poly (3,4-ethylenedioxythiophene) poly (styrenesulfonate) (PEDOT:PSS).

Main challenges of this technology are associated with inefficient exciton transport, poor long-term stability, low large-area deposition yield and low ultimate efficiency limits. Development in device efficiency, increase in lifetime and reduction in cost are required for industrial scale manufacturing (Zendehdel, Nia et al. 2020).

2.4.2.6 Organic-Inorganic Halide Perovskite Technology

Perovskite solar cells have been raised from solid-state dye-sensitized solar cells and have quickly illustrated as one of the most promising emerging thin-film PV technologies, achieving the certified efficiencies of 25.2% in few years of development in lab-scale devices (NREL 2020). The use of low-cost materials and simple fabrication process make them of growing interest.

The term "perovskite" refers to the ABX_3 crystal structure. A usually refers to methylammonium or formamidinium, caesium, rubidium ions. Recently, the organic ion guanidinium has also been used. B refers to a metal, such as lead, tin or germanium. X is an element of the halide group (chloride, bromide or iodide) (Manser, Christians et al. 2016). An interesting property of perovskite structures is high band gap tunability in the range of 1.25–3 eV by substitution of cation or anion in the lattice; for instance, $HC(NH_2)_2Pb(I_{1-x}Br_x)_3$, $CH_3NH_3SnI_3$, and $CH_3NH_3Pb(I_{1-x}Br_x)_3$ (Zendehdel, Nia et al. 2020). A single-junction perovskite is mainly comprised of a stack of different layers like the fluorine doped tin oxide layer (FTO) or indium tin oxide (ITO), an electron transport/selective layer (ETL), the perovskite material and a hole transport /selective layer (HTL) topped by a metal contact. These layers are fabricated by different low temperature solutions or vapor deposition (Zendehdel, Nia et al. 2020).

Open circuit voltage (Voc) is one challenging parameters to improve in PV devices, although perovskite technology has achieved high Voc, higher than 1.1 V. In addition to the short lifetime of perovskite PV technology, which recently increased from minutes to several months, challenges such as the high costs, uncontrollable thin film growth and deposition, scalability and reproducibility of process, moisture and oxygen sensitivity, which can produce degradation of perovskite absorber, and toxicity concerns from the use of lead hinders the commercialization of this technology (Gomez Trillos 2018, Lunardi 2019).

2.5 Perovskite Tandem Technology

The energy conversion efficiency of a single-junction PV cell, for a band gap of 1.1 eV and considering an AM 1.5 solar spectrum, remains limited to 30% by the Shockley–Queisser limit (Hossain, Qarony et al. 2019). In order to increase the efficiency further, multijunction/tandem PV devices have been developed.

A multijunction/tandem solar cell is commonly composed of a top cell and a bottom cell. The top cell has a large-bandgap absorber to effectively convert short wavelength spectrum with minimized thermalization loss while the narrow-bandgap of bottom cell absorber harvests near-infrared photons, maximizing current density. Therefore, as the device is illuminated by

sunlight, the top cell absorbs the short wavelength photons with energies higher than its bandgap and generates a high open-circuit voltage (Voc), while the low-bandgap bottom cell absorbs the long wavelength photons with energies between the bandgaps of the top cell and bottom cell. Tandem technologies reduce thermalization loss as well as photon loss, resulting in an efficiency limit of 47.1% under the standard solar spectrum and intensity (NREL 2020).

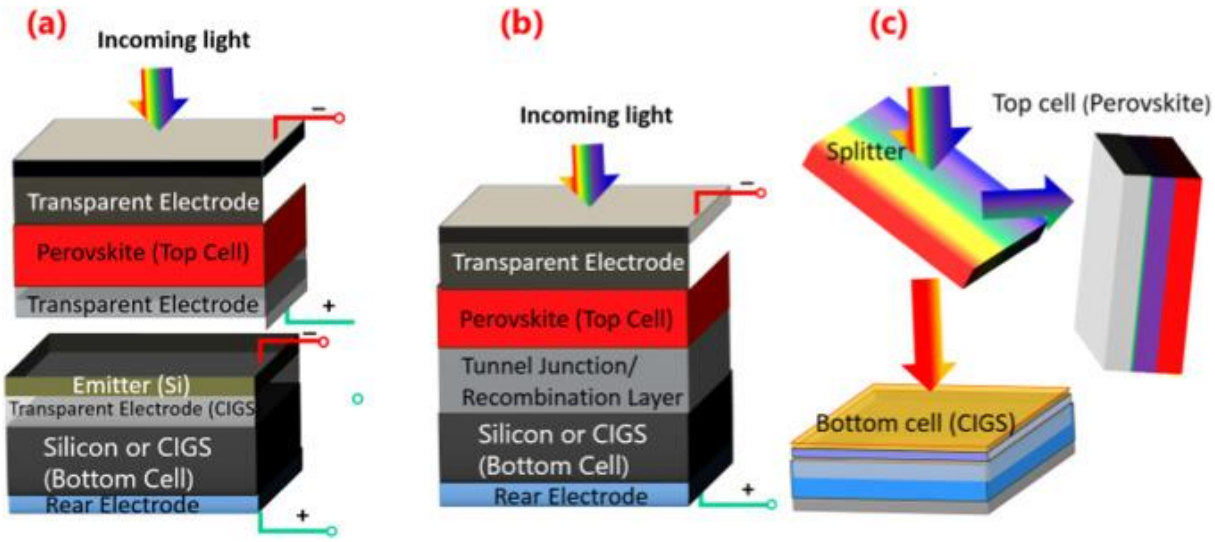

Figure: 3 Tandem technology a. 4 terminal b. 2 Terminal c. Optical splitting (Wali, Elumalai et al. 2018)

Tandem solar cells, as shown in *figure* 3, can have three architectures: two-terminal devices (2T), four-terminal devices (4T) and optical splitting in which the light is split according to the wavelength and redirected to two independent cells (Wali, Elumalai et al. 2018). The three main configurations for multijunction/tandem solar cells can be spectral splitting, monolithically integrated, and mechanically stacked devices. Although unlikely to be commercialized because of high expenses, the first configuration exhibits the highest potential in conversion efficiency, exceeding 28%, due to the minimal parasitic absorption loss (Wang, Zhu et al. 2020). The second configuration, monolithically designed, is limited by requirement of current matching, design and material selections. The last configuration, mechanical stacking or wafer bonding, is an approach that allows more freedom on cell design and material choice. In this case, the top and bottom cells are individually fabricated first and then fabrication is completed by stacking individual solar cells with electrically conductive intermediate adhesive layers to produce electrical current for the two (or more) cells.

Materials with a possibility of high band gap, such as CIGS or CZTS, are attractive for use on top of a Si base cell in a tandem solar cell. Tandem solar cells have achieved high efficiencies, beyond 43%, mostly by using III-V cells, like InGaP or GaAs, in specific conditions (Lunardi,

2018). Even with major technical challenges, like thermal expansion coefficient, fast development can be observed for two-terminal (2T) (*Figure* 1).

2.6 Perovskite/Si Tandem under Investigation

Perovskite/Si tandems have outpaced all other single junction PV technologies in power conversion efficiency (PCE), with the laboratory record of 29.1% (NREL, 2020). In spite of perovskite's merits of high absorption coefficient (≈105/cm), high carrier mobility, low trap density, tunable bandgap (from 1.17 to 2.24 eV), low cost and easy fabrication (Wang, Zhu et al. 2020), major challenges remain in the deposition of the high-quality perovskite absorbers and recombination layers onto the inverted-pyramidal-nanostructure surface of the present silicon devices.

The investigated tandem is a 2T, monolithically integrated perovskite/Si solar cell with a Si hetero-junction (SHJ) in the rear and a certified power conversion efficiency of 29.15%. It has a cell area of 106.09 mm and 1.9 V of Voc. The bottom cell of this tandem is a silicon heterojunction (SHJ) cell based on an n-type float zone (FZ) wafer, while the top cell constitutes perovskite layer in p-i-n architecture which is deposited directly on the ITO of the silicon. As this study focuses on the perovskite/Si tandem developed by the project partners of PEROSEED, detailed description of the fabrication processes of this tandem is given below.

2.6.1 Manufacturing of Silicon

The production process of c-Si wafer for the bottom cell consists of multiple stages that start with the mining of raw materials, which is mainly quartz sand. This quartz sand or silicon is an abundant, non-toxic and stable element. Mining of this element is followed by further high energy consuming processing and purification stages as high purity silicon is needed to fabricate the solar cell. To produce elemental silicon, quartz sand (SiO2) is reduced to metallurgical-grade silicon (MGS) at approximately 2000°C with carbon in smelting reduction kilns. The MGS produced are 98-99% pure and involve the following reaction.

$$Si + 2C \rightarrow Si + 2CO$$

The liquid silicon metal is drained from the bottom of the smelting kiln. Most of the silicon production plants use 11-13 MWh of electrical energy per ton of silicon (Chen, Ma et al. 2018). Subsequently, the still liquid silicon is treated with oxidative gas and slag-forming materials such as silica sand (SiO2), lime/limestone (CaO/CaCO3), dolomite (CaO-MgO) and calcium fluoride (CaF2) are added to the product to further reduce and purify it (Gomez Trillos 2018). To achieve the required electronic properties, the metallurgical-grade silicon must be refined to electronic grade silicon (EGS). Only about 2% of the raw silicon is

prepared for EGS, of which approximately 90% is used for the manufacture of semiconductor in the microelectronics or PV.

The most common method to purify MGS into EGS is by the Siemens process. This method can be broken down into three main steps: (1) the production of trichlorosilane (SiHCl3) from MGS in a fluid-bed-reactor; (2) the purification of SiHCl3; and (3) the reduction or thermal decomposition of SiHCl3 into solid polysilicon. In the first step, MGS is converted into trichlorosilane (HSiCl3), at about 300-350°C with HCl. Many impurities, such as iron (Fe), aluminium (Al), and boron (B) which react with Cl to form their halides (e.g. FeCl3, AlCl3, and BCl3), and thus, are removed (Lunardi 2019). The following reaction can be observed in this case.

$$Si + 3HCl \rightarrow HSiCl_3 + H_2$$

Trichlorosilane mixed with other gaseous chlorine compounds undergoes multiple distillations which improves the purity up to 99.999%. Subsequently, the purified trichlorosilane, mixed in hydrogen, is thermally decomposed on the surface of a heated silicon rod, heated approximately to 1100°C, to poly-crystalline silicon and HCl. The reactions associated with this process are:

$$2SiHCl_3 \rightarrow H_2SiCl_2 + SiCl_4$$
$$H_2SiCl_2 \rightarrow Si + 2HCl$$
$$H_2 + SiHCl_3 \rightarrow Si + 3HCl$$
$$HCl + SiHCl_3 \rightarrow SiCl_4 + H_2$$

The poly-crystalline silicon obtained at the end of this process has a high degree of purity. However, crystalline grain boundaries, which form electronic defects, reduce the efficiency of solar cells fabricated with it, and therefore, excludes its use in the field of microelectronics. The mono-crystalline silicon, produced from poly-crystalline silicon using the Czochralski or Float Zone methods, can be used as the basic raw material for the production of silicon wafers for microelectronic components (Saga 2010).

2.6.2 Silicon Wafer Production

Since the investigated perovskite/Si tandem consists of a FZ wafer, the float zone process has been focused onto. In the float zone, a mono-crystalline silicon seed crystal is brought into contact with one end of a poly-crystalline silicon ingot. The radio frequency (RF) coil and the melted zone move along the entire ingot. This coil, when heated, melts a small region of the polysilicon and after cooling down, forms mono-crystalline silicon with the crystallographic orientation of the seed crystal. As most impurities are less soluble in the crystal than in the melted silicon, the molten zone carries the impurities away which concentrate near the end of the crystal where they can easily be cut off. To further reduce the remaining impurity concentration, this process can be repeated. Usually, during crystal

growth, phosphine (PH_3), arsine (AsH_3) or diborane (B_2H_6) are added as dopant gas to produce the p–n junction. However, to produce a SHJ cell, as used in the investigated tandem, a layer of doped a:Si is deposited instead of doping like the p-n junction. Less energy is required for cell production as this modified junction reduces recombination and decreases the thermal budget, resulting in potential reduction in environmental impacts (Lunardi 2019).

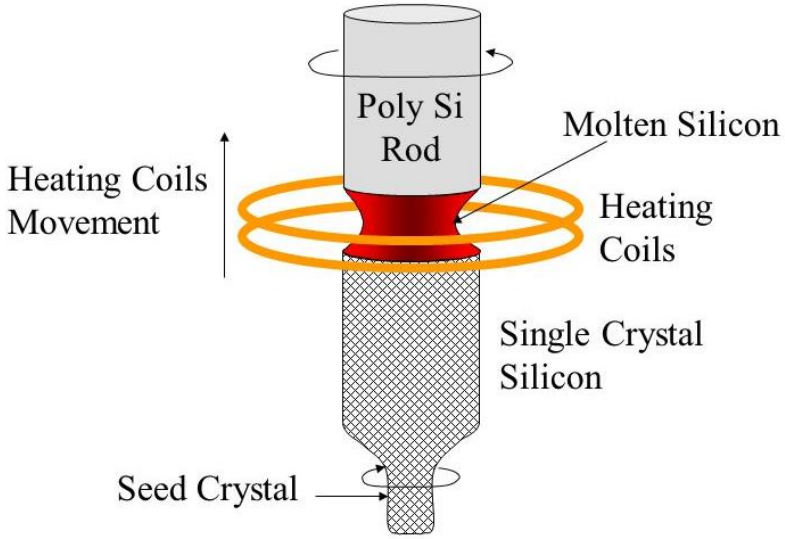

Figure: 4 Float zone process (Chao 2001)

The main advantage of the FZ technique is the very low impurity concentration, particularly oxygen and carbon, in the silicon crystal as compared to CZ silicon. In the final crystal, the dopant concentration is homogeneous and manageable, allowing very high-ohmic (1-10 KΩ cm) and narrow electrical resistivity wafers. The disadvantage of the FZ method is the relatively high cost, which is typically three to four times with respect to the finished CZ wafer.

After the production of mono-crystalline silicon, the following step is sawing it into wafer form to attain desired thickness. The wafer thickness for the investigated tandem is 260 µm. But the sawing process is typically associated with 40% material losses, known as kerf loss, which represents a large part of the wafer production cost, contributing significantly to the overall module cost. Mainly, two methods of slicing ingots are used in the industry: slurry based and electroplated diamond wires. Although diamond wire sawing is gaining a greater market share recently, the slurry based sawing method is the dominant technology due to lower costs. The slurry based sawing method cut ingots using a multi wire technique, where the silicon material is in direct contact with a moving wire made of steel, with a suspension of SiC in polyethylene glycol (Rodriguez, Guerrero et al. 2011). The wafer cutting process causes some defects to the wafer which can be removed by etching, usually 10 µm, in alkaline or acidic based solutions or a plasma etching (Gomez Trillos 2018). Furthermore, the wafers are chemically treated to enhance optical and electrical properties (Lunardi 2019).

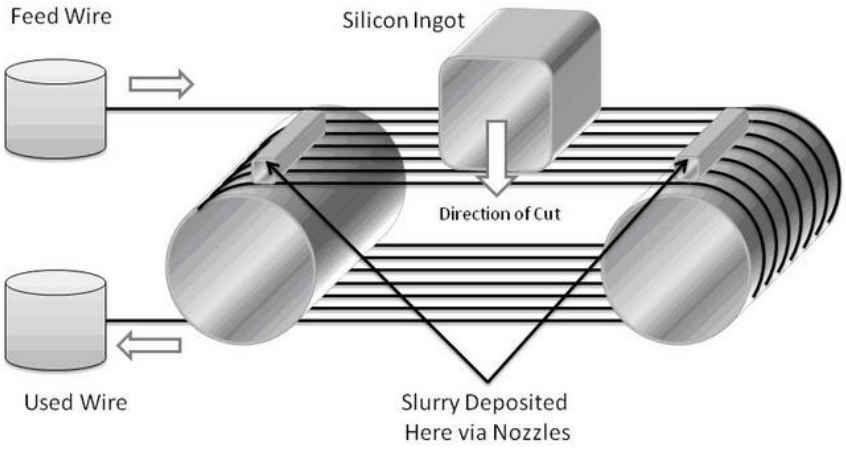

Figure: 5 Wafer Sawing (Radeker and Cunningham 2010)

Various techniques can been applied to deposit the different layers that comprise the stack, like the commonly used spin-coating, doctor blading, slot-die coating, printing, spray deposition, soft cover deposition, dip coating and vapour-based deposition (Qiu, Ono et al. 2018). Subsequently, 5 nm of Intrinsic Amorphous Silicon (a-Si:H)(i) is deposited on both sides of this wafer through plasma-enhanced chemical vapor deposition (PECVD). Following this, 5 nm thickness of Hydrogenated Amorphous Silicon (a-Si:H)(p+) is deposited on the rear by the same process, PECVD. Unhydrogenated a-Si has a very high defect density that can lead to undesirable semiconductor properties like poor photoconductivity and prevention in doping. Both the problems can be solved by introducing hydrogen during the fabrication of a-Si which showed a lower defect density and increased conductivity due to impurities (Gotoh et al., 2019). The source of Si in a:Si is silane gas (SiH_4). Following this, 95 nm thickness of hydrogenated nanocrystalline silicon oxide (nc-SiO_x:H)(n) was deposited on a-Si:H (i), on the top by PECVD.

Plasma-Enhanced Chemical Vapour Deposition:

Key advantage of the PECVD technique is that various reactive organic and inorganic monomers as well as inert materials can be used as precursors. These precursors undergo disintegration and radical polymerization as they are exposed to a high-energy plasma stream, resulting in the deposition of a thin film. Plasma is a partially or fully ionized gas which, generally, is a mixture of electrons, charged particles, and neutral atoms. Although this state has extremely high energy, the plasma has no net charge, i.e., neutral. The process gas, one or more, turns into a gas plasma when ionized with electrical energy and provides energy to the reaction process. It is an attractive process for lowering the process temperatures as deposition can occur at room temperature. Electrical energy is delivered from an external source to the process gas or gases only to form the plasma, resulting a low requirement of thermal energy (Hamedani, Macha et al. 2016).

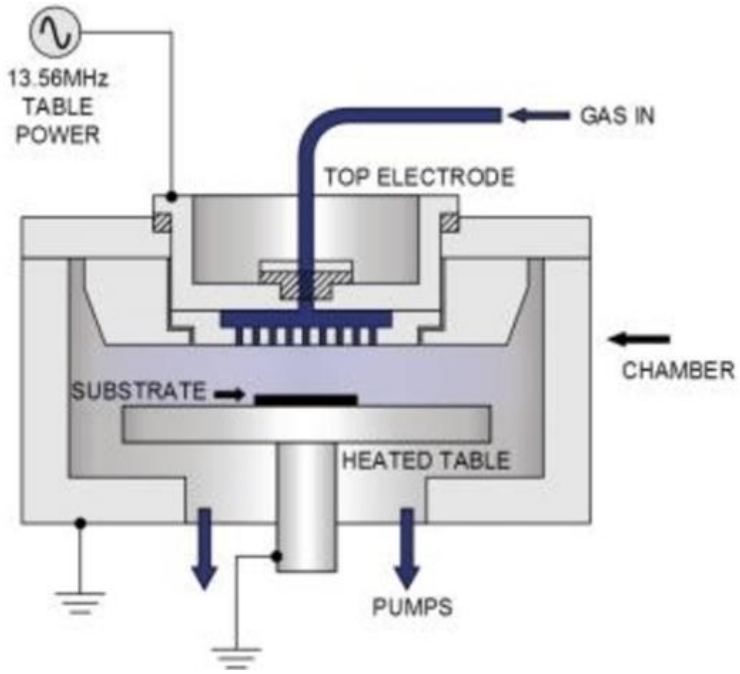

Figure: 6 Plasma-enhanced chemical vapour deposition (Oxford Instruments PlasmaLab 133 instrument manual 2006)

Further requirements for this process are: a pressure reduction system to maintain the plasma state and a reaction chamber. High deposition rate, thermal and chemical stability, high solvent and corrosion resistance are among the key advantages of PECVD, while the disadvantages include utilization of chemical precursors with high vapor pressure, such as halides or metal-carbonyl precursors with associated toxicities, and explosive gases in the plasma stream along with high cost of equipment (Hamedani, Macha et al. 2016).

Furthermore, ITO is deposited at a thickness of 20 nm on top of nc-SiO_x:H (n), on the top side of the wafer. This layer, deposited by radio frequency (RF) sputtering, is the recombination layer between the top and the bottom cell. Finally, to complete the fabrication of the bottom silicon cell, a metal contact layer is deposited on top of the a-Si:H (p+) on the rear side of the wafer. This layer is formed by two RF sputtered layers, a 140 nm deposition of aluminium doped zinc oxide (ZnO:Al) followed by a 400nm silver layer. ZnO has good photoelectric and piezoelectric properties along with characteristics like large band gap (3.36 eV), low dielectric constant and large exciton binding energy (60 meV), making it one of the typical transparent conducting oxides (Lim, Kwon et al. 2008).

Radio Frequency Sputtering:

RF sputtering is a matured process by which any thin metallic and thin inorganic insulating materials can be deposited at relatively high rates, approximately one thousand angstroms per minute, on the surface of semiconductor slices. Sputtered films are high quality and relatively pinhole free.

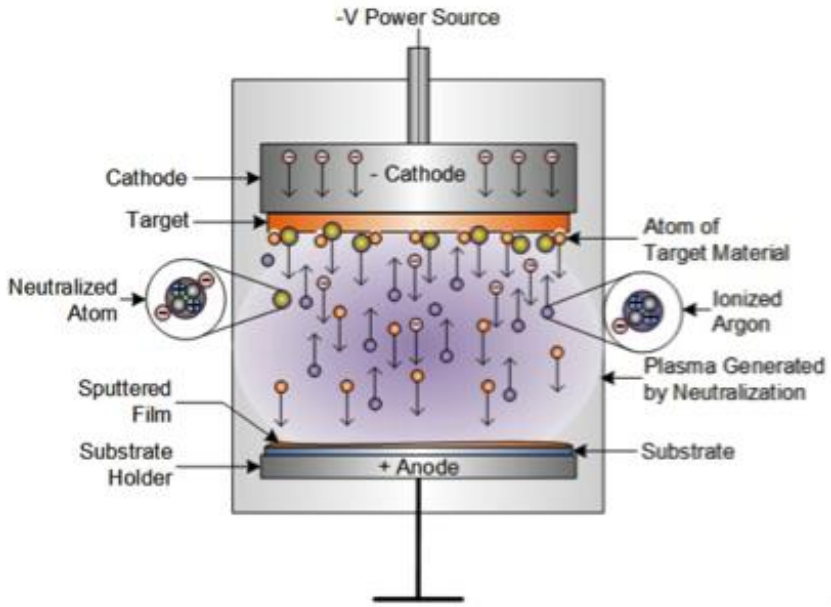

Figure: 7 Radio frequency sputtering (Hughes 2016)

When RF voltage is applied across the electrodes, the substrate, supported by the anode, is exposed to atoms sputtered from the source. The grounded plate, which supports the semiconductor substrate, is water cooled. At a distance of about one inch from this substrate is the RF cathode carrying the bulk source of the material to be deposited as a thin film. In operation, the vacuum chamber is filled with argon at a pressure of about 5 x 10^{-03} torr and when the ionized argon atoms strike the source material, atoms of the source material are sputtered off (Cash Jr and Cunningham 1970). The sputtered ZnO thin films prepared with low sputtering power have very small inherent defect concentration while those deposited at high power have low resistivity with high carrier concentrations due to the arrival of energetic depositing particles (Cash Jr and Cunningham 1970).

2.6.3 Perovskite Cell Manufacturing

An organic ETL, fullerene (C_{60}), of 18 nm thickness is deposited by thermal evaporation on top of the ITO of the bottom cell. This ultra-thin deposition is the bottom most layer of the perovskite top cell. C_{60} is a carbon allotrope which is composed entirely of carbon, in the shape of hollow spheres or ellipsoids. Although C_{60} is relatively insoluble in polar solvents, such as water, its solubility is relatively high in aromatic and moderate in organic solvents (Shinohara 2016). The use of such organic material has displayed significant improvement in the electron extraction from the photoexcited perovskite to the C_{60}, as compared to the commonly employed TiO_2 (Wojciechowski, Leijtens et al. 2015). Organic layers do not require high temperature sintering steps, facilitating fabrication at low temperature which is suitable for temperature sensitive substrates. Additionally, this organic layer has achieved both high stabilized power output and long-term operational stability for perovskite solar

cells. Although little is known regarding the chronic effects of toxicity of fullerene on the environment, the risk of C_{60} on the environment can be assumed to be low at present and for the near future (Shinohara 2016).

Thermal Evaporation Deposition:

Thermal evaporation is one of the common methods of PVD for deposition of metal and non metallic substances. This process involves heating a solid material inside a high vacuum chamber to a temperature which produces some vapor pressure. Inside the vacuum chamber, even a relatively low vapor pressure is sufficient to raise a vapor stream, resulting in low energy consumption (Hardy 2013). This evaporated material traverses the chamber and hits the substrate, sticking to it as a coating or film. Ultra-thin metal films, deposited by thermal evaporation do not require buffer layers because of the more moderate process and could replace the transparent metal oxide electrode such as TiO_2 (Wojciechowski, Leijtens et al. 2015).

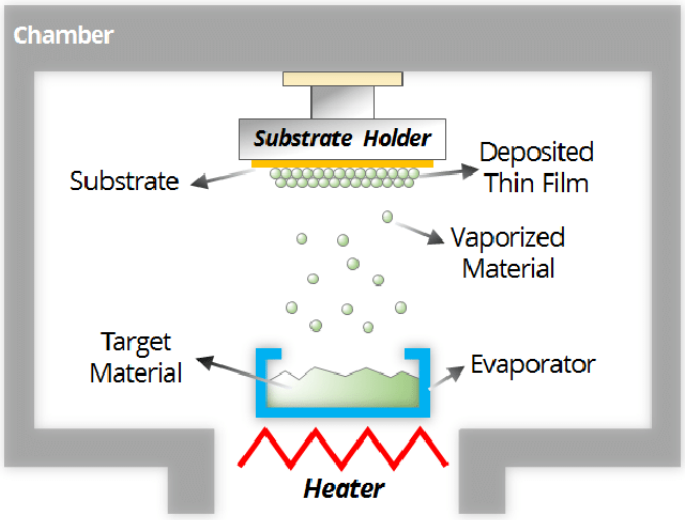

Figure: 8 Schematic diagram of thermal evaporation deposition (Park, Quan et al. 2016)

On top of the thermal evaporated fullerene ETL, 500 nm thickness of perovskite absorber is deposited by spin coating. This layer can be composed of caesium, methylammonium (MA), formamidinium (FA), lead, iodine and bromine with the formula $Cs_{0.05}(FA_{0.77}MA_{0.23})_{0.95}Pb(I_{0.77}Br_{0.23})_3$. The MA based perovskites are limited by intrinsic moisture and thermal stability issues. Such challenges in stability can be solved by using FA based mixed-cation perovskite, although the control of nucleation and crystal growth is difficult in large-areas for such perovskite absorber (Bu, Liu et al. 2020). Mixed halides, that incorporate Br in its composition, contribute to more stability in humid conditions (Zhang 2019). Caesium is also associated with increasing the stability of this material but it is a scarce material. Additionally, the presence of lead(II)halide materials has raised environmental concerns as the lead vapour/dust released from processing facilities threatens workers‘ health and safety (Espinosa, Serrano-Luján et al. 2015).

Spin Coating Deposition:

Spin coating is a well-developed technique used to deposit films in small areas. In this process a small amount of solution is dropped onto a substrate, spun to coat the substrate surface and eliminate the excess of solution and subsequently, dried. The deposited layer thickness can be controlled by the concentration of the solution and the rotation speed (Gomez Trillos 2018). Furthermore, dimethyl formamide (DMF) and dimethyl sulfoxide (DMSO), in the ratio of DMF 4:1 DMSO, is dropped onto the substrate as a deposition solvent. If the process is not controlled thoroughly, this technique can lead to the production of a film with pinholes and small grain sizes with low performance (Mesquita, Andrade et al. 2018). The application of an antisolvent, as a following step, can enhance crystallization and film morphology, where chlorobenzene or toluene is poured on top of the film during the spinning program. Antisolvent-induced cracks may appear in FA based perovskite films but decrease when additional MA cation was added in the precursor (Bu, Liu et al. 2020). Although areas up to 100 cm^2 can be produced through spin coating, commercialization of this technology was limited due to non-uniform film production, high amount of wasted precursors and use of hazardous solvents (Cai, Zhang et al. 2015).

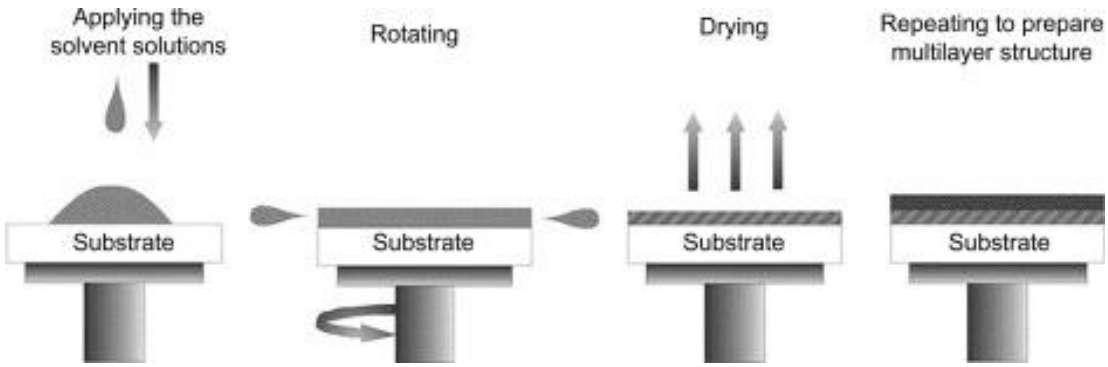

Figure: 9 Spin coating deposition method (Mishra, Bhatt et al. 2019)

After the deposition of the perovskite absorber layer, 200 nm of Ag is deposited by thermal evaporation at room temperature, which acts as the top metal contact layer. Gold, silver and aluminium are among the common materials used for metal contacts due to higher work function and better energy band alignment (Celik, Song et al. 2016). Besides, an ultra thin HTL, approximately 0.6 nm in thickness, of 4-bromobenzyl phosponic acid-based self-assembled monolayer is deposited through spin coating at the interface between the ITO layer and the perovskite layer. Such modification leads to an increase in photovoltage, from 0.979V to 1.029V, and consequently, an improved power-conversion efficiency (Fisher 2020). Furthermore, the investigated tandem developed in Helmholtz Zentrum Berlin uses 25 µg of ethanol for each cell as the deposition solvent.

The protective layer is pivotal for a solid-state solar cell as it inhibits the back-electron-transfer from the electron-collecting substrate, which is an undesired parasitic process in solar cells (Kavan, Steier et al. 2017). Such a layer is transparent and pinhole-free to fully block charge carrier recombination between the electrode contact and the photon absorber. Although TiO_2, and in some cases Al_2O_3, was exclusively used for this layer, SnO_2 deposited by atomic layer deposition (ALD) has recently emerged as a powerful alternative to it. Henceforth, 20 nm of SnO_2 is deposited on top of the HTL by ALD.

Atomic Layer Deposition (ALD):

ALD is a gas-phase thin film deposition method which can produce high quality films at relatively low temperature. Such a process involves the surface of a substrate being exposed to alternating precursors, which do not overlap but instead are introduced sequentially with self-limiting surface reactions. The precursors include oxides, metals, sulfides, and fluorides. For deposition of SnO_2, tetrakis(dimethylamino)tin(IV) (TDMASn, 99.99%-Sn), heated at 55°C, and ozone at 118°C is used as precursors, while pure oxygen and nitrogen gas is used for production of ozone (13% in O_2) and as the carrier gas, respectively (Matsui, Seo et al. 2017). The process ensures accurate thickness films, excellent conformality, uniformity over large areas and reproducibility. This process is widely used to deposit diffusion barriers and passivation of active layers as it delivers high density films with no pinholes. Key disadvantage of the ALD process is its high equipment cost.

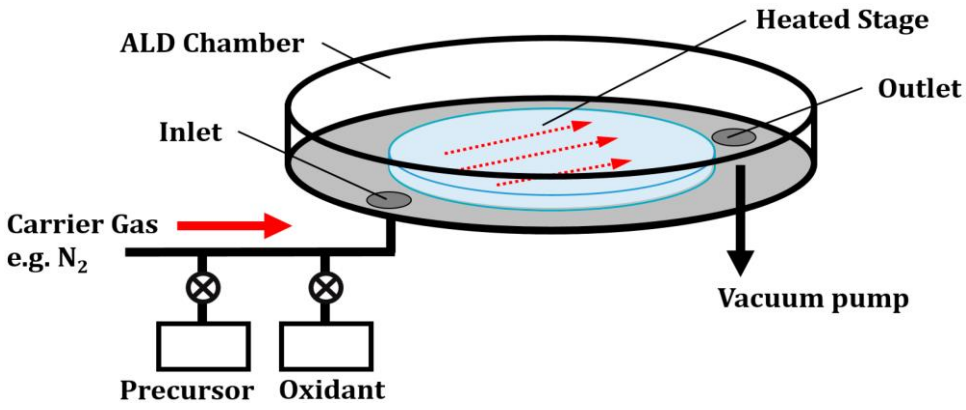

Figure: 10 Atomic layer deposition (Ono, Qi et al. 2018)

Subsequently, 100 nm thickness of indium zinc oxide (IZO) is deposited on top of the protective layer. This layer constitutes the front electrode and is deposited by RF sputtering. Deposition of IZO is done using the oxide ceramic targets In_2O_3 and ZnO, 89.3 wt. % and 10.7 wt. % respectively, and substrate temperature during the deposition is confirmed to be lower than 50°C (Ito, Sato et al. 2006). Ito et al. further demonstrated that total gas pressure

of Ar or Ar+H_2 is kept at 0.5 Pa and introducing H_2 gas into the process increases carrier density.

To achieve a reduction of the reflection losses, an antireflection coating is also deposited on top of the IZO beside the Ag layer. This layer is composed of 100 nm thickness of lithium fluoride (LiF), deposited by thermal deposition. Such layers on the cell increase the photon flux reaching the PV medium, while reflecting part of the incident energy that results only unwanted cell heating. Serving as a radiation barrier, an optical-coupling element and a protective agent against debris, impact and other environmental aggressors, antireflection coatings are critical to the performance and environmental robustness of PV systems.

The following *Table* 1 shows the architecture of the investigated perovskite/Si tandem, based on the data provided by the project partners.

Table 1 Architecture of the investigates perovskite/Si tandem (Helmholtz Zentrum Berlin)

Subcell	Layer	Composition	Thickness	Deposition process
Perovskite Top Cell	Antireflection Coating	LiF	100 nm	Thermal Evaporation
	Metal contact Layer	Ag	200 nm	Thermal Evaporation
	Front Electrode	IZO	100 nm	RF Sputtering
	Protective Layer	SnO_2	20 nm	ALD
	Electron Transporting Layer	C_{60}	18 nm	Thermal Evaporation
	Perovskite Absorber	$Cs_{0.05}(FA_{0.77}MA_{0.23})_{0.95}Pb(I_{0.77}Br_{0.23})_3$	500 nm	Spin Coating
	Hole Transport Layer	Phosphonic Acid Monolayer	~0.6 nm	Spin Coating
Heterojunction Silicon Bottom Cell	Recombination Layer	ITO	20 nm	RF Sputtering
	n-type Hydrogenated Nanocrystalline Siliconoxide	nc-SiO_x:H(n)	95 nm	PECVD
	Intrinsic Amorphous Silicon	a-Si:H(i)	5 nm	PECVD
	Mono-crystalline Silicon Wafer	c-Si(n)	260 µm	Floatzone
	Intrinsic Amorphous Silicon	a-Si:H(i)	5 nm	PECVD

	Layer	Composition	Thickness	Deposition process
	p-type Hydrogenated Amorphous Silicon	a-Si:H(p+)	5 nm	PECVD
	Metal Contact Layer (Back)	ZnO:Al	140 nm	RF Sputtering
		Ag	400	RF Sputtering

2.7 Installation, Use and End-of-Life

At present, there are no utility scale perovskite or perovskite/Si tandem solar installations but only lab-scale. Therefore, the installation and use factors associated with a utility scale c-Si installation are analysed. Installation of such a utility scale solar power plant requires immense amount of site maintenance prior to installation, followed by various balance of system (BOS) components, such as wiring, inverters, mounting structures, etc. As suggested by the researchers, the energy requirement during the installation phase could be as low as ~ 40 kWh/m^2 or as high as ~ 500 kWh/m^2 (Nawaz and Tiwari 2006, Zhou and Carbajales-Dale 2018).

During the use phase, the panels themselves do not produce waste or emissions. However, plant maintenance activities, such as lawn mowings and panel cleanings, require energy and produce emissions. Throughout the lifetime of a solar plant, the modules will require frequent washings to remove dirt and debris from the panel surface, producing waste water, until the site has reached the end of its lifetime and is subsequently decommissioned.

The lifetime of perovskite solar cells is extremely short, approximately 5 years, calculated based on lab-tested efficiencies and small-scale installations (Kadro and Hagfeldt 2017). The lifetime can be increased by substituting the component A in the perovskite formula ABX_3 of the crystal structure. This is possible as change of the component A has less impact in the optoelectronic properties of the overall material. Although partial substitution with Caesium or other organic groups has extended the lifetime to more than 1000 hours, researchers believe that a minimum of 10 years lifetime is required for commercialization.

As the current PV installations reach the final decommissioning stage, recycling and material recovery will be preferable to panel disposal. But the recycling of PV panels is still negligible, as most of these devices are on service or there are low economic incentives, and therefore, most of the efforts have been devoted to the improvement of efficiency or stability of this technology rather than recycling or handling of waste materials (Gomez Trillos 2018). But end-of-life management for PV technology is crucial as it will spawn new industries, support

considerable economic value creation and is consistent with a global shift to sustainable long-term development (Weckend, Wade et al. 2016).

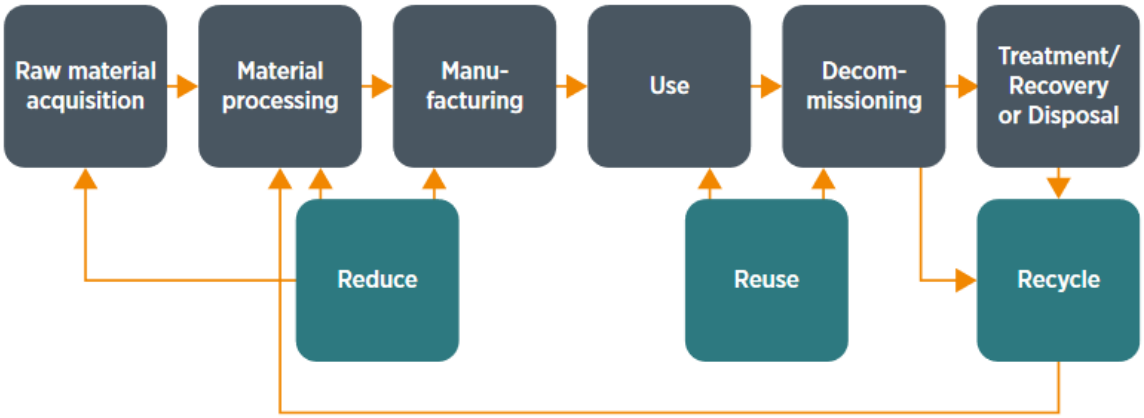

Figure: 11 Life cycle of PV technology (Fthenakis 2000)

Existing recycling technology includes reuse and recycling of the most important parts of the panel in three different types of treatment processes, namely: physical, thermal and chemical treatment processess. In most of the cases, the PV module is separated from the mounting system and the electric installation before going to landfill, allowing separation of specific components based on their waste types. These components are then treated in a recycling plant which further allows the recovery of steel, aluminium and copper. Such BOS components are often neglected in LCA studies; however, there are some studies that analysed the environmental impact profile of these materials.

In the physical treatment process, the panels are primarily dismantled by removing the surrounded Al frame, along with the junction-boxes and embedded cables, and are shredded and crushed to favour separation processes (Chowdhury, Rahman et al. 2020). Further recycling steps for the perovskite top cell and the c-Si bottom cell takes place after the physical treatment. Recycling methods for the newly emerging perovskite solar cells strategize to isolate the lead materials within the panels. Tsao showed that the addition of chlorobenzene, ethanol, and dimethylformamide (DMF) are necessary to separate different layers of the perovskite PV layers while keeping the lead isolated (Tsao 2016). Binek et al. developed a step by step recycling procedure that ensured safe toxicity levels while saving as much material as possible (Binek, Petrus et al. 2016). The steps are as follows-

- Removal of back contact layer with adhesive tape.
- Separation of HTL by submerging the remaining material in chlorobenzene.
- Converting the photo absorber layer into iodide (PbI_2) and methylammonium iodide (MAI) by submerging the material in a bed of double distilled water.

- Submerging the remaining material in DMF for further lead removal.
- Separation of ETL by DMF submergence, leaving behind the glass top layer only.

Recovery of further material is done by using the thermal and chemical treatment. Typically c-Si is composed of more than 90% of non-hazardous waste, such as glass, polymer and aluminium, while thin-film panels are over 98% non-hazardous. The hazardous waste in c-Si consists of mainly silver, tin and lead traces , while the 2% potential hazardous waste in thin films include copper, zinc indium, gallium, selenium, cadmium, tellurium and lead (Weckend, Wade et al. 2016). Such reuse and recycle strategy allows material recovery of major components, such as glass, aluminium and copper for c-Si panels, which can be recovered at cumulative yields greater than 85% of total panel mass (Weckend, Wade et al. 2016). Besides, valuable metals like silver and copper represent a value opportunity if recovered. Hence, landfill may not be the best option since it does not recover potentially valuable materials from PV modules. Overall costs can be offset by recovering materials that would otherwise be lost to landfills. However, unless the recycling facility runs off of renewable energy sources, emissions from fossil fuels contribute to global climate change.

Another effective strategy to manage the end of life of PV technologies is proper policy implementation. For instance, the EU's Waste Electrical & Electronic Equipment (WEEE) directive requires all the producers and importers to accept responsibility for the end of life treatment of their products or they are subjected to large fines (Román 2012). Globally, there is a lack of such regulations and enforcements on solar panel recycling, particularly in Asia, threatening their natural environment (Weckend, Wade et al. 2016).

2.8 Future Developments

An emerging c-Si PV technology, that has drawn significant attention due to its reputation as high performance solar cells, is the passivated emitter and rear cell (PERC) technology. With an expected share of around 60% in the world's PV market in 2027, this technology may be the dominant technology in the future (Trube, Fischer et al. 2018). This technology has already been implemented in the industry and a p-type PERC cell has achieved an efficiency of approximately 25% (Lunardi 2019).

Additionally, two other thin-film PV technologies are recently emerging beside the perovskite technology. They are copper zinc tin sulfide (Cu_2ZnSnS_4, or CZTS) and colloidal quantum dot photovoltaics (QDPV). CZTS is an alternative technology with respect to CIGS that replaces indium with more abundant materials, which has a certified cell efficiency of 12.6%. Besides, the constantly improving QDPV technologies, at present, has a certified cell efficiency of 16.6% and uses solution processed nanocrystals to absorb the photon (Zendehdel, Nia et al. 2020). Incomplete knowledge of surface chemistry of quantum dots (QD) and low open-circuit voltages limit this technology.

Nevertheless, the target of all these emerging technologies remains the same. It is to employ non hazardous, earth-abundant materials that can be engineered by relatively simple processing methods to achieve desired stable electronic and optical properties, and subsequently, increase the power conversion efficiency. This can promise a gate for large-scale manufacturing and deployment of such emerging PVs.

Chapter 3 State of the Art LCA Studies on Perovskite Solar Cells

The life cycle inventory (LCI) datasets and life cycle impact assessment methods used in this study are in harmony with the recent literature. As perovskite can be used in solar cells in numeruos configurations, different results associated with the environmental footprint are published in the literature. In this context, the selection was limited to studies on perovskite thin film solar cells, perovskite/Si tandem and end-of-life stage of photovoltaic cells. Moreover, only studies with detailed and complete life cycle inventories (i.e., raw materials and energy input and output flows) of the cell are selected to maintain high-quality information. This allowed for a more consistent comparison of the obtained results from different studies, keeping the definition of baseline information harmonized.

The perovskite/Si tandem technology is still in the development phase. Only a few companies, such as Saule Technologies, and research groups have reached the technology readiness level (TRL) 7-8 (system prototype demonstration in operational environment and qualifying), while the investigated tandem in this study has reached TRL 5-6 (technology validation and demonstration in relevant environment). The TRL is a method for estimating the maturity of technologies during the development phase, ranging from TRL 1 (basic principles observed) to TRL 9 (system proven in operational environment or competitive manufacturing). The race to TRL 9 has resulted in the development of a multitude of cell components, configurations and fabrication processes which, in turn, determine a large number of combinations. Therefore, the quantity of material and energy inflow and outflow in the LCI datasets, within all the LCA studies of perovskites published in literature so far, has high degree of diversity and refers only to the lab-scale fabrication. Consequently, it is important to highlight that as the life cycle inventories represent lab-scale synthesis, it fails to represent a scaled-up industrial production.

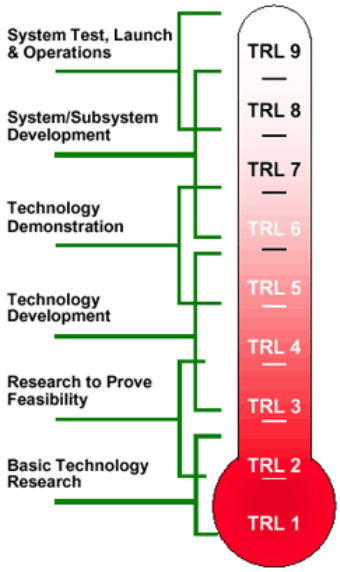

Figure: 12 NASA Technology Readiness Levels

A careful inspection of the selected studies reported in *Table* 2 revealed that only four studies by Itten & Stucki, Celik et al., Lunardi et al. and Lunardi, considered tandem structures while only the first three are cradle-to-grave analyis, i.e, included end of life scenarios.

Table 2 Studies on LCA of perovskite and perovskite/Si tandem solar cells. Own table.

Index	Title	Author	Type	Date	FU	Archetecture	Reference
01	Solution and vapour deposited lead perovskite solar cells: Ecotoxicity from a life cycle assessment perspective. Solar Energy Materials and Solar Cells	Espinosa, N., et al.	Cradle to gate	2015	1 kWh	Vapour deposition: FTO/TiO2/MAPbI3/Spiro-OMeTAD/Ag Spin coating: ITO/PEDOT:PSS/MAPbI3/ PCBM/Al	(Espinosa, Serrano-Luján et al. 2015)
02	Tin and Lead Based Perovskite Solar Cells under Scrutiny: An Environmental Perspective. Advanced Energy Materials	Serrano-Lujan, L., et al.	Cradle to grave	2015	1kWh	Glass-ITO/PEDOT:PSS/ MAPbI3/ PCBM/Al Glass-FTO/TiO2/MAPbI3/Spiro-OMeTAD/Ag Glass-FTO/Compact TiO2/MASnI3 + MesoporousTiO2/Spiro-OMeTAD/Au	(Serrano-Lujan, Espinosa et al. 2015)
03	Perovskite photovoltaics: life-cycle assessment of energy and environmental impacts.	Gong, J., et al.	Cradle to gate	2015	1 m^2	TiO2 module: FTO/Mesoporous TiO2/MAPbI3/Spiro-OMeTAD/Au ZnO module: ITO/ZnO/MAPbI3/Spiro-OMeTAD/Au	(Gong, Darling et al. 2015)
04	Life cycle assessment of titania perovskite solar cell technology for sustainable design and manufacturing.	Zhang, J., et al.	Cradle to gate	2015	1 cm^2	FTO glass/TiO2 nanotube (TNT)/MAPbI3/Iodine liq el./Pt glass	(Zhang, Gao et al. 2015)
05	Life Cycle Assessment (LCA) of perovskite PV cells projected from lab to fab.	Celik, I., et al.	Cradle to gate	2016	1 m^2	Solution based: FTO/SnO2/MAPbI3/CuSCN/MoOx-Al Vacuum based: FTO/SnO2/MAPbI3/CuSCN/MoOx-Al HTL free: FTO/SnO2/MAPbI3/C-Paste	(Celik, Song et al. 2016)

Index	Title	Author	Type	Date	FU	Archetecture	Reference
06	Comparison of life cycle environmental impacts of different perovskite solar cell systems.	Zhang, J. et al.	Cradle to cradle	2017	1 cm^2 conv. to 1 kWh	MASnI3: FTO/Compact TiO2/ Mesoporous TiO2/ MASnI3/ Spiro-OMeTAD/ Gold	(Zhang, Gao et al. 2017)
						MAPbI3: FTO/Compact TiO2/ Mesoporous TiO2/ MAPbI3/ Spiro-OMeTAD/ Gold	
						FAPbI3: FTO/Compact TiO2/ Mesoporous TiO2/ FAPbI3/ Spiro-OMeTAD/ Gold	
						CsPbBr3: FTO/Compact TiO2/ Mesoporous TiO2/ CsPbBr3/ Spiro-OMeTAD/ Gold	
						MAPbI2Cl: FTO/Compact TiO2/ Mesoporous TiO2/ MAPbI2Cl / Spiro-OMeTAD/ Gold	
07	Highly efficient 3rd generation multi-junction solar cells using silicon heterojunction and perovskite tandem: Prospective life cycle environmental impacts.	Itten, R. & Stucki, M.	Cradle to grave	2017	1 kWh	PSC Pessimistic ITO/SbO2/MAPbI3/NiO/Ag	(Itten and Stucki 2017)
						PSC Optimistic ITO/SbO2/MAPbI3/NiO/Ag	
						SHJ-PSC Pessimistic Ag/ITO/NiO/MAPbI3/SbO2/SHJ/ ITO/Ag	
						SHJ-PSC Optimistic Ag/ITO/NiO/MAPbI3/SbO2/SHJ/ ITO/Ag	
08	Environmental analysis of perovskites and other relevant solar cell technologies in a tandem configuration	Celik, I. et al.	Cradle to end of use	2017	1 m^2 conv. to 1 kWh	CZTS/PKPb: Glass/Mo/CZTS/CdS/ITO/PEDOT:PSS/MAPbI3/PC BM/Al	(Celik, Phillips et al. 2017)
						CIGS/ PKPb: FTO Glass/mp-TiO2/MAPbI3/ SpiroOMeTAD/MoO3/(ZnO/ZnOAl)/CdS/CIGS/Mo/Glass	
						Si/ PKPb: ITO/MoO3/SpiroOMeTAD/MAPbI3/PCBM/ZnO:In/p-aSi/i-aSi/n-type FZ Si Wafer/i-aSi/n-aSi/ITO/Ag	
						PKSn,Pb / PKPb: ITO/NiO/MAPbI3/PCBM/ITO/PEDOT:PSS/MASnI3/ PCBM/Ag	
09	A life cycle assessment of perovskite/silicon tandem solar cells.	Lunardi, M.M. et al.	Cradle to grave	2017	1 kWh	Au/ SHJ bottom cell /TiO2/MAPbI3/Spiro OMeTAD/MoO3/ITO	(Monteiro Lunardi, Wing Yi Ho-Baillie et al. 2017)
						Ag/ SHJ bottom cell /TiO2/MAPbI3/Spiro OMeTAD/MoO3/ITO	
						Al/Si(p)/Si(n)//ITO/PEDOT:PSS/MAPbI3/PCBM/ZnO/ITO	

Index	Title	Author	Type	Date	FU	Archetecture	Reference
10	Perovskite solar cells: An integrated hybrid lifecycle assessment and review in comparison with other photovoltaic technologies.	Ibn-Mohammed, T. et al.	Cradle to gate	2017	1 m^2	Au/Spiro OMeTAD/MAPbI3/Mesoporous TiO2/TiO2/FTO anode/FTO glass	(Ibn-Mohammed, Koh et al. 2017)
						Cu/CuSCN/CsFAPbIBr/Mesoporous TiO2/TiO2/FTO anode/FTO glass	
11	Life Cycle Assessment of Perovskite Solar Cells.	Gomez Trillos, J. C.	Cradle to cradle	2018	1 m^2 conv. to 1 kWh	FTO glass/TiO2/MAPbI3 (Solv2)/Spiro-OMeTAD/Au	(Gomez Trillos 2018)
						FTO glass/TiO2/MAPbI3 (Solv3)/Spiro-OMeTAD/Au	
12	Relative impacts of methylammonium lead triiodide perovskite solar cells based on life cycle assessment.	Alberola-Borràs, J.A., et al.	Cradle to grave	2018	1 cm^2	FTO glass/TiO2/MAPbI3 (Solv2 + TiO2 scaffold)/Spiro-OMeTAD/Au	(Alberola-Borràs, Vidal et al. 2018)
						FTO glass/TiO2/MAPbI3 (Solv2)/Spiro-OMeTAD/Au	
						FTO glass/TiO2/MAPbI3 (Solv3)/Spiro-OMeTAD/Au	
						FTO glass/TiO2/MAPbI3 (Solv2 + TiO2 scaffold)/Spiro-OMeTAD/Au	
13	Life cycle assessment of silicon based tandem and advanced silicon solar modules	Lunardi, M. M.	Cradle to gate	2019	1kWh	FTO glass/ITO/TiO2/PEDOT:PSS/MAPbI3/ Spiro-OMeTAD/PCBM/ZnO ink/Ag	(Lunardi 2019)
						FTO glass/ITO/TiO2/PEDOT:PSS/MAPbI3/ Spiro-OMeTAD/PCBM/ZnO ink/Al	
						FTO glass/ITO/TiO2/PEDOT:PSS/MAPbI3/ Spiro-OMeTAD/PCBM/ZnO ink/Au	
14	This study	Khan, A. A.	Cradle to grave	2020	1 m^2 conv. to 1 kWh	LiF/IZO/SnO2/Phosphonic acid/Ag/ $Cs_{0.05}(FA_{0.77}MA_{0.23})_{0.95}Pb(I_{0.77}Br_{0.23})_3$/ITO/C60/nc-SiO:H(n)/a-Si:H(i)/s-Si/a-Si:H(i)/Silicon nanoparticles:H/ZnO:Al/Ag (+ Encapsulation and front contacts)	

3.1 Results of LCA Studies on Organic-Inorganic Halide Perovskite Technology

Among the cradle to gate studies listed in Table 2, the LCA study of Espinosa et al. considers a solution and vapour deposited lead perovskite solar cell. They assume a functional unit (FU) of 1 kWh and 1,700 kWh/m^2/yr for solar insolation, 15.4% and 11.5% efficiency and 1 year lifetime. Regarding the investigated environmental impacts, the authors identified global warming potential (GWP) of 5.48 and 5.24 kgCO_2eq/kWh (depending on efficiency) and a energy payback time (EPBT) of 17.32 to 16.54 years if the process energy required to produce a 1 cm^2 solar cell is 0.146 and 0.108 kWh.

Considering 1 m^2 as FU, Gong et al. showed that 82.5 and 60.1 gCO_2eq/kWh could be released into the environment for TiO_2 and ZnO solar cells, respectively, and 7.78 kWh of manufacturing energy is required to fabricate 1 m^2 of each. With the same FU, Celik, et al. calculated a GWP impact of 99 to 147 gCO_2eq/kWh and the EPBT between 1.05 to 1.54 years. This study assumed a solar insolation of 1,700 kWh/m^2/yr, 0.75 performance ratio, 15% efficiency and 5 years lifetime. In 2017, for the same FU, Ibn-Mohammed, T. et al. reported a GWP of 92.34 and 47.35 gCO_2eq/kWh and EPBT of 0.39 and 0.15 years for $MAPbI_3$ and CsFAPbIBr perovskite solar cells, respectively.

Using 1 cm^2 as the FU, the study carried out by Zhang et al. found a GWP impact of 2.88 gCO_2eq/kWh. Insolation assumed in this study ranged between 1000 to 1863 kWh/m^2/yr. Furthermore, the performance ratio of 0.75, efficiencies from 6.5 to 25 % and the lifetime of 20 to 30 years was used in this LCA.

3.2 Results of LCA Studies on Perovskite/Si Tandem Technology

Among the three cradle-to-grave LCA studies of the tandem configuration, Itten and Stucki analysed that, depending on the efficiency, the GWP of a monolithic silicon heterojunction-perovskite tandem cell structure is between 0.05 to 0.08 kgCO_2eq/kWh. All three studies have the common assumptions of 1 kWh FU, an insolation of 1,700 kWh/m^2/yr and a performance ratio of 0.75. Itten and Stucki, Celik et al. and Lunardi et al. considered 30, 5 and 20 years of lifetimes, respectively. In the second study, Celik, I. et al. showed that the GWP and EPBT are 168.4 gCO_2eq/kWh and 13 to 13.5 months, respectively, for Si/perovskite tandem solar cells with an efficiency of 6%. In the third LCA, also conducted in 2017, Lunardi et al. found that the GWP and EPBT were 294 gCO_2eq/kWh and between 1.3 to 1.7 years for different scenarios, respectively. In this case, the efficiency was 24 to 27%, depending on the configuration of the tandem cell. The fourth LCA was a cradle to cradle study, in which Gomez Trillos 2018, found out that the GWP of the perovskite/Si tandem was 118.5 gCO2eq/kWh. The EPBT was 1 and 1.79 years for an insolation of 950 and 1,700 kWh/m^2/yr, respectively. The efficiency of the tandem was 26% and the lifetime was considered 5 years.

However, it is important to address that these impacts, considered over 20 to 30 years of lifetime for the modules, are unrealistic because of the challenges with stability of this technology. Besides, large uncertainties are associated with studies that use secondary process data from the literature because supplementary materials, such as chemical solvents, associated energies and fabrication processes are often ignored.

3.3 Results of LCA Studies on End-of-Life Stage

Understanding the future of photovoltaic recycling is a research area gradually gaining interest as the International Renewable Energy Agency (IRENA) state that if the growth in worldwide installed solar capacity continues, global PV waste materials could be worth over $15 billion by 2050 (Weckend, Wade et al. 2016). Although description of the end of life stage of photovoltaics can be observed in some studies, such as the studies conducted by Chowdhury et al. and Kadro and Hagfeldt, these processes are often left out of the LCAs. Among the three selected LCA studies mentioned in *Table* 3, Latunussa et al. found out that the global warming potential of recycling 1000 kg of c-Si PV waste panel is 370 kg CO_2eq. Stolz and Frischknecht showed that 256 g CO_2eq. is emitted for the treatment of per kg PV waste without the mounting structures or electric installations. Lastly, Lunardi et al. calculated that the GWP impacts are mostly produced by the silicon feedstock (solar and electronic grade) as high energy is required to recover the silicon and reuse it. Although no concrete value is provided for the GWP, this author showed that recycling, particularly thermal and chemical recycling, has lower impacts on the ecosystem than landfill and incineration.

Table 3 Studies on LCA of End-of-Life stage. Own table.

Index	Title	Author	Date	Functional Unit	Reference
1	Life Cycle Assessment of an innovative recycling process for crystalline photovoltaic panels	Latunussa et al.	2016	Recycling of 1000 kg of c-Si PV waste panel	(Latunussa, Ardente et al. 2016)
2	Life Cycle Assessment of Current Photovoltaic Module Recycling	Stolz and Frischknecht	2017	Recycling of 1 kg of used framed c-Si	(Stolz, Frischknecht et al. 2017)
3	Comparative Life Cycle Assessment of End-of-Life Silicon Solar Photovoltaic Modules	Lunardi et al.	2018	1kg of Silicon-based PV waste modules	(Lunardi, Alvarez-Gaitan et al. 2018)

Chapter 4 Life Cycle Assessment of Perovskite/Silicon Solar Cell Tandems

4.1 Methodology

The complicated processes and the diverse resources used over the lifetime of a product involve potential environmental impacts. Among the several tools and methodologies used to calculate those effects, a common method accredited by the International Organisation for Standardisation (ISO) is the Life Cycle Assessment (LCA). The first LCA was conducted for different containers of beverages for the Coca Cola Company, in the late 1960s, as concern for the environment grew with the increased energy demands and diminishing natural resources (Hunt, Franklin et al. 1996). This methodology is described as an analysis that addresses the environmental aspects and potential environmental impacts (e.g. use of resources and the environmental consequences of releases) throughout a product's life cycle from raw material acquisition through production, use, end-of-life treatment, recycling and final disposal (i.e. cradle-to-grave) (Finkbeiner, Inaba et al. 2006).

An LCA accounts for the environmental impacts of the material and energy inputs and outputs throughout a product or service lifetime. Additionally, an LCA identifies the potential transfer of environmental impacts from different mediums at different times on different life cycle stages (Bjørn, Owsianiak et al. 2018). This is the key strength of an LCA which allows the comparison of environmental impacts of different product systems. Such a result can assist decision-makers to select the product or process that causes the least impact to the environment and identify opportunities to improve the environmental aspects of products at various points in their lifecycle. Consequently, this approach has increased the awareness of human activity impacts on the environment and further, provided a standardized method with a scientific basis to assess environmental trade-offs in the life cycle of a product or service. To give the reader of the study a possibility of judgement, it is important to keep the transparency as many simplifications and assumptions are made during an LCA (Curran 2015).

The two different approaches to perform an LCA study are the attributional and consequential approaches. While the attributional LCA evaluates one complete life cycle chain by assigning emissions from each step of the process, the consequential LCA analyses a wider system by assessing the consequences of selecting the use of one material over another. The attributional approach is useful in benchmarking and comparing different technologies or products whereas the latter is useful for decision making policy levels (Rödger, Hammond et al. 2016).

ISO 14040 and ISO 14044 Standards

LCA methodology is currently standardized upon the two universal standards ISO 14040 and 14044. These standards are as follows:

I. **ISO 14040 :** 'Environmental management- Life cycle assessment- Principles and framework' (ISO)

II. **ISO 14044 (2006b):** 'Environmental management– Life cycle assessment- Requirements and guidelines' (Standardization 2006)

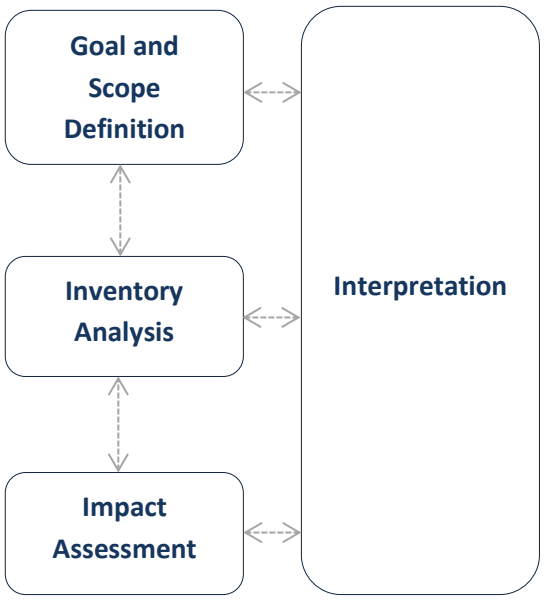

Figure: 13 The four stages in LCA (Finkbeiner, Inaba et al. 2006, Finkbeiner 2014)

The flow diagram of the LCA (*Figure* 13), in accordance to the standard protocol of ISO 14040 and 14044, is organized in four different stages- (i)IGoal and Scope Definition, (ii) Life Cycle Inventory (LCI), (iii) Life Cycle Impact Assessment (LCIA) and (iv) Interpretation. Detailed descriptions of these four stages are given in the following part of this chapter.

4.2 Goal and Scope

This step must explicitly state the purpose of the study, the application of the results and the audience to whom the results will be disclosed. Other items to be stated in this step are (Mukherjee 2014):

- Product system to be studied
- Functional unit
- System boundaries
- Allocation procedures
- Impact assessment methodology
- Assumptions

The goal of this research is to conduct a life cycle assessment (LCA) of a perovskite/silicon solar cell tandems, developed by Helmholtz Zentrum Berlin (HZB) within the research project of PEROSEED. The environmental impacts GWP (midpoint indicator), EPBT, human toxicity, freshwater eutrophication and eco-toxicity as well as the energy use throughout their entire life cycle will be investigated. Moreover, this study aims to perform a comparison of the environmental impacts between this perovskite/Si tandem and established solar cell technologies which are readily available on the market. This study is funded by the Helmholtz Association of German Research Centres and is supervised by the German Aerospace Center - Institute of Networked Energy Systems.

A cradle-to-gate LCA of the perovskite/Si tandem, that includes the raw material acquisition, material processing and manufacturing of the modules, will be used to compare with modules of other photovoltaic technologies. Subsequently, another cradle-to-grave analysis which includes further phases of the life cycle, such as use phase and end-of-life phase will be carried out to analyse the impacts throughout the complete life cycle.

Furthermore, a sensitivity analysis with the operational lifetime, conversion efficiency and location of production as a basis and uncertainty analysis will be conducted for all uncertain parameters.

The goal and scope of this LCA can be further specified by the following points:

- **Product System to be Studied**

  This study comprises all the materials used over the 5 years lifetime of perovskite/Si tandem solar cells, including components that would be required to produce a complete module in case of practical use. *Figure 14* shows the prime focus of the studied system, which is the perovskite/Si tandem solar cell itself.

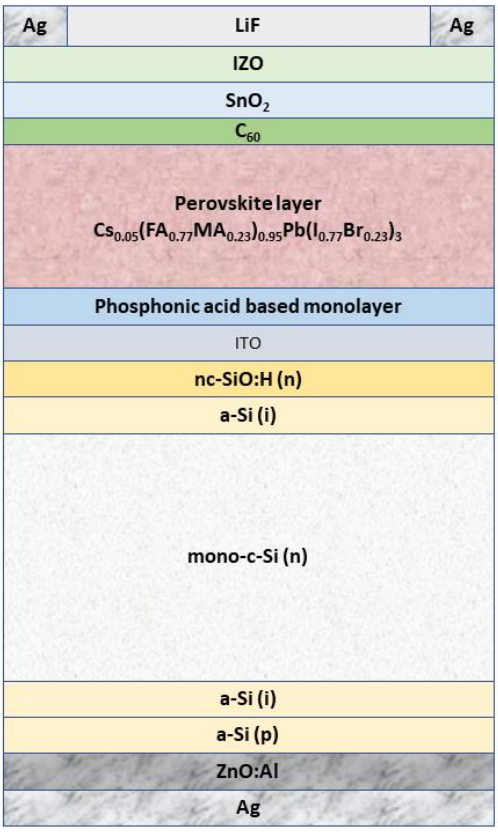

Figure: 14 Investigated Perovskite/Si Tandem Solar Cell. (Köhnen, Jošt et al. 2019)

- **Functional Unit (FU)**

The impacts produced by a FU of 1m^2 surface area of the tandem are analysed, as area units provide simplicity regarding the manufacturing of modules. However, the recommended FU for LCA regarding photovoltaic electricity is kWh which makes comparison with other energy generating technology possible (Raugei, Frischknecht et al. 2016). Therefore, within this study the impacts for generation of 1 kWh of electricity by the developed perovskite/Si solar cell tandem are also analysed.

- **System Boundary**

The system boundary for this study includes the production and manufacturing stage, the use phase and the end-of-life phase of the perovskite/Si tandem module (*Figure 15*). For the sake of having a more systemic view, elements belonging to complete modules such as encapsulation, connections and frames and that to the balance of system (BOS) such as inverters, cabling and supporting structure, are included in this analysis. On the other hand, the geographical system boundary is limited to the European Union, particularly Germany. This means that all the products and background systems required for manufacture are selected whenever possible with origin in Germany or the European Union. For the calculation of impacts, the electricity and energy matrices used are of the EU/Germany as well.

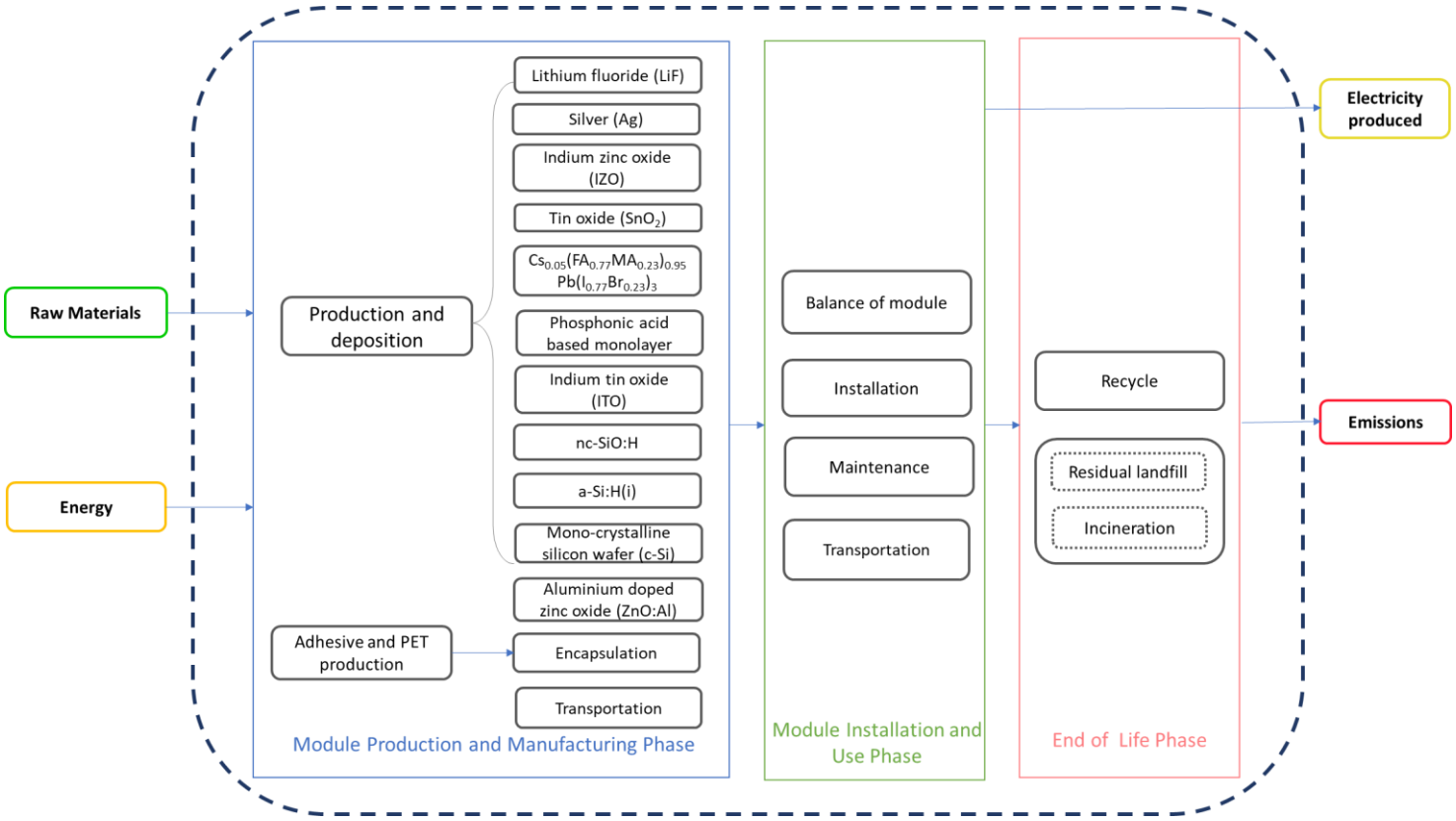

Figure: 15 System boundary. Own Figure.

- **Allocation Procedures**

Allocations are made on a mass basis. The allocation cut off approach is used, where the primary production of materials is always allocated to the primary user of a material. In this case, when recycling is introduced, producers of wastes do not receive any credit for recycling or re-use of products resulting from any waste treatment but the recyclable materials are available burden-free to recycling processes.

- **Impact Assessment Methodology**

The ReCiPe 2016, V1.1 impact assessment method is utilized for this comprehensive assessment as it provides multiple choices and better reflect current policies and values which allow actors to look at environmental impact with regards to different ideological perspectives (Andersson and Listén 2014). This assessment method contains both midpoint and endpoint characterisation (Huijbregts, Steinmann et al. 2016), however, only the former is employed in this work. The selected environmental impact categories are listed in *table* 4. In addition, the cumulative energy demand method included in Brightway2 is used to perform the calculations, both in cradle-to-gate and cradle-to-grave analysis.

Table 4 List of environmental impacts considered for this LCA. Own table.

Impact Category	Unit
Ecotoxicity, Freshwater	1,4-DCB eq.
Ecotoxicity, Marine	1,4-DCB eq.
Ecotoxicity, Terrestrial	1,4-DCB eq.
Fossil Resource Scarcity	kg oil-eq/unit of resource
Freshwater Eutrophication	kg P-eq. /kg
Global Warming, 100 year timescale	kg CO2eq/ kg GHG
Ionizing Radiation	kBq Co-60 to air eq/kBq
Land Occupation	m2·annual crop eq.
Land Transformation	m2·annual crop eq.
Marine Eutrophication	kg N-eq. /kg
Mineral Resource Scarcity	kg Cu-eq/kg ore
Ozone Formation, Damage to Ecosystems	kg NOx-eq/kg
Ozone Formation, Damage to Humans	kg NOx-eq/kg
Particulate Matter Formation	kg PM2.5-eq/kg
Stratospheric Ozone Depletion, 100 year t.	kg CFC11-eq/ kg ODS
Terrestrial Acidification	kg SO2-eq/kg
Toxicity, Carcinogenic	1,4-DCB eq.
Toxicity, Non-carcinogenic	1,4-DCB eq.
Water Consumption	m3-eq

- **Assumptions**

The weight of the tandem panels is assumed to be 15.6 kg/m^2, including the encapsulation, frame, glass and other elements of the module (2017). The module

materials include ethyl vinyl acetate (EVA), aluminium frame, polymer back-sheet, cover glass, tabbing and solder (Lunardi 2019).

While the efficiency of the investigated tandem is known to be 29.15%, the performance ratio (PR) and degradation rate is assumed to be 0.75 and 0.7 %/year, respectively. The PR is a value that represents the degree of use of a PV system, specifying the effect of losses on the PV system's rated output due to array temperature, incomplete utilisation of the irradiation, and system component inefficiencies or failures. Besides, due to stability challenges, a lifetime of 5 year is selected which is later extended to 20 years during the sensitivity analysis. Additionally, the grid conversion efficiency is considered 31.5% for the calculation of the Energy Payback Time. Furthermore, this LCA assumes an insolation of 1,700 kWh/m^2/year which is typical of southern European countries and representative of a world average in LCA studies of renewable energy. In addition to that, an insolation of 1,117 kWh/m^2/year, the average conditions in the city of Freiburg im Breisgau in Baden-Württemberg, Germany, is also analysed but spectral and temperatures are neglected in the calculations. These parameters are used in *equation* 1 of the following equations.

$$\boldsymbol{\varepsilon}_{lifetime} = \sum_{i=1}^{Lifetime} I \times \eta \times PR \times (1 - DR)^{i-1} \qquad (eq.\ 1)$$

$$Impact\ Category\ \left(\frac{Unit}{kWh}\right) = \frac{Impact\ Category\ (\frac{Unit}{m^2})}{\boldsymbol{\varepsilon}\ (\frac{kWh}{m^2})} \qquad (eq.\ 2)$$

Equations 1 and 2 are adopted from the studies of Celik et al. (Celik, Phillips et al. 2017). The former is used to calculate the energy generated over the lifetime, while the latter calculated the value of the impact category per kWh of electricity produced by the system. Although primary calculations are performed on an area basis for convenience, they are later converted into impacts per kWh of electricity output by using the *equation* 2. Denotations used in *equation* 1 signify the following;-

ε = electricity generated
η= efficiency
I= insolation
y= lifetime (years)
PR= performance ratio
DR= degradation rate
I= year after installation

4.3 Life Cycle Inventory (LCI)

This step is designated for compilation and quantification of inputs and outputs (inventory) from primary and secondary sources for the investigated system. Input data can include energy, components, materials, services, waste for treatment and natural resources. On the other hand, output data include products, waste for treatment, emissions and residuals. Beside data collection, this phase also includes calculation procedure, allocation and recycling. However, the LCI may lead to the revision of goal and scope later due to limitations or expansion of the LCA.

The software Brightway2 (Mutel 2017) is used to develop the inventory and carry out this life cycle assessment. This python based, open source and developing software does not try to replace softwares like SimaPro or OpenLCA, but instead offers possibilities of developing codes for flexible execution of LCA to researchers willing to break the limits of conventional LCA tools. On the other hand, the ecoinvent 3.6 (cut-off system model) is used as background data to perform the analysis (Wernet, Bauer et al. 2016).

The life cycle processes included in the inventory of the two terminal, monolithic, single-heterojunction perovskite/Si tandem solar cells complements the processes described in *Chapter 2.* The energy required for the manufacturing process of each layer was estimated employing the data from literature and the thickness, and hence the amount of material, employed in each layer. Overall, the inventory for this study is developed from information collected directly from researchers involved with project of PEROSEED and scientific papers of other practitioners, a summary of which is presented in Table A 1- A 42 in the annex.

The following sections present the specifications and a few considerations for the different layers of the cell modelled in this study. All inputs and outputs refer to the FU of 1 m^2.

Inventory for Perovskite Top Cell Manufacturing

The fabrication of perovskite/Si tandem is an additive process, where each layer is subsequently deposited on top of the previous one. In order to model the inventory for the top most layer, the anti-reflection coating, data from the study conducted by Gomez Trillos 2018 is considered a benchmark. Gomez Trillos modelled for a layer thickness of 150 nm and considered the deposition efficiency of the thermal evaporation process to be 15% (Gomez Trillos 2018), all else being equal, the data is modified for 100 nm. The inventory for silver deposition, as the top metal contact layer, by thermal evaporation is modified for 200 nm thickness. This layer is also modelled after the same author and the same deposition efficiency is considered when calculating the mass of silver requirement for the investigated tandem.

The inventory for the following transparent conductive oxide (TCO) layer, indium zinc oxide, is modelled modifying the ecoinvent processes. In order to produce the IZO targets, 89.2 wt.% In_2O_3 and 10.7 wt.% ZnO are used (Ito, Sato et al. 2006). The sputtering target production inventory for indium tin oxide (ITO), available in ecoinvent 3.6 database, was modified by replacing ITO with IZO to model the sputtering target for IZO. This database also considered 15% sputtering utilization rate. Furthermore, the energy consumption and material use by TCO sputtering processes are modelled as described by Louwen et al. (Louwen, Van Sark et al. 2015). While Louwen et al. calculated for 80 nm layer thickness, this study has adjusted the inventory for 100 nm. In case of SnO_2, the buffer layer, the ALD process is also modelled as shown by Louwen et al. but modified for 20 nm. Tetrakis(Dimethylamino)tin(IV) used as deposition solvent is not included in the calculations due to insufficient data. Instead, tin dioxide was included in the inventory as a proxy for this compound.

The inventory for the fullerene derivative C60 of the final layer of the top cell, the electron transport layer, is modelled after García-Valverde et al. but modified for 18 nm of thickness (García-Valverde, Cherni et al. 2010).

While building the inventory for the hole transport layer, no data for the phosphonic acid is found in the database. Consequently, the oxyacid phosphoric acid (H_3PO_4) is used instead of the dihydroxy form phosphonic acid. Ethanol is used as the deposition solvent and only a few watts of power are consumed in this process, as per the project partners.

Although, a perovskite layer with formula $Cs_{0.05}(FA_{0.77}MA_{0.23})_{0.95}Pb(I_{0.77}Br_{0.23})_3$ is used for the investigated tandem, the scarce element caesium is excluded from the analysis because of its unavailability in the database. Zang et al. indicates that both lithium and cesium have similar extraction and production processes (Zhang, Gao et al. 2017) and, therefore, a similar environmental impact profile. To account for the impact caused by the inclusion of this Cesium, Lithium was used as a proxy of the element instead (Table A 1). Gomez Trillos used an absorbing perovskite layer with formula $FA_{0.85}MA_{0.15}PbI_3$ which is also 500 nm in thickness. The inventory for this layer is developed from the studies of Espinosa et al., Gong et al., Gomez Trillos and Zang et al. (Espinosa, Serrano-Luján et al. 2015, Gong, Darling et al. 2015, Zhang, Gao et al. 2017, Gomez Trillos 2018). Energy consumption considered for spin-coating of this layer is an approximate provided by the project partners.

Inventory for Silicon Bottom Cell Manufacturing

The inventory of the recombination layer is built by modifying the ecoinvent data of sputtering indium tin oxide for 20 nm thickness. Additionally, water and electricity are added to the inventory as shown by Louwen et al. for radio frequency sputtering process (Louwen, Van Sark et al. 2015).

The following layer, which is the silicon layer, is a combination of multiple sub-layers. As initial material, $1m^2$ of FZ mono-crystalline silicon wafer is used in the investigated tandem. Nevertheless CZ mono-crystalline silicon is considered for this study as the process data for modelling FZ wafers are unavailable. The inventory is modified from the ecoinvent database 3.6 for 260 µm of wafer thickness and the kerf loss is considered to be 180 µm. Furthermore, the cells are assumed to be treated and textured according to the inventories provided by Louwen et al. but the waste water produced is not taken into account. This is due to the fact that waste water is absent in the Brightway2 biosphere.

After this treatment, the silicon wafer is sandwiched between two 5nm sub-layers of a-Si:H(i). The inventory for this PECVD process is adopted and adjusted from Louwen et al. as it is modelled for 300nm thickness. The inventory for the a-Si:H(p+) sub-layer is assumed similar to the a-Si:H(i). Due to the use of nitrogen trifluoride and silane, gas abatement is also included in this study and modelled after Louwen et al. The inventory of the final sub-layer of the silicon layer, 95 nm of hydrogenated nanocrystalline silicon oxide (nc-SiO_x:H(n)), is also similar to the a-Si:H(i). In contrast, silane (SiH4) is included with an addition of process gasses like 2% phosphine (PH3) as dopant source, carbon dioxide (CO2) and hydrogen (H2) (Lambertz, Grundler et al. 2011).

Finally, the inventories of both the metal contact are adopted from Louwen et al. Since the ZnO layer considered in this study is doped with aluminium, 3 wt.% of Al is additionally considered in the inventory (Wang, Li et al. 2011). The sputtering utilization rate for both the layers is considered 74% while modifying the inventory for 140 nm ZnO:Al and 400nm Ag. However, the inventories related to the materials used are limited and, in many cases, not included in background data provided by databases such as Ecoinvent.

Inventory for PV Panel Manufacturing

The inventory of PV panel manufacturing used in this study includes encapsulation and module elements present in the database Ecoinvent 3.6, modifying the inventory by replacing the silicon cells for the perovskite/Si tandem cells. The unit process and exchange data of this step are adopted from the photovoltaic laminate and panel production in Europe developed by Frischknecht et al. (Frischknecht, Itten et al. 2015). This also includes transportation of the tandem modules to the market.

Inventory for Module Installation and Use

To install the manufactured panel, the balance of system (BOS) is required. In addition to the photovoltaic modules, elements used in the inventory of the BOS included inverter, transformer, wiring and mounting structures used in PV installations (Jean, Brown et al. 2015). While an inverter of 2.5 kW, considered according to the peak power per square meter per module, is available in Ecoinvent 3.6, electric installations are available only for 3kWp plants at buildings. Among the four installations considered, the energy necessary to build the structures for open ground, flat-roof and slanted-roof installations are modelled after Gomez Trillos, while that of the facade installation is assumed based on interpolation. Transportation of the BOS from the market to the site was modeled after Jungbluth et al. (Jungbluth, Stucki et al. 2012).

During the use phase, PV modules do not consume a significant amount of materials or energy; therefore, only an approximation of the materials required for their maintenance during the operation is considered during this phase. According to the inventories of Jungbluth & Stucki, 20 litres of tap water per year is considered for cleaning the surface of the modules (Jungbluth, Stucki et al. 2012). Furthermore, three leakage scenarios are assessed as studied by Gomez Trillos, even though LCA is an inappropriate methodology to assess the effects on a small scale. While in the first scenario no leakage is accounted for, the second scenario included the loss of lead and iodine to the ground, and both elements are lost to the water in the third scenario.

Inventory for Module End of Life

As there are no current standard methods for recycling of PV tandem modules, the inventories of different scenarios of this phase are developed based on one factor-availability of data. This factor shaped the scope of the end of life of the module into two scenarios: 1. Recycling and 2. Combination of residual landfill and incineration.

Although there are some inventories available for waste silicon panels, inventories for perovskite/Si tandem waste are unavailable. Therefore, EoL inventories are built only for the silicon bottom cell. Afterall, the perovskite/Si tandem panel comprises an overall similar material composition, as silicon-only panels, with glass and aluminium dominating by weight (Kadro and Hagfeldt 2017).

The inventory of the recycling process developed by Latunussa et al. is considered as a benchmark for modelling this step (Latunussa, Ardente et al. 2016). Besides treatment of c-Si PV modules, the calculations included laminated glass, metals or electric and electronic waste from internal wires. Although the average weight of c-Si PV modules considered by Stolz et el is 13.2 kg/m^2 (Stolz, Frischknecht et al. 2016), 15.6 kg/m^2 is considered a more appropriate assumption of weight of the investigated tandem. This FU does not include PV plant components such as inverters or external cables. Moreover, the materials used in the mounting system and the electric installations are not included in the bill of materials along

with the losses due to breakage or cutting. Additionally, the recovery of glass cullets and Al and Cu scrap used in the analysis are modeled from the study by Stolz & Frischknecht. Finally, inventories for both the scenarios, residual landfill and incineration, are modelled from the study performerd by Rashedi & Khanam (Rashedi and Khanam 2020). For these two scenarios in this study, it is assumed that 91% of the 1 m^2 mono-Si PV waste goes to landfill, while approximately 9% is incinerated.

4.4 Life Cycle Impact Assessment (LCIA)

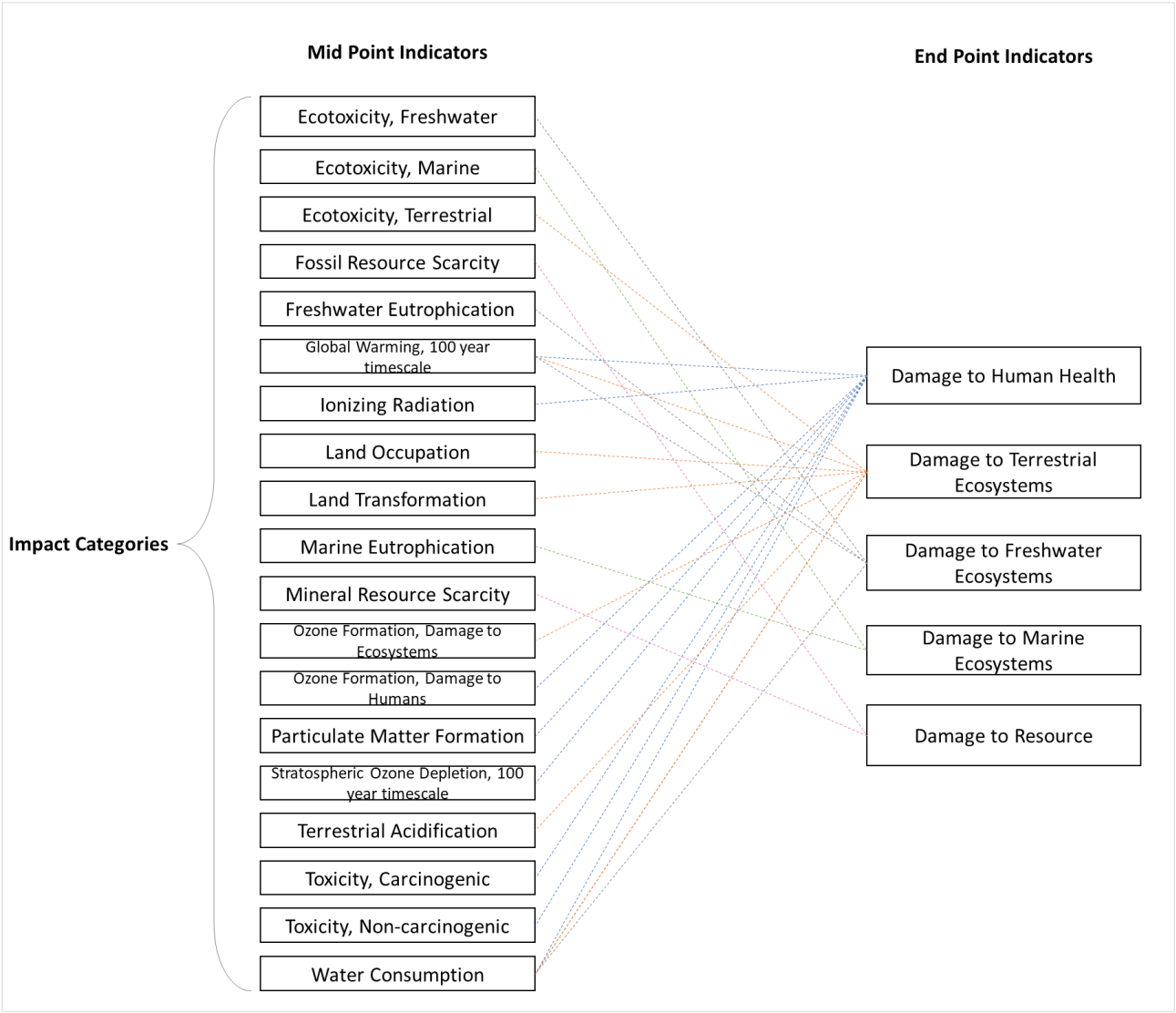

Figure: 16 Selected impact categories in ReCiPe 2016 V1.1 method. (Huijbregts, Steinmann et al. 2016).

Within this step of the LCA the potential environmental impacts of input and output flows are evaluated (e.g., global warming potential, eco-toxicity, ozone depletion and energy payback time) (Zendehdel, Nia et al. 2020). It is accomplished by converting the emissions and resource extraction into a limited number of impact categories by means of

characterization factors, known as methods. Such impacts are defined as a negative effect on human health, natural environment or natural resources by a product or process during its lifecycle. These impact categories are the classes that represent the potential environmental issues of concern and its selection is defined according to the goal and scope. Although an LCA may include optional elements, such as normalization, grouping and weighting, they are not a part of the scope of this LCA study.

The two mainstream ways of approaching characterization factors are midpoint-oriented and endpoint-oriented (Figure 16). Among the two, the midpoint-oriented characterization has a stronger relation to the environmental flows and a relatively low uncertainty as it relies primarily on scientific information and well-proven facts (Huijbregts, Steinmann et al. 2016). On the other hand, the endpoint-oriented indicators are broader and are related to the endpoint impacts (damage to human health, ecosystems and resource availability). While endpoints have the advantage of presenting information more clearly to non-LCA practitioners on the environmental relevance of the environmental flows, they also have a bigger uncertainty. Therefore, the midpoint-oriented approach is considered in this study. *Figure* 16 provides a list of the midpoint indicators taken into account for this study. The LCIA of the investigated model obtained from Brightway2 are shown in *Table* A 43, 44, 45 and 46, of which Table A 43 depicts that 293.84 kg CO2eq/ kg GHG are produced per square meter only during the cradle-to-gate stage. For the cradle-to-grave assessment, the impacts and CED from later life stages are added to that of the cradle-to-gate to obtain the impacts over the lifecycle. *Table* A 45 further describes that a cradle-to-grave produces an additional ˜115 kg CO2eq/ kg GHG on average, making a total of aprox. 409 kg CO2eq/ kg GHG emissions per square meter of the investigated tandem.

The result obtained by means of the *equation* 3, which is adopted from the study of Frischknecht et al. to calculate the energy pay back time (EPBT) (Frischknecht, Itten et al. 2015) are summarised in *table* A 46. EPBT can be defined as the period required by a renewable energy system to generate the amount of energy required in the different life cycle stages of the product.

$$EPBT = \frac{Emat + Emanuf + Etrans + Einst + EEOL}{(\frac{Eagen}{\eta G}) - Eaoper} \qquad (eq.\ 3)$$

$$EROI = \frac{Lifetime}{EPBT} \qquad (eq.\ 4)$$

Denotations used in this equation signify-

$Emat=$ primary energy demand to produce materials comprising the PV system

$Emanuf=$ primary energy to manufacture the PV system
$Etrans=$ primary energy to transport materials used during the life cycle
$Einst=$ primary energy used during the install of the system
$EEOL=$ primary energy demand for the end-of-life management
$Eagen=$ annual electricity generation
$Eaoper=$ annual energy demand for operation and maintenance in primary energy terms (not considered in this study)
$\eta G=$ conversion factor from primary energy to electricity, 31.5% for germany (Wernet, Bauer et al. 2016)

Additionally, Celik et al. derived the indicator energy return on investment (EROI) from EPBT and energy generated over the lifetime (Celik, Phillips et al. 2017). This indicator is also adopted in this study as it calculates how much energy can be obtained when an amount of energy is invested in a certain conversion technology.

4.5 Interpretation

This final step shows the LCI and LCIA results, analyses the critical points for future improvements. To check if the assumptions, methods and data are in harmony with the previously stated goal and scope, the evaluation may consider completeness check, sensitivity check, consistency checks and other checks (Protocol 2012).

Results of the cradle-to-gate and cradle-to-grave analysis for both the environmental impact categories and the cumulative energy demand per kWh are presented in the following part of this chapter. Thereafter, the result is interpreted in terms of EPBT and EROI. A layer-wise and subsequently, a lifecycle stage-wise breakdown of the environmental impacts are included where the respective share of different impacts can be seen. Finally, the sensitivity analysis and the uncertainty analysis can be found in the latter part of this chapter.

4.5.1 Impacts of Perovskite/Si Tandem Solar Panel

The *equation* 1 revealed that for average conditions of Europe (1,700 kWh/m^2/year) and Freiburg, the city in southern Germany (1,117 kWh/m^2/year), the energy generated over lifetime of 5 years are 1,870 kWh/m^2 and 1,205 kWh/m^2 respectively. The panel efficiency assumed in all cases is 29.15%. Subsequently, *equation* 2 showed that while 0.157 and 0.244 kg CO2eq/ kg GHG are produced per kWh of output during the cradle-to-gate analysis, 0.217 and 0.337 kg CO2eq/ kg GHG are produced in the cradle-to-grave for Europe and Freiburg respectively. The average of the four installations and that of the two EoL scenarios are considered to derive the average cradle-to-grave impacts and CED (*Table* 6 and 7). Other impacts per kWh of output for the investigated tandem are listed in following *Table* 5 and 6.

Table 5 Impacts per kWh energy output from cradle-to-gate lifecycle of perovskite/Si tandem solar panel. Own table.

Impact Category Unit per kWh	Perovskite/Si Tandem Solar Panel	
	Cradle-to-Gate Europe (1,700 kWh/m²)	Cradle-to-Gate Freiburg (1,117 kWh/m²)
Ecotoxicity, Freshwater 1,4-DCB eq.	8.8×10^{-05}	1.4×10^{-04}
Ecotoxicity, Marine 1,4-DCB eq.	7.9×10^{-04}	1.2×10^{-03}
Ecotoxicity, Terrestrial 1,4-DCB eq.	4.2×10^{-03}	6.5×10^{-03}
Fossil Resource Scarcity kg oil-eq/unit of resource	4.3×10^{-02}	6.7×10^{-02}
Freshwater Eutrophication kg P-eq. /kg	1×10^{-05}	1.6×10^{-05}
Global Warming, 100 year timescale kg CO2eq/ kg GHG	1.6×10^{-01}	2.4×10^{-01}
Ionizing Radiation kBq Co-60 to air eq/kBq	1.6×10^{-02}	2.6×10^{-02}
Land Occupation m2·annual crop eq.	4.5×10^{-03}	7×10^{-03}
Land Transformation m2·annual crop eq.	4.26×10^{-05}	6.8×10^{-05}
Marine Eutrophication kg N-eq. /kg	4.4×10^{-06}	6.8×10^{-06}
Mineral Resource Scarcity kg Cu-eq/kg ore	1.4×10^{-03}	2.1×10^{-03}
Ozone Formation, Damage to Ecosystems kg NOx-eq/kg	3.5×10^{-04}	5.4×10^{-04}
Ozone Formation, Damage to Humans **kg NOx-eq/kg**	3.4×10^{-04}	5.3×10^{-04}
Particulate Matter Formation kg PM2.5-eq/kg	2.9×10^{-04}	4.5×10^{-04}
Stratospheric Ozone Depletion, 100 year t. kg CFC11-eq/ kg ODS	5.4×10^{-04}	8.5×10^{-04}
Terrestrial Acidification kg SO2-eq/kg	1.5×10^{-03}	2.3×10^{-03}
Toxicity, Carcinogenic 1,4-DCB eq.	1.1×10^{-02}	1.7×10^{-02}
Toxicity, Non-carcinogenic 1,4-DCB eq.	6.6×10^{-03}	1×10^{-02}
Water Consumption m3-eq	6.6×10^{-03}	1×10^{-02}

Impact Categories Unit per kWh	Gate-to-Grave (Europe/Freiburg)							Cradle-to-Grave Average (Europe/Freiburg)
	Installation and Supporting Structure				Use	End of Life		
	Open Ground Module	Flat-Roof	Facade	Slanted-Roof		Scenario 1	Scenario 2	
Ecotoxicity, Freshwater 1,4-DCB eq.	1.58×10^{-04} / 2.46×10^{-04}	1.2×10^{-04} / 1.86×10^{-04}	1.24×10^{-04} / 1.9×10^{-04}	1.25×10^{-04} / 1.9×10^{-04}	4.82×10^{-09} / 7.49×10^{-09}	9.07×10^{-07} / 1.4×10^{-06}	4.14×10^{-06} / 6.43×10^{-06}	2.2×10^{-04} / 3.5×10^{-04}
Ecotoxicity, Marine 1,4-DCB eq.	4.6×10^{-04} / 7.15×10^{-04}	4×10^{-04} / 6.2×10^{-04}	4.07×10^{-04} / 6.3×10^{-04}	4.08×10^{-04} / 6.34×10^{-04}	8.31×10^{-09} / 1.29×10^{-08}	2.24×10^{-06} / 3.48×10^{-06}	6.51×10^{-06} / 1×10^{-05}	1.2×10^{-03} / 1.8×10^{-03}
Ecotoxicity, Terrestrial 1,4-DCB eq.	2.88×10^{-02} / 2.47×10^{-02}	2.7×10^{-02} / 4.26×10^{-02}	2.77×10^{-02} / 4.3×10^{-02}	2.76×10^{-02} / 4.29×10^{-02}	7.8×10^{-08} / 1.22×10^{-07}	3.56×10^{-05} / 5.54×10^{-05}	4.2×10^{-05} / 6.5×10^{-05}	3.2×10^{-02} / 4.9×10^{-02}
Fossil Resource Sc. kg oil-eq/unit of res.	1.48×10^{-02} / 2.29×10^{-02}	1.14×10^{-02} / 1.8×10^{-02}	1.03×10^{-02} / 1.6×10^{-02}	1.06×10^{-02} / 1.65×10^{-02}	9.65×10^{-07} / 1.5×10^{-06}	9.5×10^{-04} / 1.47×10^{-03}	2.53×10^{-04} / 3.9×10^{-04}	5.5×10^{-02} / 8.6×10^{-02}
Freshwater Eutr. kg P-eq. /kg	7.44×10^{-06} / 1.15×10^{-05}	6.5×10^{-06} / 1×10^{-05}	6.59×10^{-06} / 1.02×10^{-05}	6.62×10^{-06} / 1.03×10^{-05}	2.93×10^{-10} / 4.56×10^{-10}	1.12×10^{-07} / 1.72×10^{-07}	2.9×10^{-08} / 4.5×10^{-08}	1.7×10^{-05} / 2.7×10^{-05}
Global Warming kg CO2eq/ kg GHG	6.2×10^{-02} / 9.6×10^{-02}	4.3×10^{-02} / 6.74×10^{-02}	4.2×10^{-02} / 6.6×10^{-02}	4.4×10^{-02} / 6.84×10^{-02}	3.66×10^{-06} / 5.69×10^{-06}	3.1×10^{-03} / 4.8×10^{-03}	2×10^{-02} / 3.2×10^{-02}	2.17×10^{-01} / 3.37×10^{-01}
Ionizing Radiation kBq Co-60 to air eq/kBq	2.87×10^{-03} / 4.46×10^{-03}	2.1×10^{-03} / 3.3×10^{-03}	2.1×10^{-03} / 3.3×10^{-03}	2.21×10^{-03} / 3.44×10^{-03}	1.65×10^{-06} / 1.8×10^{-06}	2.3×10^{-04} / 3.5×10^{-04}	4×10^{-05} / 6.24×10^{-05}	1.9×10^{-02} / 2.9×10^{-02}
Land Occupation m2·annual crop eq.	5.6×10^{-02} / 8.8×10^{-02}	1.25×10^{-03} / 1.94×10^{-03}	1.28×10^{-03} / 1.99×10^{-03}	1.31×10^{-03} / 2.04×10^{-03}	1.19×10^{-07} / 1.85×10^{-07}	2.4×10^{-04} / 3.7×10^{-04}	5.34×10^{-05} / 8.3×10^{-05}	2×10^{-02} / 3×10^{-02}
Land Transformation m2·annual crop eq.	1.56×10^{-05} / 2.42×10^{-05}	7.75×10^{-06} / 1.27×10^{-05}	9×10^{-06} / 1.4×10^{-07}	8.16×10^{-06} / 1.27×10^{-05}	7.63×10^{-10} / 1.18×10^{-09}	1×10^{-06} / 1.56×10^{-06}	1.12×10^{-07} / 1.73×10^{-07}	5.4×10^{-05} / 8.4×10^{-05}
Marine Eutrophication kg N-eq. /kg	8.2×10^{-07} / 1.27×10^{-06}	5.65×10^{-07} / 8.77×10^{-07}	6.17×10^{-07} / 9.58×10^{-07}	6.11×10^{-07} / 9.5×10^{-07}	3.76×10^{-11} / 5.84×10^{-11}	8.14×10^{-09} / 1.26×10^{-08}	1.17×10^{-07} / 1.8×10^{-07}	5.1×10^{-06} / 7.9×10^{-06}
Mineral Resource Sc. kg Cu-eq/kg ore	3.2×10^{-03} / 4.9×10^{-03}	1.91×10^{-03} / 3×10^{-03}	2×10^{-03} / 3.11×10^{-03}	2×10^{-03} / 3.12×10^{-03}	4.9×10^{-08} / 7.6×10^{-08}	8.79×10^{-06} / 1.36×10^{-05}	7.8×10^{-06} / 1.2×10^{-05}	3.6×10^{-03} / 5.7×10^{-03}

Impact Categories Unit per kWh	Gate-to-Grave (Europe/Freiburg)							Cradle-to-Grave Average (Europe/Freiburg)
	Installation and Supporting Structure				Use	End of Life		
	Open Ground Module	Flat-Roof	Facade	Slanted-Roof		Scenario 1	Scenario 2	
Ozone Formation, E. kg NOx-eq/kg	2.23×10^{-04} / 3.47×10^{-04}	1.66×10^{-04} / 2.58×10^{-04}	1.67×10^{-04} / 2.6×10^{-04}	1.7×10^{-04} / 2.65×10^{-04}	9×10^{-09} / 1.4×10^{-08}	2.6×10^{-05} / 4×10^{-05}	5.83×10^{-06} / 9×10^{-06}	5.5×10^{-04} / 8.5×10^{-04}
Ozone Formation, H. kg NOx-eq/kg	2.17×10^{-04} / 3.38×10^{-04}	1.62×10^{-04} / 2.52×10^{-04}	1.63×10^{-04} / 2.53×10^{-04}	1.66×10^{-04} / 2.58×10^{-04}	8.8×10^{-09} / 1.36×10^{-08}	2.56×10^{-05} / 4×10^{-05}	5.79×10^{-06} / 8.9×10^{-06}	5.4×10^{-04} / 8.3×10^{-04}
PM Formation kg PM2.5-eq/kg	2.63×10^{-04} / 4.08×10^{-04}	2.2×10^{-04} / 3.4×10^{-04}	2.22×10^{-04} / 3.45×10^{-04}	2.25×10^{-04} / 3.5×10^{-04}	6.51×10^{-09} / 1×10^{-08}	9.25×10^{-06} / 1.43×10^{-06}	1.76×10^{-06} / 2.73×10^{-06}	5.3×10^{-04} / 8.2×10^{-04}
Strat. Ozone Dep. kg CFC11-eq/ kg ODS	3.49×10^{-08} / 5.42×10^{-08}	2.9×10^{-08} / 4.5×10^{-08}	2.92×10^{-08} / 4.54×10^{-08}	2.96×10^{-08} / 4.6×10^{-08}	1.89×10^{-12} / 2.93×10^{-12}	0/0	3×10^{-09} / 4.64×10^{-09}	5.4×10^{-04} / 8.5×10^{-04}
Terrestrial Acid. kg SO2-eq/kg	6.5×10^{-04} / 1.02×10^{-03}	5.6×10^{-04} / 8.7×10^{-04}	5.67×10^{-04} / 8.8×10^{-04}	5.7×10^{-04} / 8.9×10^{-04}	1.45×10^{-08} / 2.26×10^{-08}	1.92×10^{-05} / 3×10^{-06}	4.13×10^{-06} / 6.4×10^{-06}	2×10^{-03} / 3.2×10^{-03}
Toxicity, Carcinogenic 1,4-DCB eq.	3.4×10^{-03} / 5.3×10^{-03}	1.85×10^{-03} / 2.8×10^{-03}	2.2×10^{-03} / 3.4×10^{-03}	2.2×10^{-03} / 3.4×10^{-03}	2.76×10^{-07} / 4.28×10^{-07}	0/0	5.56×10^{-05} / 8.64×10^{-05}	1.4×10^{-02} / 2.1×10^{-02}
Toxicity, Non-carc. 1,4-DCB eq.	8.7×10^{-02} / 1.35×10^{-01}	8.52×10^{-02} / 1.32×10^{-01}	8.53×10^{-02} / 1.32×10^{-01}	8.54×10^{-02} / 1.32×10^{-01}	2.12×10^{-07} / 3.23×10^{-07}	7.7×10^{-05} / 1.2×10^{-04}	1.9×10^{-04} / 2.96×10^{-04}	9.2×10^{-02} / 1.4×10^{-01}
Water Consumption m3-eq	6.4×10^{-04} / 1×10^{-03}	4.6×10^{-04} / 7.1×10^{-04}	4.65×10^{-04} / 7.2×10^{-04}	4.7×10^{-04} / 7.33×10^{-04}	1.07×10^{-05} / 1.67×10^{-05}	1.16×10^{-05} / 1.8×10^{-05}	1.92×10^{-04} / 3×10^{-04}	7.2×10^{-03} / 1.1×10^{-02}

Table 6 Impacts per kWh energy output from cradle-to-grave lifecycle of perovskite/Si tandem solar panel. Own table.

4.5.2 Cumulative Energy Demand (CED)

Table 7 CED per kWh for thr investigated perovskite/Si tandem solar panel. Own table.

Cumulative Energy Demand MJ-eq/kWh	Cradle–to-Gate (Europe/ Freiburg)	Gate-to-Grave (Europe/Freiburg)							Cradle-to-Grave (Europe/ Freiburg)
		Installation and Supporting Structure				Use	End of Life		
		Open Ground Module	Flat-Roof	Facade	Slanted-Roof		Scenario 1	Scenario 2	
Renewable Energy Resources, Biomass	7.4×10^{-02}/ 1.25×10^{-01}	1.5×10^{-02}/ 2.4×10^{-02}	1.16×10^{-02}/ 1.8×10^{-02}	1.18×10^{-02}/ 1.84×10^{-02}	1.23×10^{-02}/ 1.92×10^{-02}	2.1×10^{-06}/ 3.2×10^{-06}	6×10^{-03}/ 9.2×10^{-03}	2.6×10^{-04}/ 4×10^{-04}	9×10^{-02}/ 1.5×10^{-01}
Non-Renewable Energy Resources, Fossil	1.97 /3.3	$6.8x\ 10^{-01}$/ 1.05	5.26×10^{-01}/ 8.17×10^{-01}	4.7×10^{-01}/ 7.36×10^{-01}	4.8×10^{-01}/ 7.6×10^{-01}	4.4×10^{-05}/ 6.8×10^{-05}	4.4×10^{-02}/ $6.8x\ 10^{-02}$	1.2×10^{-02}/ 1.8×10^{-02}	2.5 / 4.18
Renewable Energy Resources, Geothermal	3.4×10^{-03}/ 5.8×10^{-03}	5.7×10^{-04}/ 8.9×10^{-04}	4.5×10^{-04}/ 7×10^{-04}	4.6×10^{-04}/ $7.1x\ 10^{-04}$	4.6×10^{-04}/ 7.2×10^{-04}	1.5×10^{-07}/ 2.3×10^{-07}	7.8×10^{-05}/ 1.2×10^{-04}	9.8×10^{-06}/ 1.5×10^{-05}	4×10^{-03}/ 6.6×10^{-03}
Non-Renewable Energy Resources, Nuclear	3.1×10^{-01}/ 5.2×10^{-01}	5.4×10^{-02}/ $8.4x\ 10^{-02}$	4.21×10^{-02}/ 6.5×10^{-02}	4.13×10^{-02}/ 6.4×10^{-02}	4.2×10^{-02}/ 6.5×10^{-02}	2.2×10^{-05}/ $3.4x\ 10^{-05}$	4.1×10^{-03}/ 6.4×10^{-03}	6.9×10^{-04}/ 1×10^{-03}	3.6×10^{-01}/ 6×10^{-01}
Non-Renewable Energy Resources, Primary Forest	6.7×10^{-05}/ 1.13×10^{-04}	4.02×10^{-05}/ 6.25×10^{-05}	1.36×10^{-05}/ 2.11×10^{-05}	1.86×10^{-05}/ 2.9×10^{-05}	1.4×10^{-05}/ 2.2×10^{-05}	5.5×10^{-10}/ 8.6×10^{-10}	1.6×10^{-06}/ 2.5×10^{-06}	2.7×10^{-07}/ 4.3×10^{-07}	9×10^{-05}/ 1.4×10^{-04}
Renewable Energy Resources, Kinetic, Wind	4.5×10^{-02}/ 7.6×10^{-02}	4.6×10^{-03}/ 7.14×10^{-03}	3.5×10^{-03}/ 5.4×10^{-03}	3.54×10^{-03}/ 5.5×10^{-03}	3.6×10^{-03}/ 5.6×10^{-03}	2×10^{-06}/ 3.2×10^{-06}	2×10^{-04}/ 3.2×10^{-04}	6.7×10^{-05} / 1×10^{-04}	5×10^{-02}/ 8×10^{-02}
Renewable Energy Resources, Potential, Water	2.24×10^{-01}/ 4×10^{-01}	6.12×10^{-02}/ 9.5×10^{-02}	4.4×10^{-02}/ 6.8×10^{-02}	2.56×10^{-02}/ 7×10^{-02}	7.3×10^{-02}/ 4.7×10^{-02}	4.2×10^{-06}/ 6.5×10^{-06}	2×10^{-03}/ 3.1×10^{-03}	4.4×10^{-04}/ 6.8×10^{-04}	2.9×10^{-01}/ 4.7×10^{-01}
Renewable Energy Resources, Solar	9.1×10^{-04}/ 1.5×10^{-03}	3.72×10^{-05}/ 5.78×10^{-05}	1.84×10^{-05}/ 2.86×10^{-05}	1.8×10^{-05}/ 2.82×10^{-05}	1.78×10^{-05}/ $2.78x\ 10^{-05}$	1.2×10^{-09}/ 1.9×10^{-09}	2.22×10^{-06}/ 3.4×10^{-06}	2×10^{-06}/ 3.2×10^{-06}	9.3×10^{-04}/ 1.5×10^{-03}
Total	**2.64 / 4.43**	8.15×10^{-01}/ 1.266	6.3×10^{-01}/ 9.7×10^{-01}	5.77×10^{-01}/ 9×10^{-01}	6×10^{-01}/ 9.2×10^{-01}	7.5×10^{-05}/ 1.15×10^{-04}	5.6×10^{-02}/ 8.7×10^{-02}	$1.3x\ 10^{-02}$/ 2×10^{-02}	**3.34 / 5.5**
Total kWh-eq/kWh	**0.73/1.23**								**0.93/1.53**

The direct and indirect energy used throughout the life cycle, which includes the energy consumed during the production, installation, use and EoL of the raw and auxiliary materials, are represented by the cumulative energy demand (CED) (Huijbregts, Rombouts et al. 2006). Although the ISO standards on life cycle assessment (2006a) do not explicitly address nor require an energy consumption indicator (Frischknecht, Wyss et al. 2015), this study considered analysing CED to facilitate calculation of the energy payback time (EPBT). Therefore, the CED per kWh output by the investigated tandem for both cradle-to-gate and cradle-to-grave analysis are listed in *table* 7. This table showed that while 2.6 and 4.4 MJ eq. are required per kWh of output during the cradle-to-gate analysis, 3.3 and 5.5 MJ eq. are required in the cradle-to-grave for Europe and Freiburg respectively. In addition, this table also revealed that approximately 86% of this demanded energy is supplied from non-renewable sources while only 14% of the total came from renewable sources.

From the *figure* 17, it is clear that approx. 80 % share of cumulative energy is demanded by the production and manufacturing phase of the lifecycle. Although the CED is similar for all installations, only that of the open ground module was higher. Therefore, an average CED is taken into account to provide a complete view. On the other hand, the CED during the use phase is negligible, while approx. 1.6% and 0.4% are demanded during recycling and scenario 2, residual landfill and incineration, respectively.

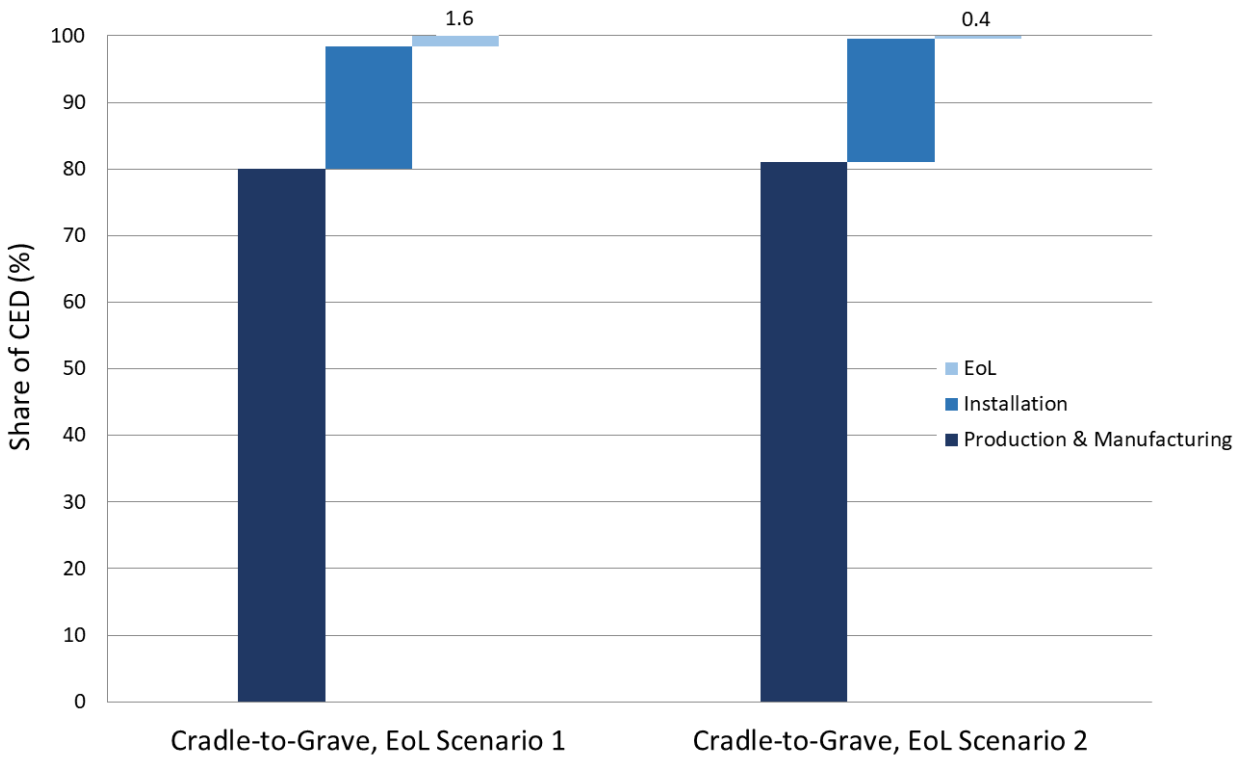

Figure: 17 Share of different lifecycle stages to CED for the perovskite/Si tandem solar panel. Own figure.

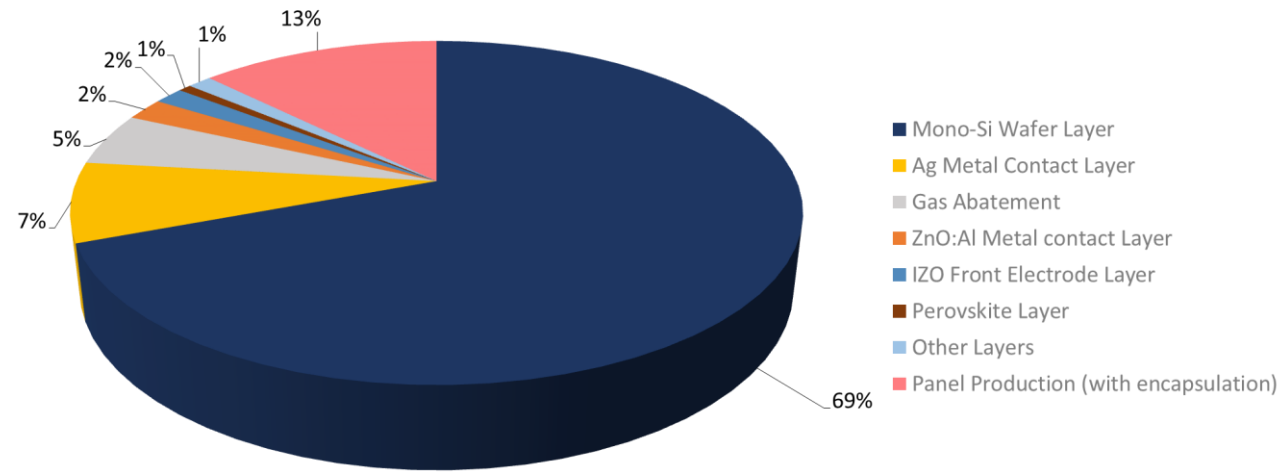

Figure: 18 Share of different components to the CED of the Perovskite/Si tandem solar panel from the cradle-to-gate analysis. Own figure.

A further look into the cradle-to-gate analysis revealed that the major share of this CED (69%) is associated with mono-Si wafer production. According to the *figure* 18 the second and third most energy demanding processes are the panel production (approx. 13%) and the metallization with silver (7%).

4.5.3 Energy Pay Back Time (EPBT) and Energy Return on Investment (EROI)

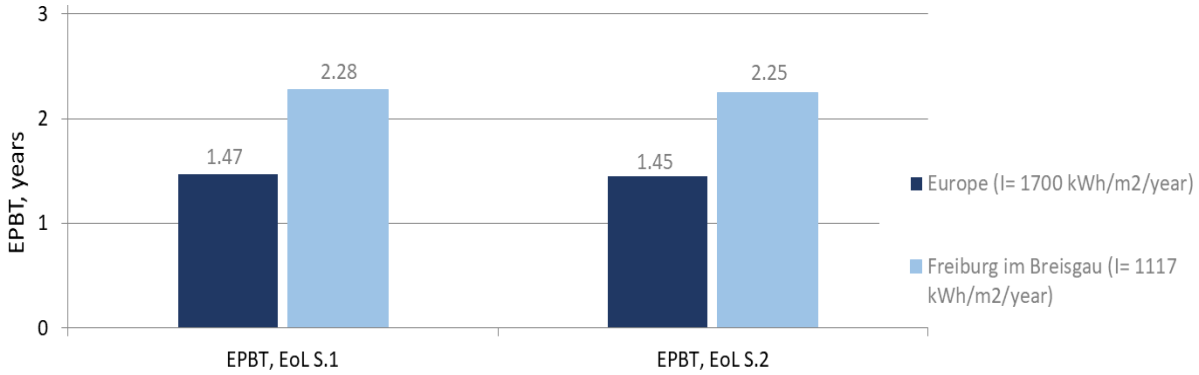

Figure: 19 EPBT for the Perovskite/Si tandem solar panel from Cradle-to-Grave analysis. Own figure.

As depicted in *figure* 19, the EPBT for the investigated tandem solar panel is 1.47 and 2.28 years for Europe and Freiburg, respectively, when recycling is considered as EoL fate. On the other hand, when residual landfill and incineration are considered the EPBT for Europe and Freiburg are consecutively 1.45 and 2.25 years. The difference between the two EoL scenarios is calculated to be approx. 8 days.

From the EPBT, the EROI for the investigated tandem solar cells are calculated to be 3.4 and 2.2 for average conditions of Europe and Freiburg, respectively. In other words, this suggested that 3.4 and 2.2 times more energy can be produced out of this system than invested in it during manufacturing, installation, operation, and EoL.

4.5.4 Layer-wise and Life Cycle Stage-Wise Breakdown of Environmental Impacts

The contributional analysis shown *figure* 20 reveals that the mono-Si wafer production held the most share of impacts among all the layers, followed by the silver metal contact layers. Moreover, the layers associated with silver showed high marine ecotoxicity and significant mineral resource scarcity. However, the panel production held the second major share of overall impacts, particularly in the categories terrestrial ecotoxicity and non-carcinogenic toxicity, when the cradle-to-gate analysis is considered. The perovskite layer, which contains small quantities of toxic Pb, represented the third largest share of terrestrial ecotoxicity.

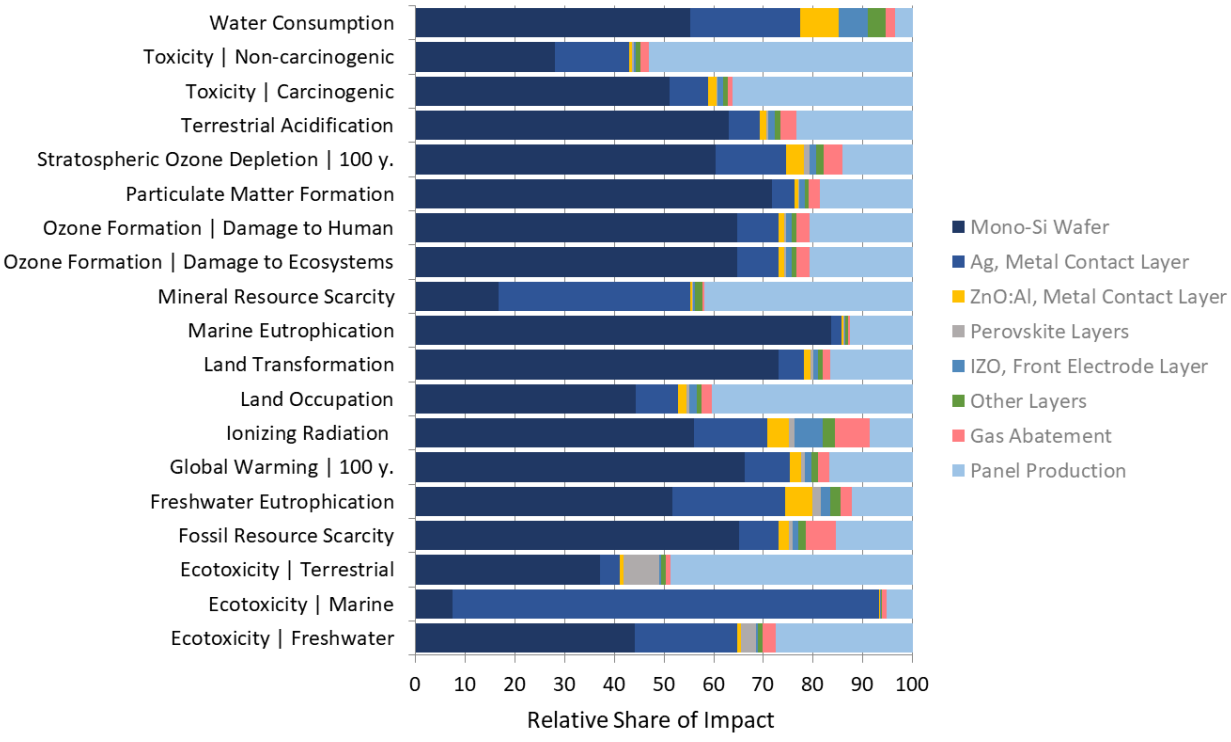

Figure: 20 Relative share of impacts from the cradle-to-gate analysis of the perovskite/Si tandem solar panel. Own figure.

The *figure* 21 showed a comparison of the relative impact in different impact categories of the four different installations. Only the categories that showed a difference of over 20% among the installations are presented in this figure. It is evident that the open ground module installation has a greater share of impacts than the other three installations, with the highest share in land occupation. The reason is that open ground installations are

typically for large, utility-scale PV power stations where PV modules are held by racks or frames that are attached to ground-based mounting supports in arrays.

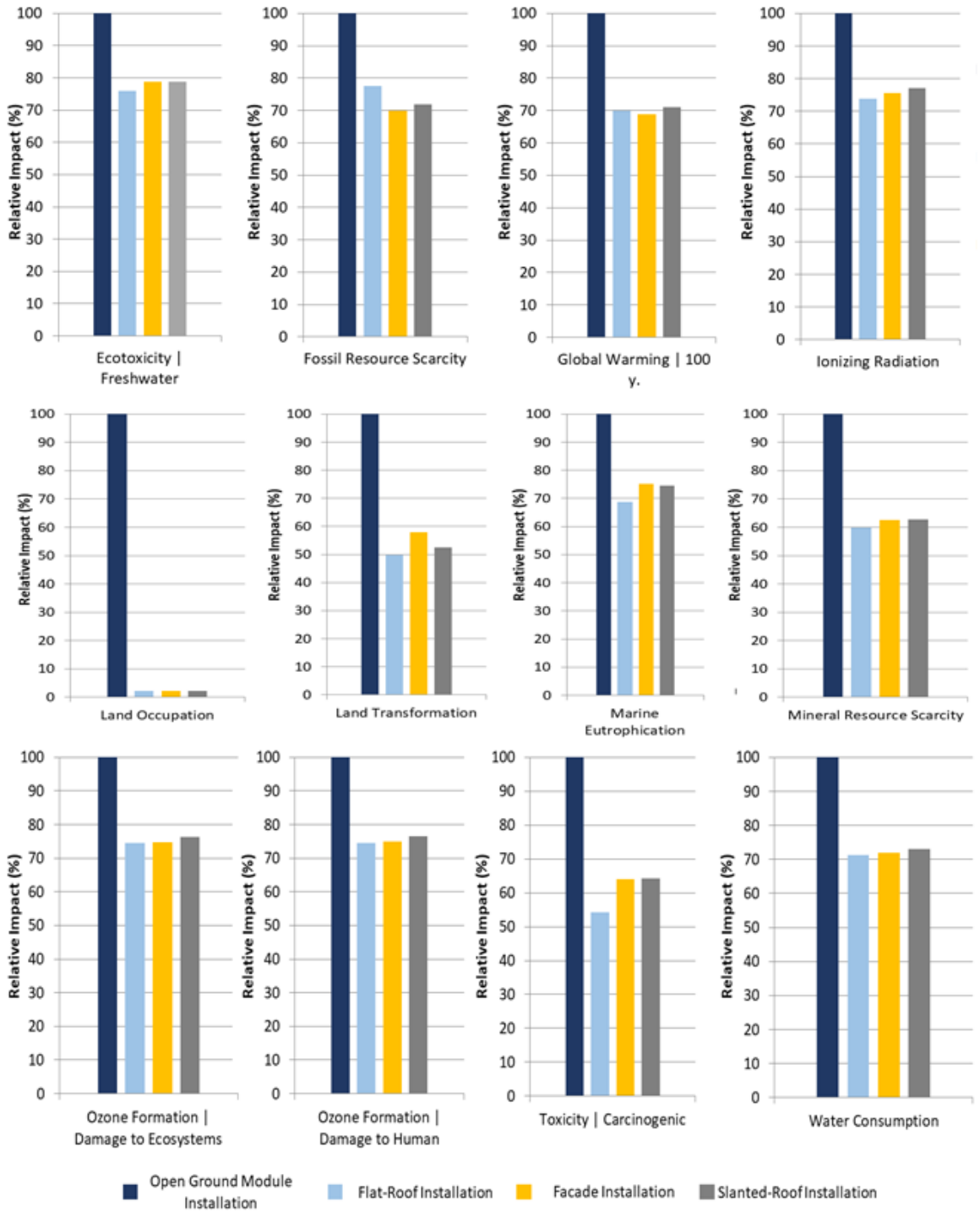

Figure: 21 Comparison between the relative impacts of different impact categories (>20% difference) of the 4 types of installations. Own figure.

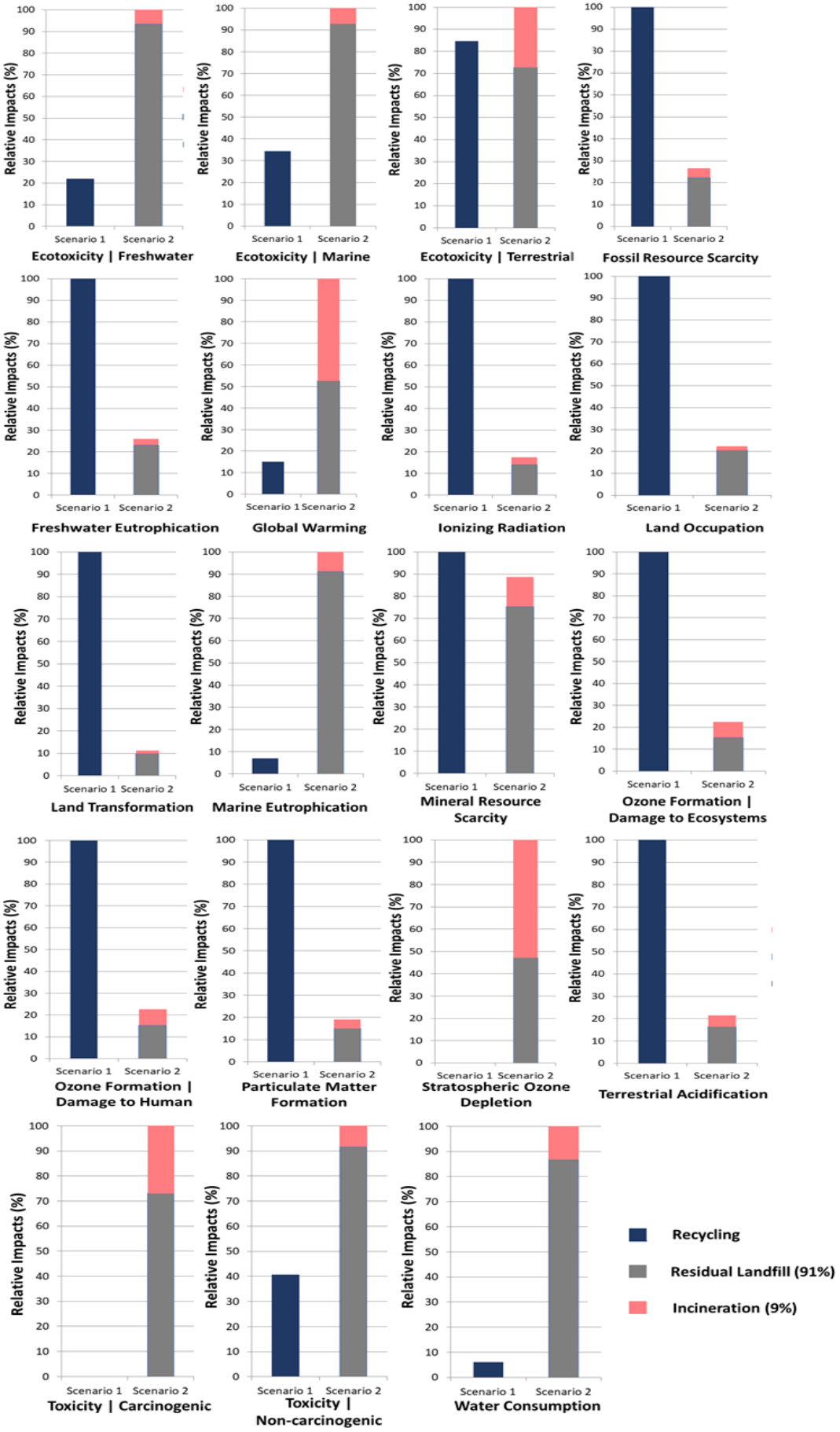

Figure: 22 Comparison between the relative impacts of different impact categories of the EoL scenarios. Own figure.

Moreover, no difference is observed in the impacts between the no-leak and leakage to air and water scenarios during the use phase of the investigated tandem solar panel which can be seen in table A 45. Nevertheless, this result must be taken with caution, since it does not imply that a release of these emissions to the ground, water or air cannot have local impacts over the environment or human health. Maintenance activities in the use phase also produce a fraction of emission via mowers primarily, which can cause great noise pollution within a certain area as well as ground contamination from gasoline use (Fthenakis and Kim 2011) but not considered in this study. Apart from this, significant differences are observed for different EoL scenarios of the waste panel, which are shown in *figure* 22. Although EoL scenario 1 represented a small share in the category global warming, 0.003 kg CO2eq/ kg GHG per kWh in comparison to 0.02 kg CO2eq/ kg GHG per kWh for scenario 2, it showed high shares in many other categories such as terrestrial acidification, ozone formation, freshwater eutrophication and land transformation among others. It is to be noted that scenario 1 held no share in the impact categories Stratospheric Ozone Depletion and Toxicity, Carcinogenic. In addition, this scenario showed a very small share of water consumption and marine eutrophication.

The *figure* 23, on the contrary, represents the approx. share of global warming by the overall the cradle-to-grave analysis along with the relative environmental flow (EF) contributions. Roughly 72% of the total emission is generated by the production and manufacturing stage and almost 85% of the generated emission is accounted for by carbon dioxide, mostly from the production of electricity. Methane follows CO_2 and represents approx. 10% share of the emissions. Overall, the process that contributed the most to global warming impacts is electricity production, followed by hard coal mining. In addition, waste treatment processes such as waste plastic, polyethylene and mineral oil among others, and production processes such as flat glass, aluminium and pig iron production along with their transportation also held noteworthy contribution to this share.

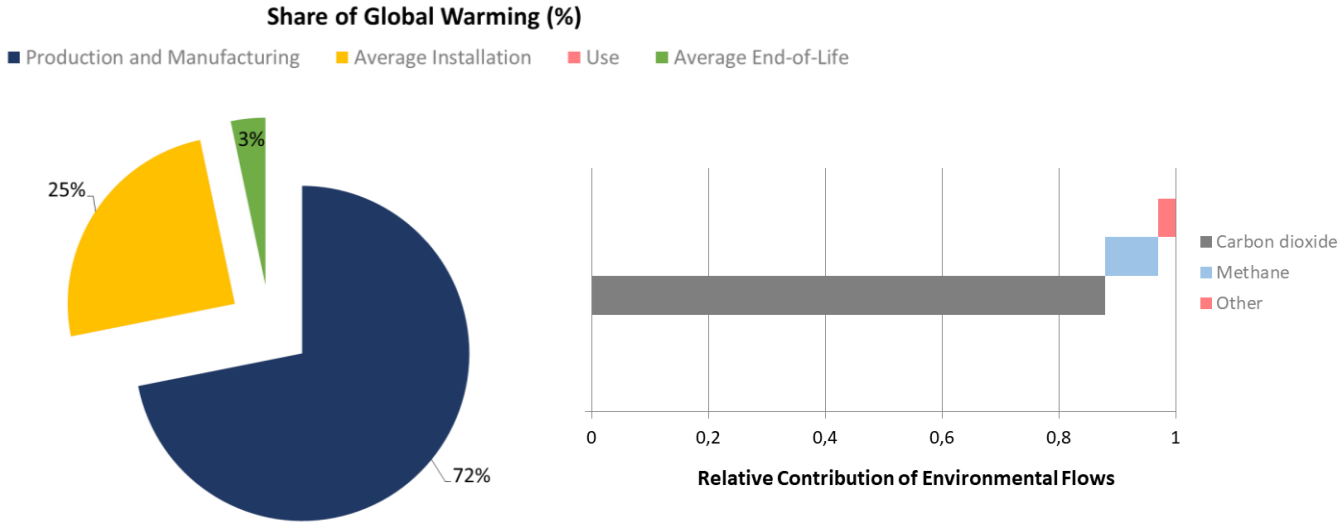

Figure: 23 Approx. share of Global Warming and relative contribution of environmental flows from the cradle-to-grave analysis. Own figure.

4.5.5 Sensitivity Analysis

The sensitivity analysis is the relative importance of an independent parameter related to the value of another dependent parameter (Giglioli and Saltelli 2000). Selected parameters, such as irradiance, efficiency, lifetime, performance ratio and degradation rate are associated with uncertainty. Therefore, the effect of these independent parameters over the EPBT and CO_2 emissions was assessed.

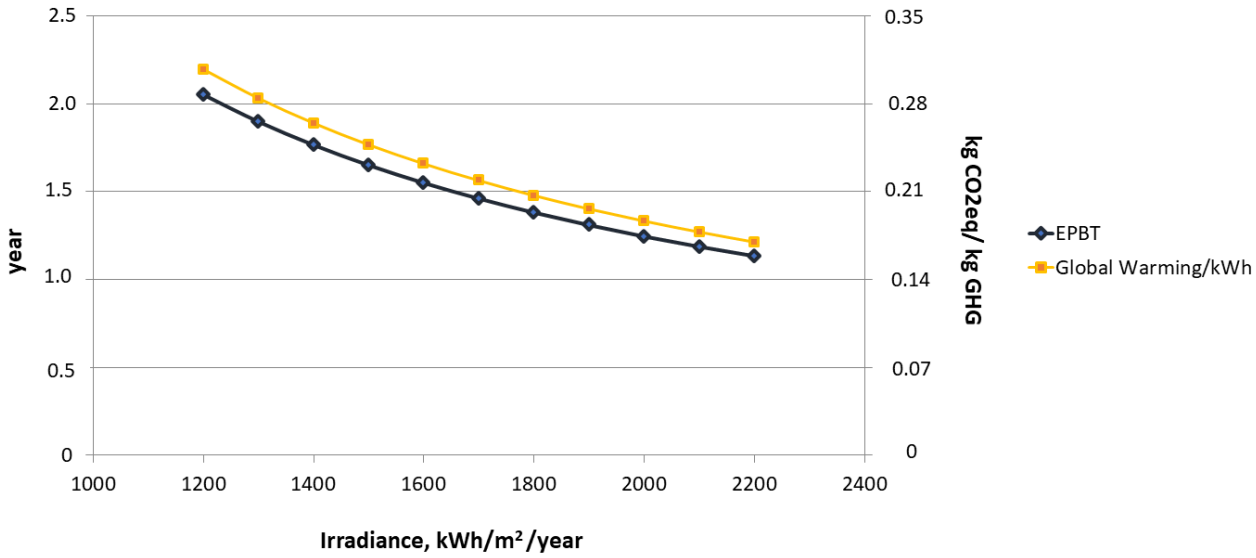

Figure: 24 Sensitivity analysis showing the effect of irradiance on EPBT and global warming per kWh output from the perovskite/Si tandem solar panel (cradle-to-grave). Own figure.

As the *figure* 24 shows, both the EPBT and global warming impacts per kWh have an inverse relation with irradiance. In other words, as irradiance increased the EPBT and global warming impacts per kWh decreased. However, this meant that the inverse relation is limited till a certain increase in irradiance and further increase in irradiance will not affect the two selected parameters.

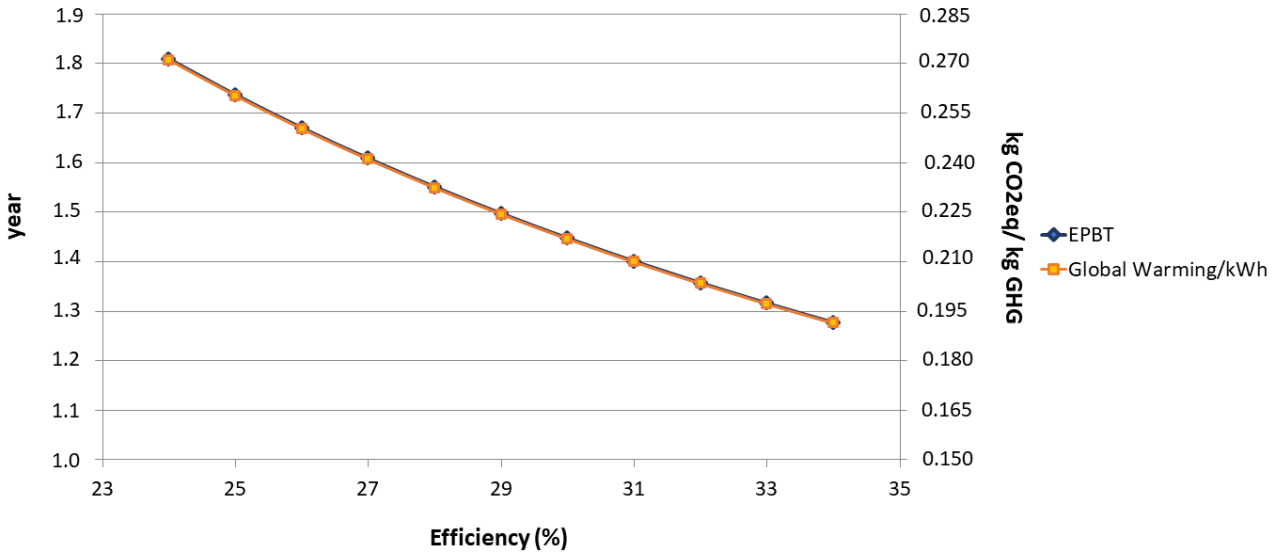

Figure: 25 Sensitivity analysis showing the effect of efficiency on EPBT and global warming per kWh output by the perovskite/Si tandem solar panel (cradle-to-grave). Own figure.

As the efficiency of the perovskite/Si tandem solar panel increases, the EPBT and global warming impacts per kWh decrease almost linearly as shown in *figure* 25. Therefore, an increased efficiency would further reduce both the EPBT and global warming impacts of the investigated tandem solar panel.

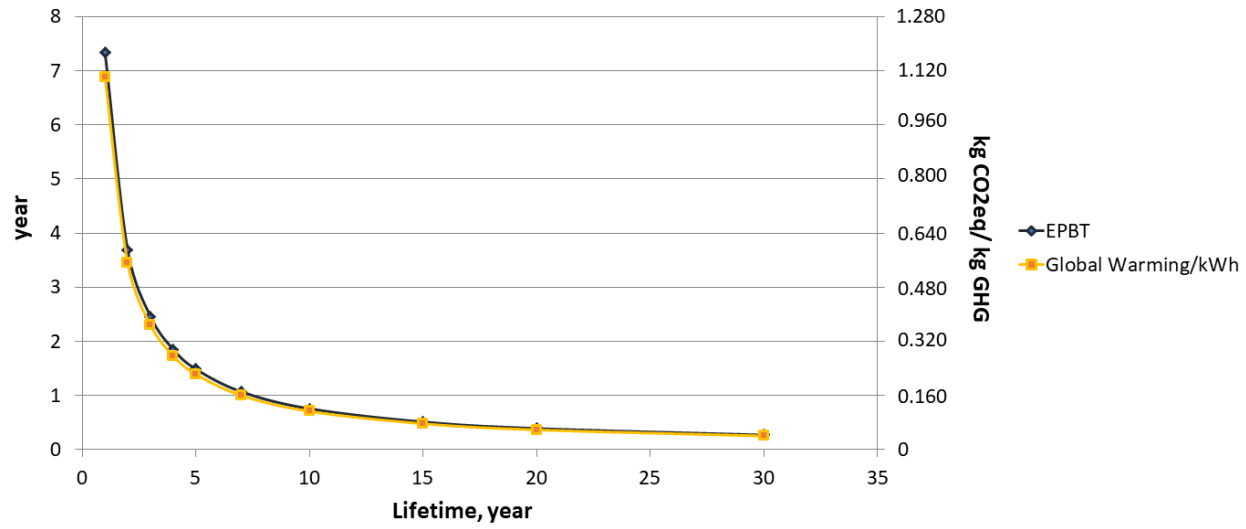

Figure: 26 Sensitivity analysis showing the effect of lifetime on EPBT and global warming per kWh output by the perovskite/Si tandem solar panel (cradle-to-grave). Own figure.

The sensitivity analysis in *figure* 26 revealed the inverse relationship that exists between the lifetime and the parameters EPBT and global warming impacts per kWh as well. This also suggests that the impacts per kWh can be reduced with an increased lifetime. Moreover, if the lifetime is shorter than EPBT, then the panel does not give back the energy necessary for its production, which means that it does not pay back the energy.

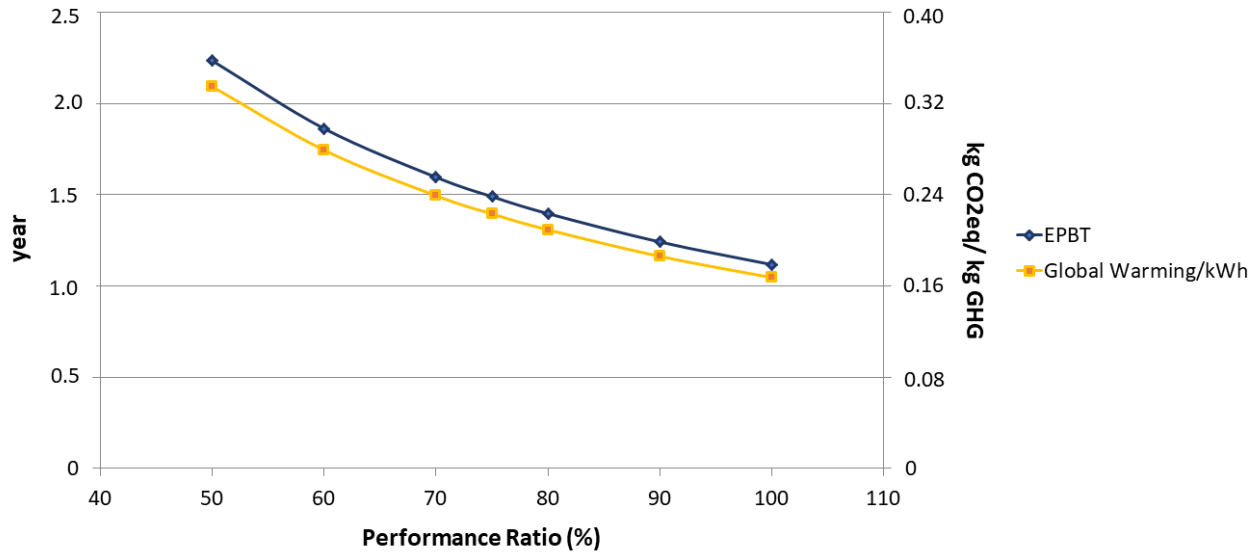

Figure: 27 Sensitivity analysis showing the effect of performance ratio on EPBT and global warming per kWh output by the perovskite/Si tandem solar panel (cradle-to-grave). Own figure.

With the increase in PR, it is observed from *figure* 27 that both the parameters, EPBT and global warming impacts, decrease. It means that this parameter too, shows the same linear inverse relation.

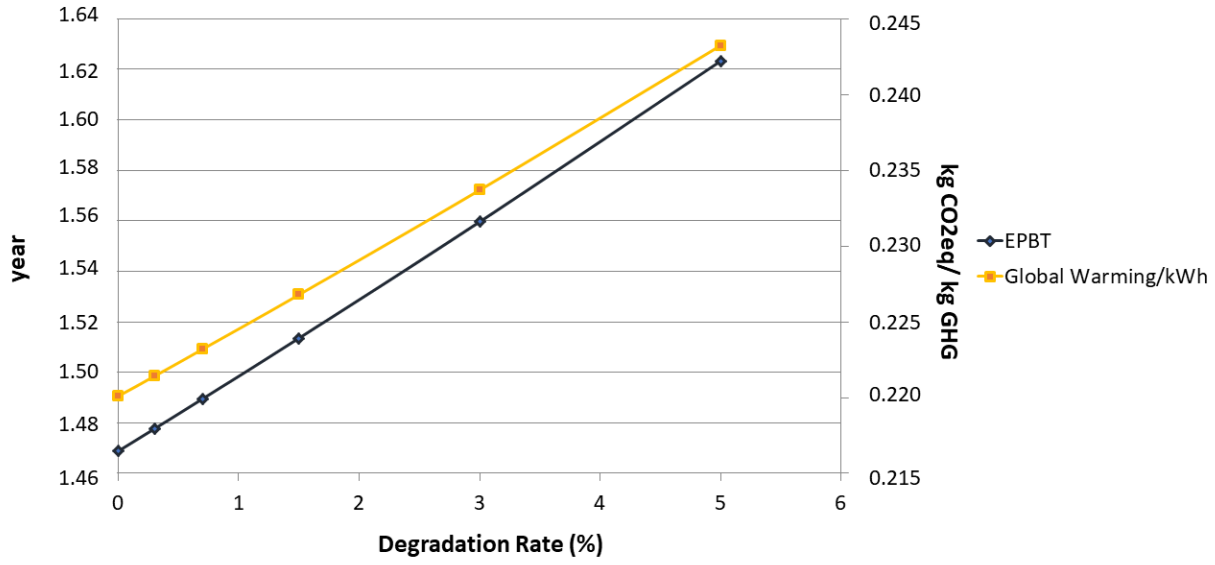

Figure: 28 Sensitivity analysis showing the effect of degradation rate on EPBT and global warming per kWh output by the perovskite/Si tandem solar panel (cradle-to-grave). Own figure.

Finally, the *figure* 28 representing the sensitivity analysis represents the effect of degradation rate on EPBT and global warming impacts per kWh. Both the EPBT and global warming impacts increase linearly with the increase in DR. It can also be observed that an increase in DR has slightly more effects on the EPBT than the global warming impact.

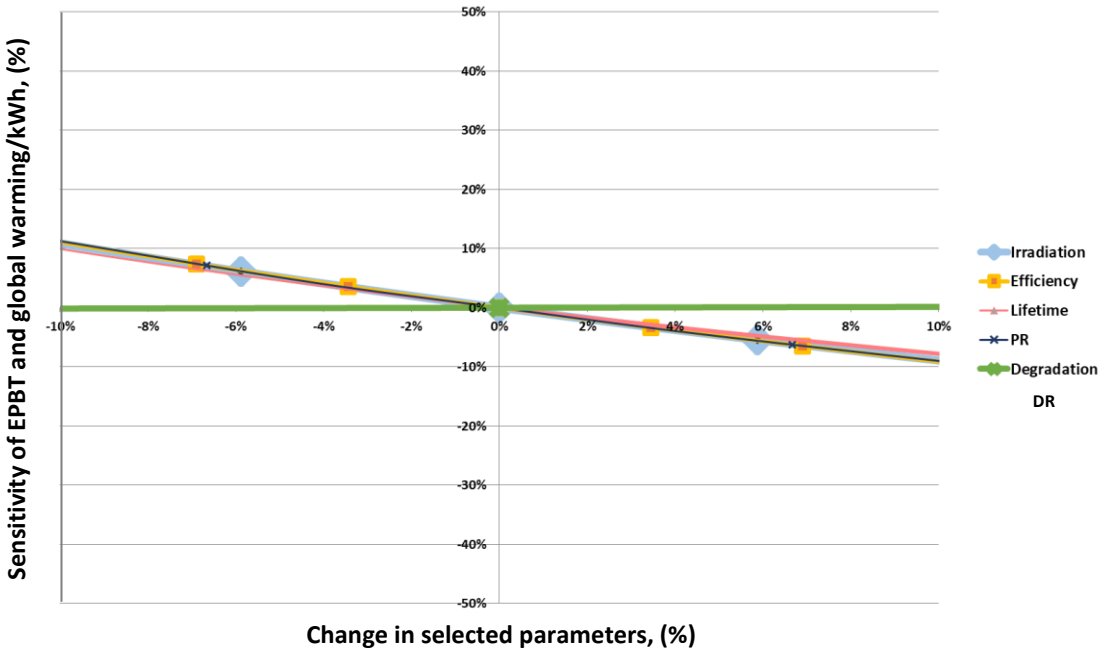

Figure: 29 Overview of the sensitivity of the selected parameters on EPBT and global warming per kWh for the perovskite/Si tandem solar panel (cradle-to-grave). Own figure.

The results of the sensitivity analyses obtained so far are compiled together in *figure* 29 to compare the sensitivity of the criteria to different parameters. The x-axis represents the change of the parameters irradiation, efficiency, lifetime, PR and DR while the y-axis represents the sensitivity of both the EPBT and global warming per kWh. The irradiation, efficiency, lifetime, PR and DR of the investigated solar panel is considered as the reference for this plot. In this case, both the criteria presented the same sensitivity for their respective parameters and are found most sensitive to parameters such as the performance ratio, irradiance and efficiency, followed by lifetime. However, change in the parameter DR showed negligible sensitivity to the two criteria (2% increase for the first 100% increase in DR).

4.5.6 Uncertainty Analysis

The Monte Carlo method was employed for the uncertainty analysis, where all uncertainty distributions that are defined in the flows, parameters and characterisation factors are taken into account for the simulation. This is accomplished by substituting the point estimates with random numbers obtained from probability density functions and then building models of the possible results (Hongxiang and Wei 2013). To perform Monte Carlo analysis for the midpoint impact categories ReCiPe 2016, 1.1 (20180117) and CED, this study used the software Brightway2 as a tool employing 1000 iterations. However, no data of uncertainty was considered during the data collected of this study.

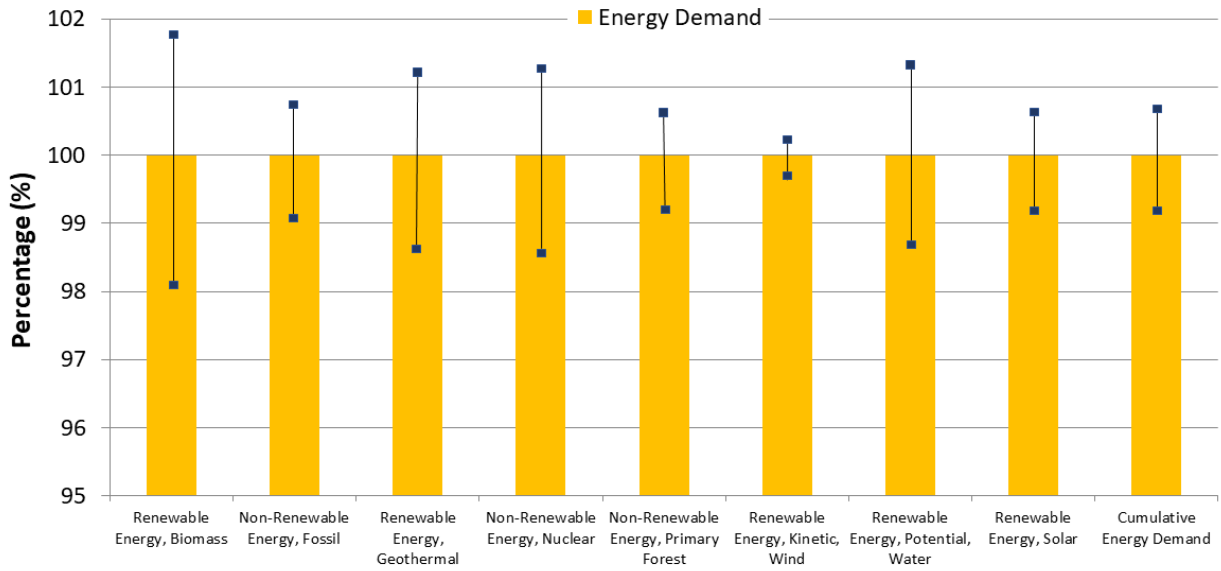

Figure: 30 Relative uncertainty with an 95% of confidence of the cradle-to-grave CED for the perovskite/Si tandem solar panel. Own figure.

With 95% of confidence, the Monte Carlo analysis from cradle-to-grave revealed that the mean uncertainty obtained for the different CED categories for the perovskite/Si tandem is 0.78%. The confidence level was calculated manually using the results of the Monte Carlo analysis from Brightway2 as this feature is absent in this software. The margin of error, as seen in *figure* 30, is highest for the category Renewable Energy, Biomass which is ±1.86%, followed by Non-Renewable Energy, Nuclear (±1.36%) and Renewable Energy, Geothermal (±1.28%) and Water (±1.2%).

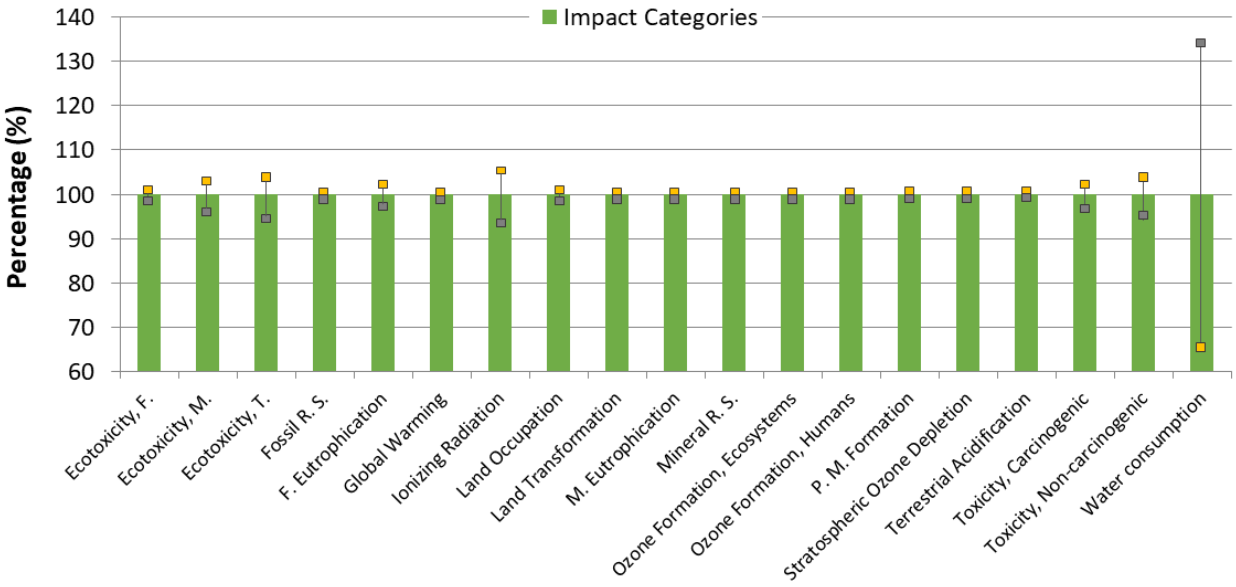

Figure: 31 Relative uncertainty (cradle-to-grave) with an 95% of confidence of the impact category ReCiPe 2016, 1.1 (20180117), Midpoint for the perovskite/Si tandem solar panel. Own figure.

With the same confidence, the Monte Carlo analysis further revealed that although the results of the categories ranged from 93% to 107%, that of only the water consumption ranged from 66% to 134%. A higher degree of uncertainty is observed for ionizing radiation

(± 7%), followed by terrestrial ecotoxicity (± 4.24%) and non-carcinogenic (± 3.9%) toxicity. The uncertainties of fossil resource scarcity, global warming, land transformation, marine eutrophication, mineral resource scarcity, ozone formations, particulate matter formation, stratospheric ozone depletion and terrestrial acidification is found to be below ±1% of the mean as shown in *figure* 31. It must be noticed that the uncertainties regarding the midpoint ReCiPe 2016, 1.1 (20180117) impact categories are higher than the uncertainties found for CED.

Chapter 5 Discussion of Results

In this chapter, the results of the LCA for the investigated perovskite/Si tandem solar panel is compared with those tandem solar panels mentioned in *chapter* 3 to evaluate the difference in global warming impacts and EPBT. Another comparison is made among the EPBTs of the investigated panel and other PV technologies. Subsequently, the CO_2 eq. emission of the investigated tandem is compared with other energy technologies to provide an overview of their position. In addition, comparison of results when different LCA softwares are chosen as the tool is also included later in this chapter which revealed some unexpected results.

5.1 Comparison with other LCA studies of perovskite/Si tandem

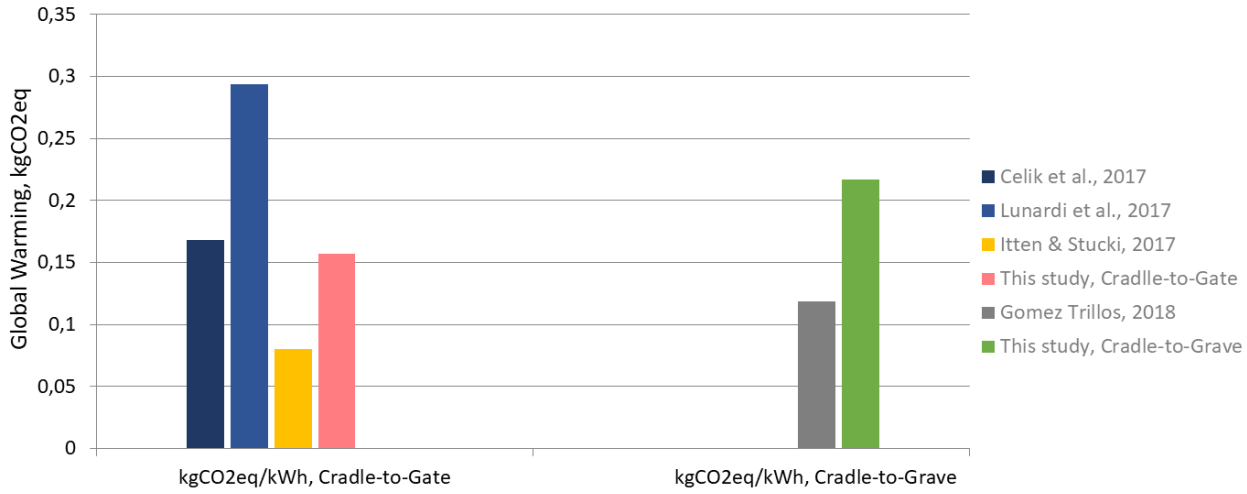

Figure: 32 Global warming impacts of investigated Perovskite/Si tandem in comparison to other Perovskite/Si tandems for 1,700 kWh/m^2/yr. Own figure.

The *figure* 32, plotted in accordance to the literature review in chapter 3, shows the difference in global warming impacts for both cradle-to-gate and cradle-to-grave analyses for perovskite/Si tandems of different architectures. Among the cradle-to-gate analyses, the tandem architecture by Itten and Stucki showed the lowest impacts as it had the highest lifetime, 30 years. Both the tandems investigated by Celik et al. and this study considered a 5 years lifetime but the lower efficiency of the former (6%) resulted in higher global warming impact than the latter. Although Lunardi et al. considered 20 years of lifetime, lower efficiency (24-27%) and material selection for different layers of this architecture resulted in higher impacts. For the cradle-to-grave analysis, the EoL scenario selection resulted in a higher impact even though both architectures had 5 years of lifetime. Other factors such as software, impact assessment method and background data can also have a significant effect on this result. On the other hand, a comparison of the EPBTs of the same architectures is shown in *figure* 33.

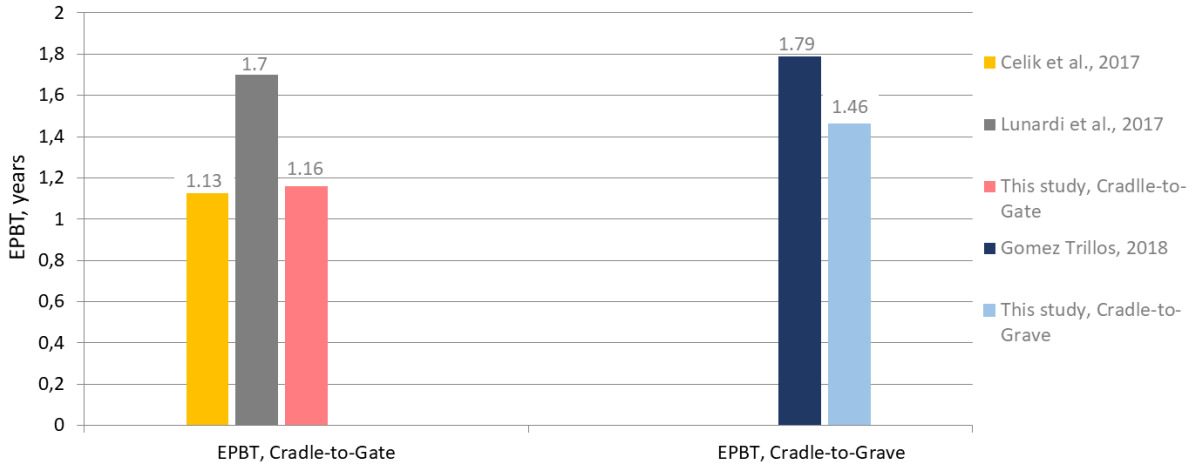

Figure: 33 EPBT of investigated Perovskite/Si tandem in comparison to other Perovskite/Si tandems for 1,700 kWh/m^2/yr. Own Figure.

The investigated tandem of this study has a lower CED which resulted in a lower EPBT when compared to the tandem architectures studied by Lunardi et al. 2017 for cradle-to-gate and Gomez Trillos 2018 for the cradle-to-grave analysis. However, the EPBT the tandem architecture analysed by Celic et al. 2017 required 3.6 months less for EPBT than that of this study.

5.2 Comparison of CO_2 eq. Emission with Other Photovoltaic Technologies

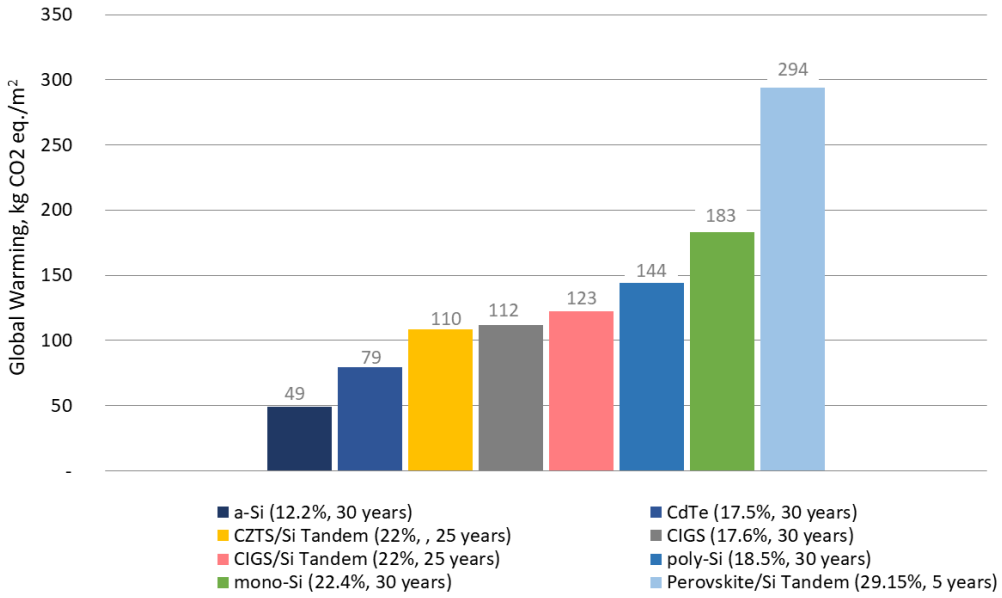

Figure: 34 CO_2 eq. emission by the investigated Perovskite/Si tandem in comparison to other PV technologies 1,700 kWh/m^2/yr, cradle-to-gate. Own Figure.

For the average global insolation value 1,700 kWh/m^2/year and a PR of 0.75 and 30 year lifetime, the CO_2 eq. emission per square meter and EPBT of mono-Si, poly-Si, a-Si, CdTe and CIGS (Celik, Mason et al. 2017) are compared with that of the tandem developed by HZB.

Celik et al. 2017 used the TRACI impact categories for their calculation. Moreover, for 25 years lifetime, all else equal, the same of perovskite/Si tandem is compared to that of CIGS/Si and CZTS/Si (Lunardi 2019). In this case, the author used ReCiPe impact categories for his calculation.

It is revealed from the *figure* 34 that the investigated tandem has the highest emission of CO_2 eq. when compared to other PV technologies. Among others, a key parameter that resulted in this difference is the lifetime of the panels as shown in the sensitivity analysis. On the other hand, the *figure* 35 depicted the promising prospects of the investigated tandem among other PV technology in regard to EPBT. The efficiencies followed by the lifetimes of the PV technologies are shown in brackets for the *figures* 34 and 35.

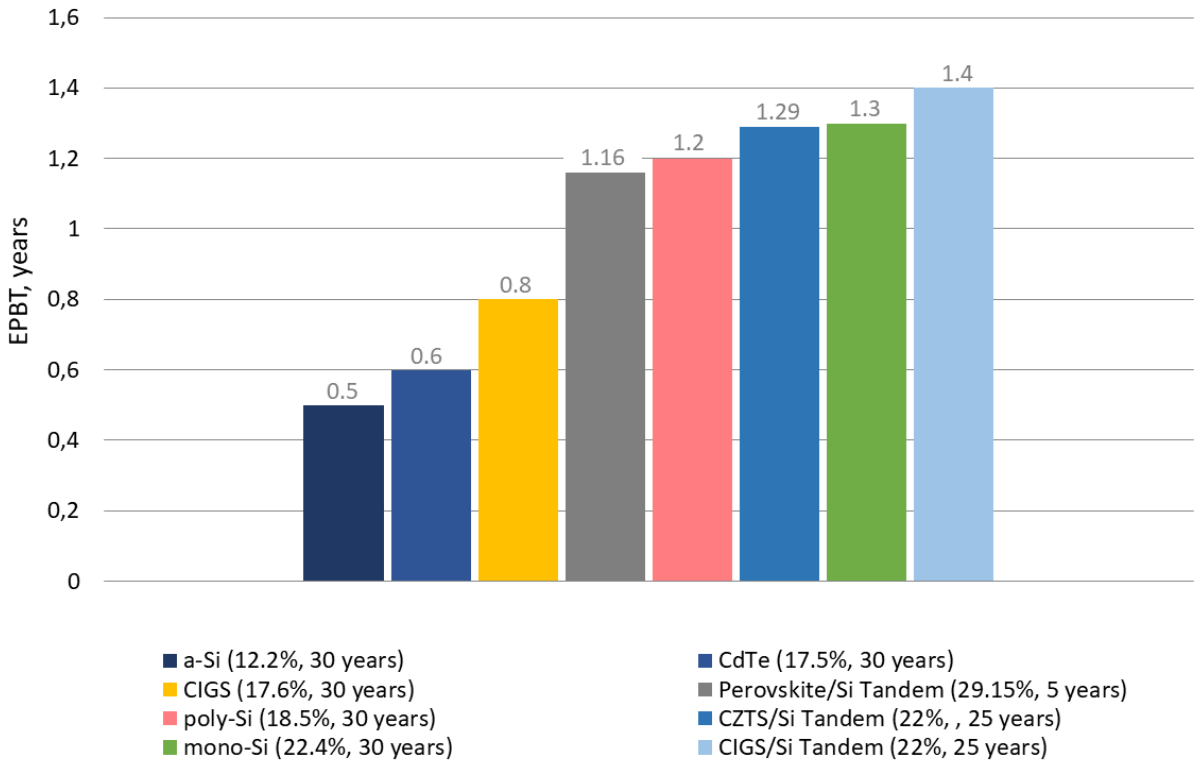

Figure: 35 EPBT of investigated Perovskite/Si tandem in comparison to other PV technologies for 1,700 kWh/m^2/yr, cradle-to-gate. Own Figure.

In addition, the *figure* 36 shows a comparison among the cradle-to-grave emissions per kWh between different energy technologies, which has been adopted from IPCC to provide an impression of the position of the investigated solar tandem (Schlömer, Bruckner et al. 2014). The solar PV considered for this plot represents primarily a-Si solar panels. The emission from mono-Si and ploy-Si PV technologies is adopted from *figure* 34 to provide a complete picture. Nevertheless, the difference in emission of the investigated tandems from coal and gas provides motivation for a transition towards a cleaner energy.

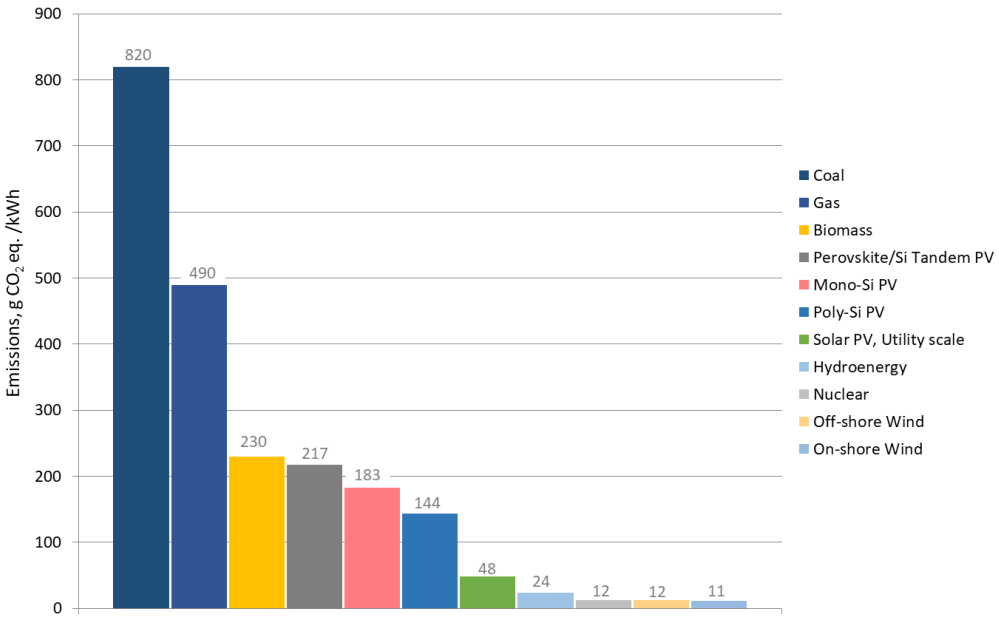

Figure: 36 Comparison among the emissions per kWh between different energy technologies (Schlömer, Bruckner et al. 2014)(Edited).

5.3 Uncertainties and Error Analysis

To develop more confidence on the results obtained, this study considered evaluation of the effects of software selection on the results. Therefore, two other LCA softwares, namely SimaPro (9.1) (Pré Consultants 2016) and OpenLCA (1.10.2) (OpenLCA 2013), are used to conduct the LCIA again for the impact category ReCiPe 2016. The results are listed below in the *table* 8.

Table 8 Comparison of LCIA results of the perovskite/Si tandem solar cell for softwares Brightway 2, SimaPro and OpenLCA. Own table.

Name	Brightway2 Units/m²	SimaPro Units/m²	OpenLCA Units/m²	Comparison Brightway2/SimaPro in % (reference Brightway2)	Comparison Brightway2/OpenLCA in % (reference Brightway2)
Global warming	290.8	281.8	203	96.9	69.8
Strat. ozone depletion	1.59×10^{-4}	1.32×10^{-4}	1.17×10^{-4}	83.1	73.5
Ionizing radiation	32.7	29.7	44.8	91	137.2
O. formation, Human health	0.67	0.6	0.39	91.3	57.9
Fine PM. formation	0.5	0.5	0.3	94.6	56.3
O. formation, T. ecosystems	0.7	0.6	0.4	89	56.4
Terrestrial acidification	0.94	0.91	0.65	96.24	68.8
Freshwater eutrophication	0.02	0.17	0.16	731.4	706.8
Marine eutrophication	0.02	0.01	0.016	68	104.6
Terrestrial ecotoxicity	4.2	743.3	272.4	17586	6444
Freshwater ecotoxicity	0.17	20.7	14.3	12000.3	8424.3
Marine ecotoxicity	3.3	28.8	20.6	870.9	623
Human carc. toxicity	2.1	19.8	12.6	925.8	588.9
Human non-carc. toxicity	15.1	407.5	242.5	2696.4	1604.4
Land use	6	6.8	5	112.6	83.3
Land transformation	0.08				
Mineral res. scarcity	3	2.4	1.4	80.3	47.7
Fossil res. scarcity	78.8	75	58.2	95.2	73.8
Water consumption	12.9	12.3	12.1	95.16	93.7

This *table* 8 showed that in most cases, the results obtained from Brightway2 are higher than that of SimaPro. The results obtained from OpenLCA are lowest in most cases but calculated the highest impacts for ionization radiation. However, the few impact categories marked in red in the *table* 8 showed extremely high difference when compared to Brightway2, particularly terrestrial ecotoxicity and freshwater ecotoxicity. Additionally, the impact category land transformation is absent in both SimaPro and OpenLCA.

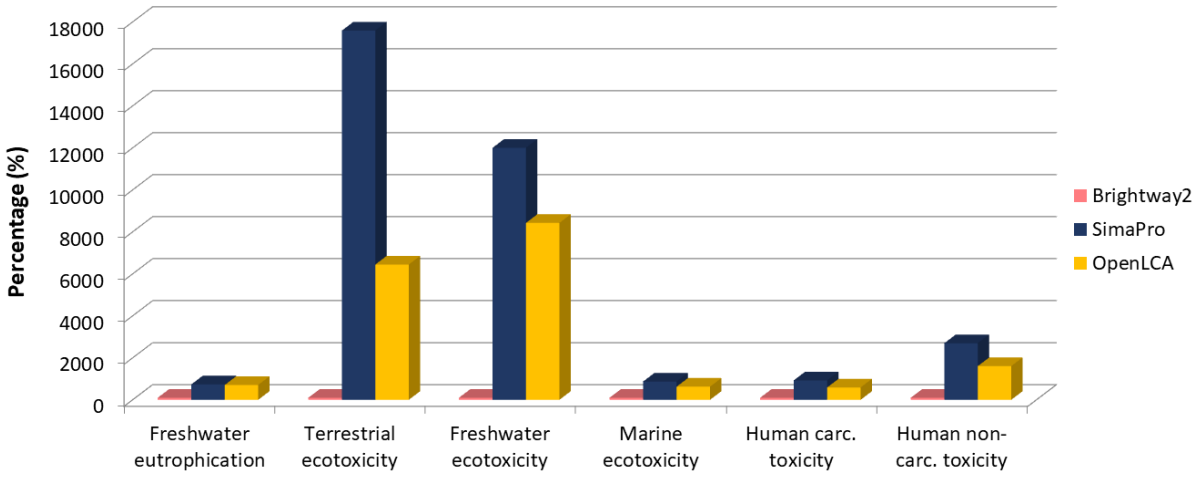

Figure: 37 Comparison of LCIA results (>200% difference) of the perovskite/Si tandem solar cell for softwares Brightway2, SimaPro and OpenLCA. Own figure.

To provide a better view of the difference in results, the impact results with high difference are plotted in the *figure* 37. From this figure, it is evident that the results from Brighway2 for the mentioned impact categories are unreliable and do not portray the complete impacts. This makes comparisons of the results obtained using different software within these impact categories difficult, due to their considerable divergence. Similarly, a trend of accounting lower impacts is observed for the a-Si and nc-SiO layers when Brightway2 is used. Nevertheless, Brightway2 accounts for highest impacts for the mono-Si wafer layer among the compared tools and has proved to provide similar results for selected impact categories such as global warming as the ones obtained using other tools.

Apart from this, certain life cycle processes and their respective impact contributions were difficult to account for. For example, sufficient data on the downstream processes, such as decommissioning and EoL of the perovskite modules were unavailable which limited the accuracy of the results. Furthermore, as the results were represented for lab-scale production with a Technology Readiness Level (TRL) between 5 to 6 (technology validation and demonstration in relevant environment) it likely underestimated the true life cycle impacts as compared to that of the industrial-scale production. Assumptions in selection of manufacturing inputs such as silicon type, grid electricity and transportation may also contribute significantly to variability in estimates of the life cycle impacts. Moreover, the uncertainty analysis presented in this study showed that the background data itself contains some variability.

Chapter 6 Conclusion and Future Research Work

A cradle-to-gate and a cradle-to-grave LCA were conducted in this study to evaluate and compare the environmental impacts of the state of the art perovskite/Si tandem solar panels developed by Helmholtz Zentrum Berlin (HZB) with other studies. While the former approach considered upto encapsulated tandem PV panels, the latter further analysed upto two EoL scenarios. The efficiency of this two terminal, monolithic, silicon-heterojunction perovskite tandem solar cells tandem was considered to be 29.15% and results were observed for a lifetime of 5 years for the average insolation conditions of Southern Europe (1,700 kWh/m^2/yr) and Freiburg (1,117 kWh/m^2/yr). To develop both environmental and energy profiles, aspects such as Cumulative Energy Demand (CED), Energy Payback Time (EPBT) and energy Return on Energy Invested (EROI) were assessed along with the *ReCiPe 2016, 1.1 (20180117), Midpoint* impact assessment methodology employing the software Brightway2.

In the cradle-to-gate analysis, the tandem layers, particularly the mono-Si wafer and the metal Ag layer, were found responsible for most of the impacts. Two key parameters that drove the impacts of mono-Si wafers were its wafer thickness (Hsu, O'Donoughue et al. 2012) and kerf loss. The layers associated with silver mainly represented the major share of marine ecotoxicity while the lead containing perovskite layer showed significant terrestrial ecotoxicity. The second most impacting process observed from this analysis was the panel production which included encapsulation, glass and framing. The share of CO_2 eq. emissions were found to be approx. 66% and 9% for mono-Si wafer and Ag layers, respectively, and around 17% for the panel production. The CED also showed a similar trend, with the highest share demanded for mono-Si wafer (69%), followed by the panel production (13%) and Ag layers (7%). This provides an orientation towards diminishing the environmental impact by reducing the wafer thickness and kerf loss of mono-Si wafer and substituting silver to produce the PV panels.

Simultaneously, the cradle-to-grave analysis revealed that the impact in the different impact categories was mainly driven by perovskite/Si tandem panel production and manufacturing. The share of CO_2 eq. emissions in this case were found to be approx. 72% for production and manufacturing and 25% for average panel installation which included BOS components such as inverters and cables. For the use phase a negligible share of impacts were observed. In addition, no change was observed among the no leakage and leakage scenarios during this stage, inferring that the local effects of this leakage cannot be ascertained through this kind of analysis. The low results analysed for the toxicity categories in Brightway2 could be one of the reasons for this no visible change. Lastly, the results validated that CO_2 eq. emissions by the recycling process was very low when compared with the other scenario. This is due to the recovery of materials such as glass and Si that can be reused to manufacture new solar cells and modules. However it should be noted that this process also represented the highest share in terrestrial acidification, ozone formation, freshwater eutrophication and

land transformation among others. Nevertheless, the CED from the gate-to-grave phase of the investigated solar panel represented approx. 20% of the total. A difference of approx. 4 months in EPBTs of the two analyses was found, which concluded that inclusion of the downstream life cycle phases are important to completely describe the effects of electricity production from the PV technologies.

The toxic pollutants emitted from the PV life cycle can affect both human health and ecosystem quality. Overall, approx. 85% of the total GWP emissions emitted by the investigated PV was represented by CO_2, while methane represents almost 5%. Key processes that contributed to this share were (i) electricity generation, (ii) treatment processes for waste materials such as waste plastic, polyethylene and mineral oil among others, (iii) flat glass, aluminium and pig iron production and lastly, (iv) their respective transportation.

The sensitivity analysis indicated that at least 10 years of lifetime with the assumed efficiency, all else equal, is required to have an equal or lower impact per kWh of electricity in all impact categories. Therefore, the lifetime of the perovskite/Si tandem must increase. A similar conclusion was drawn from the sensitivity analysis as well.

When the software SimaPro (9.1), OpenLCA (1.10.2) and Brightway2 were compared using the background data ecoinvent 3.6 and the impact assessment method ReCiPe 2016 in all cases, important differences were detected particularly in the impact categories Terrestrial ecotoxicity, Freshwater ecotoxicity and Human non-carcinogenic toxicity among others toxicity categories. After analysing the characterisation factors included in this impact assessment method, it was found that the differences might arise as a consequence of different or missing characterization factors in Brightway2.

This opens an opportunity to harmonise the LCIA results developed from different LCA softwares by equally implementing the characterization factors among all the softwares for the respective impact category, making it comparable in future. In addition, detailed study on the environmental effects of the EoL of perovskite solar panels is recommended for the future as information regarding this is rather limited.

Additionally, the background data contained some uncertainties that limited the accuracy of the results. Therefore this study recommends more adequate and better quality information collection as future work, so that the rendered results generated using those background data can be used with a higher confidence.

Finally, a multi criteria analysis is recommended as future work to provide a holistic view of the social and economic possibilities of this perovskite/Si tandem solar panel. With such assessments a more comprehensive assessment can be done which can aid in the sustainable adoption of this efficient, environmentally–benign and durable technology.

Bibliography

(2017). "Solar Panels 101: Understanding Module Size and Weight." https://www.intermtnwindandsolar.com/solar-panels-101-understanding-module-size-and-weight/ 21.08.2020.

(2020). "Perovskites take steps to industrialization." Nature Energy **5**(1): 1-1.

Abdelhady, S., M. S. Abd-Elhady and M. M. Fouad (2017). "An understanding of the operation of silicon photovoltaic panels." Energy Procedia **113**: 466-475.

Abdulrazzaq, O. A., V. Saini, S. Bourdo, E. Dervishi and A. S. Biris (2013). "Organic solar cells: a review of materials, limitations, and possibilities for improvement." Particulate science and technology **31**(5): 427-442.

Aberle, A. G. (2009). "Thin-film solar cells." Thin solid films **517**(17): 4706-4710.

Alberola-Borràs, J.-A., R. Vidal, E. J. Juárez-Pérez, E. Mas-Marzá, A. Guerrero and I. Mora-Seró (2018). "Relative impacts of methylammonium lead triiodide perovskite solar cells based on life cycle assessment." Solar Energy Materials and Solar Cells **179**: 169-177.

Andersson, S. and M. Listén (2014). Life Cycle Impact Assessment: A comparison of three contemporary methodologies.

Assadi, M. K., S. Bakhoda, R. Saidur and H. Hanaei (2018). "Recent progress in perovskite solar cells." Renewable and Sustainable Energy Reviews **81**: 2812-2822.

Binek, A., M. L. Petrus, N. Huber, H. Bristow, Y. Hu, T. Bein and P. Docampo (2016). "Recycling perovskite solar cells to avoid lead waste." ACS applied materials & interfaces **8**(20): 12881-12886.

Bjørn, A., M. Owsianiak, C. Molin and A. Laurent (2018). Main characteristics of LCA. Life Cycle Assessment, Springer**:** 9-16.

Boriskina, S. V. and G. Chen (2014). "Exceeding the solar cell Shockley–Queisser limit via thermal up-conversion of low-energy photons." Optics Communications **314**: 71-78.

Bu, T., X. Liu, J. Li, W. Huang, Z. Wu, F. Huang, Y.-B. Cheng and J. Zhong (2020). "Dynamic Antisolvent Engineering for Spin Coating of 10× 10 cm2 Perovskite Solar Module Approaching 18%." Solar RRL **4**(2): 1900263.

Cai, B., W.-H. Zhang and J. Qiu (2015). "Solvent engineering of spin-coating solutions for planar-structured high-efficiency perovskite solar cells." Chinese Journal of Catalysis **36**(8): 1183-1190.

Carbeck, J. (2016). Solar power has big limitations. This wonder material could change that. Annual Meeting of the New Champions, World Economic Forum.

Cash Jr, J. H. and J. A. Cunningham (1970). Rf sputtering method and system, Google Patents.

Celik, I., B. E. Mason, A. B. Phillips, M. J. Heben and D. Apul (2017). "Environmental impacts from photovoltaic solar cells made with single walled carbon nanotubes." Environmental Science & Technology **51**(8): 4722-4732.

Celik, I., A. B. Phillips, Z. Song, Y. Yan, R. J. Ellingson, M. J. Heben and D. Apul (2017). "Environmental analysis of perovskites and other relevant solar cell technologies in a tandem configuration." Energy & Environmental Science **10**(9): 1874-1884.

Celik, I., Z. Song, A. J. Cimaroli, Y. Yan, M. J. Heben and D. Apul (2016). "Life Cycle Assessment (LCA) of perovskite PV cells projected from lab to fab." Solar Energy Materials and Solar Cells **156**: 157-169.

Change, I. C. (2014). Synthesis Report (eds Core Writing Team, Pachauri, RK & Meyer LA)(IPCC, 2014).

Chao, T. (2001). Introduction to semiconductor manufacturing technology, SPIE PRESS.

Chen, Z., W. Ma, J. Wu, K. Wei, Y. Lei and G. Lv (2018). "A study of the performance of submerged arc furnace smelting of industrial silicon." Silicon **10**(3): 1121-1127.

Chowdhury, M. S., K. S. Rahman, T. Chowdhury, N. Nuthammachot, K. Techato, M. Akhtaruzzaman, S. K. Tiong, K. Sopian and N. Amin (2020). "An overview of solar photovoltaic panels' end-of-life material recycling." Energy Strategy Reviews **27**: 100431.

Curran, M. A. (2015). Life cycle assessment student handbook, John Wiley & Sons.

Espinosa, N., L. Serrano-Luján, A. Urbina and F. C. Krebs (2015). "Solution and vapour deposited lead perovskite solar cells: Ecotoxicity from a life cycle assessment perspective." Solar Energy Materials and Solar Cells **137**: 303-310.

Extance, A. (2019). "The reality behind solar power's next star material." Nature **570**(7762): 429-433.

Finkbeiner, M. (2014). The international standards as the constitution of life cycle assessment: the ISO 14040 series and its offspring. Background and Future Prospects in Life Cycle Assessment, Springer**:** 85-106.

Finkbeiner, M., A. Inaba, R. Tan, K. Christiansen and H.-J. Klüppel (2006). "The new international standards for life cycle assessment: ISO 14040 and ISO 14044." The international journal of life cycle assessment **11**(2): 80-85.

Fisher, D. J. (2020). Lead Halide Perovskite Solar Cells, Materials Research Forum LLC.

Frischknecht, R., R. Itten, P. Sinha, M. de Wild-Scholten, J. Zhang, G. A. Heath and C. Olson (2015). Life cycle inventories and life cycle assessments of photovoltaic systems, National Renewable Energy Lab.(NREL), Golden, CO (United States).

Frischknecht, R., F. Wyss, S. B. Knöpfel, T. Lützkendorf and M. Balouktsi (2015). "Cumulative energy demand in LCA: the energy harvested approach." The International Journal of Life Cycle Assessment **20**(7): 957-969.

Fthenakis, V. and H. C. Kim (2011). "Photovoltaics: Life-cycle analyses." Solar Energy **85**(8): 1609-1628.

Fthenakis, V. M. (2000). "End-of-life management and recycling of PV modules." Energy Policy **28**(14): 1051-1058.

García-Valverde, R., J. A. Cherni and A. Urbina (2010). "Life cycle analysis of organic photovoltaic technologies." Progress in Photovoltaics: Research and Applications **18**(7): 535-558.

Gielen, D., F. Boshell, D. Saygin, M. D. Bazilian, N. Wagner and R. Gorini (2019). "The role of renewable energy in the global energy transformation." Energy Strategy Reviews **24**: 38-50.

Giglioli, N. and A. Saltelli (2000). "SimLab 1.1, Software for Sensitivity and Uncertainty Analysis, tool for sound modelling." arXiv preprint cs/0011031.

Gomez Trillos, J. C. (2018). Life Cycle Assessment of Perovskite Solar Cells Master Thesis Carl von Ossietzky University of Oldenburg.

Gong, J., S. B. Darling and F. You (2015). "Perovskite photovoltaics: life-cycle assessment of energy and environmental impacts." Energy & Environmental Science **8**(7): 1953-1968.

Gray, J. L. (2011). "The physics of the solar cell." Handbook of photovoltaic science and engineering **2**: 82-128.

Hamedani, Y., P. Macha, T. J. Bunning, R. R. Naik and M. C. Vasudev (2016). Plasma-enhanced chemical vapor deposition: Where we are and the outlook for the future, InTech.

Hardy, N. (2013). "What is Thin Film Deposition By Thermal Evaporation? ." Retrieved 20.07, 2020, from http://www.semicore.com/news/71-thin-film-deposition-thermal-evaporation.

Hongxiang, C. and C. Wei (2013). "Uncertainty analysis by Monte Carlo simulation in a life cycle assessment of water-saving project in green buildings." Information Technology Journal **12**(13): 2593.

Hossain, M. I., W. Qarony, S. Ma, L. Zeng, D. Knipp and Y. H. Tsang (2019). "Perovskite/silicon tandem solar cells: From detailed balance limit calculations to photon management." Nano-Micro Letters **11**(1): 58.

Hsu, D. D., P. O'Donoughue, V. Fthenakis, G. A. Heath, H. C. Kim, P. Sawyer, J. K. Choi and D. E. Turney (2012). "Life cycle greenhouse gas emissions of crystalline silicon photovoltaic electricity generation: systematic review and harmonization." Journal of Industrial Ecology **16**: S122-S135.

Hughes, M. (2016). "What is RF Sputtering? ." Retrieved 19 October, 2020, from http://www.semicore.com/news/92-what-is-rf-sputtering.

Huijbregts, M., Z. Steinmann, P. Elshout, G. Stam, F. Verones, M. Vieira, A. Hollander, M. Zijp and R. Van Zelm (2016). "ReCiPe 2016: a harmonized life cycle impact assessment method at midpoint and endpoint level report I: characterization."

Huijbregts, M. A., L. J. Rombouts, S. Hellweg, R. Frischknecht, A. J. Hendriks, D. van de Meent, A. M. Ragas, L. Reijnders and J. Struijs (2006). Is cumulative fossil energy demand a useful indicator for the environmental performance of products?, ACS Publications.

Hunt, R. G., W. E. Franklin and R. Hunt (1996). "LCA—How it came about." The international journal of life cycle assessment **1**(1): 4-7.

Ibn-Mohammed, T., S. Koh, I. Reaney, A. Acquaye, G. Schileo, K. Mustapha and R. Greenough (2017). "Perovskite solar cells: An integrated hybrid lifecycle assessment and review in comparison with other photovoltaic technologies." Renewable and Sustainable Energy Reviews **80**: 1321-1344.

IEA (2020). The Covid-19 crisis is causing the biggest fall in global energy investment in history, International Energy Agency.

IEA (2020). Global Energy Review 2020. Paris, International Energy Agency.

IRENA (2019). Future of Solar Photovoltaic: Deployment, investment, technology, grid integration and socio-economic aspects (A Global Energy Transformation: paper). Abu Dhabi, International Renewable Energy Agency.

ISE (2020). PHOTOVOLTAICS REPORT, Fraunhofer Institute for Solar Energy Systems.

ISO, E. "14040: 2009-11." Environmental management–Life cycle assessment–Principles and framework (ISO 14040: 2006).

Ito, N., Y. Sato, P. Song, A. Kaijio, K. Inoue and Y. Shigesato (2006). "Electrical and optical properties of amorphous indium zinc oxide films." Thin Solid Films **496**(1): 99-103.

Itten, R. and M. Stucki (2017). "Highly efficient 3rd generation multi-junction solar cells using silicon heterojunction and perovskite tandem: prospective life cycle environmental impacts." Energies **10**(7): 841.

Jäger-Waldau, A. (2019). "Snapshot of photovoltaics—February 2019." Energies **12**(5): 769.

Jean, J., P. R. Brown, R. L. Jaffe, T. Buonassisi and V. Bulović (2015). "Pathways for solar photovoltaics." Energy & Environmental Science **8**(4): 1200-1219.

Jungbluth, N., M. Stucki, K. Flury, R. Frischknecht and S. Büsser (2012). "Life cycle inventories of photovoltaics." ESU-Services Ltd.: Uster, Switzerland: 250.

Kadro, J. M. and A. Hagfeldt (2017). "The end-of-life of perovskite PV." Joule **1**(1): 29-46.

Kavan, L., L. Steier and M. Grätzel (2017). "Ultrathin buffer layers of SnO2 by atomic layer deposition: perfect blocking function and thermal stability." The Journal of Physical Chemistry C **121**(1): 342-350.

Köhnen, E., M. Jošt, A. B. Morales-Vilches, P. Tockhorn, A. Al-Ashouri, B. Macco, L. Kegelmann, L. Korte, B. Rech and R. Schlatmann (2019). "Highly efficient monolithic perovskite silicon tandem solar cells: analyzing the influence of current mismatch on device performance." Sustainable Energy & Fuels **3**(8): 1995-2005.

Lambertz, A., T. Grundler and F. Finger (2011). "Hydrogenated amorphous silicon oxide containing a microcrystalline silicon phase and usage as an intermediate reflector in thin-film silicon solar cells." Journal of applied physics **109**(11): 113109.

Latunussa, C. E., F. Ardente, G. A. Blengini and L. Mancini (2016). "Life Cycle Assessment of an innovative recycling process for crystalline silicon photovoltaic panels." Solar Energy Materials and Solar Cells **156**: 101-111.

Lim, S., S. Kwon and H. Kim (2008). "ZnO thin films prepared by atomic layer deposition and rf sputtering as an active layer for thin film transistor." Thin Solid Films **516**(7): 1523-1528.

Liu, Z., S. E. Sofia, H. S. Laine, M. Woodhouse, S. Wieghold, I. M. Peters and T. Buonassisi (2020). "Revisiting thin silicon for photovoltaics: a technoeconomic perspective." Energy & Environmental Science **13**(1): 12-23.

Louwen, A., W. Van Sark, R. Schropp, W. Turkenburg and A. Faaij (2015). "Life-cycle greenhouse gas emissions and energy payback time of current and prospective silicon heterojunction solar cell designs." Progress in Photovoltaics: Research and Applications **23**(10): 1406-1428.

Lunardi, M. M. (2019). LIFE CYCLE ASSESSMENT OF SILICON BASED TANDEM AND ADVANCED SILICON SOLAR MODULES, The University of New South Wales.

Lunardi, M. M., J. Alvarez-Gaitan, J. Bilbao and R. Corkish (2018). "Comparative life cycle assessment of end-of-life silicon solar photovoltaic modules." Applied Sciences **8**(8): 1396.

Luque, A. and S. Hegedus (2011). Handbook of photovoltaic science and engineering, John Wiley & Sons.

Manser, J. S., J. A. Christians and P. V. Kamat (2016). "Intriguing optoelectronic properties of metal halide perovskites." Chemical reviews **116**(21): 12956-13008.

Matsui, T., J. Y. Seo, M. Saliba, S. M. Zakeeruddin and M. Grätzel (2017). "Room-Temperature Formation of Highly Crystalline Multication Perovskites for Efficient, Low-Cost Solar Cells." Advanced materials **29**(15): 1606258.

Mesquita, I., L. Andrade and A. Mendes (2018). "Perovskite solar cells: Materials, configurations and stability." Renewable and Sustainable Energy Reviews **82**: 2471-2489.

Mishra, A., N. Bhatt and A. Bajpai (2019). Nanostructured superhydrophobic coatings for solar panel applications. Nanomaterials-Based Coatings, Elsevier**:** 397-424.

Monteiro Lunardi, M., A. Wing Yi Ho-Baillie, J. P. Alvarez-Gaitan, S. Moore and R. Corkish (2017). "A life cycle assessment of perovskite/silicon tandem solar cells." Progress in photovoltaics: research and applications **25**(8): 679-695.

Mukherjee, S. (2014). "Life Cycle Assessment Projection of Photovoltaic Cells: A Case Study on Energy Demand of Quantum Wire Based Photovoltaic Technology Research."

Mutel, C. (2017). "Brightway: An open source framework for Life Cycle Assessment." Journal of Open Source Software **12**(2).

Nawaz, I. and G. Tiwari (2006). "Embodied energy analysis of photovoltaic (PV) system based on macro-and micro-level." Energy Policy **34**(17): 3144-3152.

NREL, N. (2020). Best Research-Cell Efficiences chart.

Ono, L. K., Y. Qi and S. F. Liu (2018). "Progress toward stable lead halide perovskite solar cells." Joule **2**(10): 1961-1990.

OpenLCA, O. (2013). Modular Open Source Software for Sustainability Assessment, GreenDelta.

Park, S.-I., Y.-J. Quan, S.-H. Kim, H. Kim, S. Kim, D.-M. Chun, C. S. Lee, M. Taya, W.-S. Chu and S.-H. Ahn (2016). "A review on fabrication processes for electrochromic devices." International Journal of Precision Engineering and Manufacturing-Green Technology **3**(4): 397-421.

Pré Consultants, B. (2016). "SimaPro." URL: https://network. simapro. com/esuservices.

Premalatha, L. and N. Rahim (2017). "The Effect of Dynamic Weather Conditions on Three Types of PV Cell Technologies–A Comparative Analysis." Energy Procedia **117**: 275-282.

Protocol, G. G. (2012). "GHG protocol product life cycle accounting and reporting standard ICT sector guidance." Guide for Assessing GHG Emissions Related to Energy Used by Software.

Qiu, L., L. K. Ono and Y. Qi (2018). "Advances and challenges to the commercialization of organic–inorganic halide perovskite solar cell technology." Materials today energy **7**: 169-189.

Radeker, W. S. and W. Cunningham (2010). A hierarchy of slurry reprocessing options. TMS Conference Papers.

Rashedi, A. and T. Khanam (2020). "Life cycle assessment of most widely adopted solar photovoltaic energy technologies by mid-point and end-point indicators of ReCiPe method." ENVIRONMENTAL SCIENCE AND POLLUTION RESEARCH.

Raugei, M., R. Frischknecht, C. Olson, P. Sinha and G. Heath (2016). Methodological guidelines on net energy analysis of photovoltaic electricity, National Renewable Energy Lab.(NREL), Golden, CO (United States).

Rödger, J.-M., J. Hammond, P. Brownsort, D. Dickinson and A. Loewen (2016). "Life cycle assessment." Biochar in European Soils and Agriculture: Science and Practice **184**.

Rodriguez, H., I. Guerrero, W. Koch, A. L. Endrös, D. Franke, C. Häßler, J. P. Kalejs and H. Möller (2011). "Bulk crystal growth and wafering for PV." Handbook of Photovoltaic Science and Engineering: 218-264.

Román, E. (2012). WEEE management in Europe: learning from best practice. Waste electrical and electronic equipment (WEEE) Handbook, Elsevier**:** 493-525.

Saga, T. (2010). "Advances in crystalline silicon solar cell technology for industrial mass production." NPG Asia Materials **2**(3): 96-102.

Schlömer, S., T. Bruckner, L. Fulton, E. Hertwich, A. McKinnon, D. Perczyk, J. Roy, R. Schaeffer, R. Sims and P. Smith (2014). "Annex III: Technology-specific cost and performance parameters." Climate change: 1329-1356.

Serrano-Lujan, L., N. Espinosa, T. T. Larsen-Olsen, J. Abad, A. Urbina and F. C. Krebs (2015). "Tin-and lead-based perovskite solar cells under scrutiny: an environmental perspective." Advanced Energy Materials **5**(20): 1501119.

Shafarman, W. N., S. Siebentritt and L. Stolt (2011). "Cu (InGa) Se2 Solar Cells." Handbook of photovoltaic science and engineering **2**: 546-599.

Sharma, K., V. Sharma and S. Sharma (2018). "Dye-sensitized solar cells: fundamentals and current status." Nanoscale research letters **13**(1): 381.

Shinohara, H. (2016). "Another big discovery—metallofullerenes." Philosophical Transactions of the Royal Society A: Mathematical, Physical and Engineering Sciences **374**(2076): 20150325.

Standardization, I. O. f. (2006). Environmental Management: Life Cycle Assessment; Principles and Framework, ISO.

Standardization, I. O. f. (2006). Environmental management: Life cycle assessment; requirements and guidelines, ISO Geneva.

Stolz, P., R. Frischknecht, K. Wambach, P. Sinha and G. Heath (2016). "Life cycle assessment of photovoltaic module recycling." Uster, CH: treeze Ltd.

Stolz, P., R. Frischknecht, K. Wambach, P. Sinha and G. Heath (2017). "Life cycle assessment of current photovoltaic module recycling." IEA PVPS Task 12, International Energy Agency Power Systems Programme, Report IEA-PVPS T12 **13**: 2018.

Todorov, T., O. Gunawan and S. Guha (2016). "A road towards 25% efficiency and beyond: perovskite tandem solar cells." Molecular Systems Design & Engineering **1**(4): 370-376.

Trube, J., M. Fischer, G. Erfert, C. Li, P. Ni, M. Woodhouse, P. Li, A. Metz, I. Saha and R. Chen (2018). "International technology roadmap for photovoltaic (ITRPV)." VDMA photovoltaic equipement.
Tsao, J. (2016). Recycling Perovskite Solar Cells.

UN (2015). "Goal 7 Ensure access to affordable, reliable, sustainable and modern energy for all." Department of Economic and Social Affairs.

UNFCCC, V. (2015). "Adoption of the Paris agreement." Proposal by the President.

Wali, Q., N. K. Elumalai, Y. Iqbal, A. Uddin and R. Jose (2018). "Tandem perovskite solar cells." Renewable and Sustainable Energy Reviews **84**: 89-110.

Wang, X., R. Li and D. Fan (2011). "Study on synthesis and optical properties of Al-doped ZnO hierarchical nanostructures." AIP Advances **1**(1): 012107.

Wang, Z., X. Zhu, S. Zuo, M. Chen, C. Zhang, C. Wang, X. Ren, Z. Yang, Z. Liu and X. Xu (2020). "27%-Efficiency Four-Terminal Perovskite/Silicon Tandem Solar Cells by Sandwiched Gold Nanomesh." Advanced Functional Materials **30**(4): 1908298.

Weckend, S., A. Wade and G. A. Heath (2016). End of Life Management: Solar Photovoltaic Panels, National Renewable Energy Lab.(NREL), Golden, CO (United States).

Wernet, G., C. Bauer, B. Steubing, J. Reinhard, E. Moreno-Ruiz and B. Weidema (2016). "The ecoinvent database version 3 (part I): overview and methodology." The International Journal of Life Cycle Assessment **21**(9): 1218-1230.

Wojciechowski, K., T. Leijtens, S. Siprova, C. Schlueter, M. T. Hörantner, J. T.-W. Wang, C.-Z. Li, A. K.-Y. Jen, T.-L. Lee and H. J. Snaith (2015). "C60 as an efficient n-type compact layer in perovskite solar cells." The journal of physical chemistry letters **6**(12): 2399-2405.

Zendehdel, M., N. Y. Nia and M. Yaghoubinia (2020). Emerging Thin Film Solar Panels, InterrtechOpen.

Zhang, J., X. Gao, Y. Deng, B. Li and C. Yuan (2015). "Life cycle assessment of titania perovskite solar cell technology for sustainable design and manufacturing." ChemSusChem **8**(22): 3882-3891.

Zhang, J., X. Gao, Y. Deng, Y. Zha and C. Yuan (2017). "Comparison of life cycle environmental impacts of different perovskite solar cell systems." Solar Energy Materials and Solar Cells **166**: 9-17.

Zhang, Q., F. Hao, J. Li, Y. Zhou, Y. Wei and H. Lin (2018). "Perovskite solar cells: must lead be replaced–and can it be done?" Science and Technology of advanced MaTerialS **19**(1): 425-442.

Zhang, W. (2019). Metal Halide Perovskite Crystals: Growth Techniques, Properties and Emerging Applications.

Zhou, Z. and M. Carbajales-Dale (2018). "Assessing the photovoltaic technology landscape: efficiency and energy return on investment (EROI)." Energy & Environmental Science **11**(3): 603-608.

Annexe

Table A 1 Inventory for anti-reflection coating deposition (Gomez Trillos 2018).

	Flow	Amount	Unit
Output	Antireflective Coating	1	m^2
Input	market for lithium fluoride	1.76E-03	kg
	market for electricity, medium voltage	1.93E+00	kWh
	market for argon, crude, liquid	4.65E-02	kg

Table A 2 Inventory for sputtering, indium zinc oxide, photovoltaics.

	Flow	Amount	Unit
Output	sputtering, indium zinc oxide, photovoltaics	1	m^3
Input	chemical factory construction	5.88E+02	kg
	market group for electricity, medium voltage	2.93E+07	kWh
	building construction, multi-storey	1.47E+02	m^3
	indium tin oxide powder production, nanoscale, for sputtering target	4.77E+04	kg

Table A 3 Inventory for front electrode (Louwen, Van Sark et al. 2015).

	Flow	Amount	Unit
Output	Front Electrode	1	m^2
Input	sputtering, indium zinc oxide, photovoltaics	1E-09	m^3
	market group for electricity, high voltage	7.88	kWh
	market for tap water	640	kg

Table A 4 Inventory for buffer layer (Louwen, Van Sark et al. 2015).

	Flow	Amount	Unit
Output	Buffer Layer	1	m^2
Input	market for tin dioxide	1.39E-04	kg
	market for electricity, medium voltage	2.90E-01	kWh
	market for oxygen, liquid	8.59E-03	kg
	market for nitrogen, liquid	1.10E-01	kg
	market for tap water	2.31E+01	kg

Table A 5 Inventory for hole transport layer (Helmholtz Zentrum Berlin).

	Flow	Amount	Unit
Output	Hole Transport Layer	1	m^2
Input	market for phosphoric acid, industrial grade, without water, in 85% solution state	1.13E-06	kg
	market for ethanol, without water, in 99.7% solution state, from ethylene	2.36E-04	kg
	market for electricity, low voltage	4.29E-03	kWh

Table A 6 Inventory for metal contact layer, top (Gomez Trillos 2018).

	Flow	Amount	Unit
Output	Metal Contact Layer, Top	1	m^2
Input	market for silver	2.10E-03	kg
	market for electricity, medium voltage	3.58E+00	kWh
	market for argon, crude, liquid	6.98E-02	kg

Table A 7 Inventory for market for methylammonium iodide (Gomez Trillos 2018).

	Flow	Amount	Unit
Output	market for methylammonium iodide	1	kg
Input	market for sulfur	-0.12	kg
	market for iodine	1.04	kg
	market for hydrogen sulfide	0.14	kg
	market for methylamine	0.58	kg
	market for ethanol, without water, in 99.7% solution state, from fermentation	7.31	kg
	market for diethyl ether, without water, in 99.95% solution state	20.8	kg
	market group for heat, district or industrial, other than natural gas	8.3	MJ
	market group for electricity, low voltage	9.24	kWh
	treatment of spent solvent mixture, hazardous waste incineration	29.9	kg

Table A 8 Inventory for market for formamidinium iodide (Gomez Trillos 2018).

	Flow	Amount	Unit
Output	market for formamidinium iodide	1	kg
Input	FAAc (C3H8N2O2), production	0.66	kg
	market for solvent, organic	0.63	kg
	market for hidroidic acid	1.62	kg
	market for nitrogen, liquid	0.29	kg
	market for solvent, organic	3.87	kg
	market for steam, in chemical industry	4.45	kg
	market group for tap water	400	kg
	market for electricity, low voltage	0.79	kWh
	market for hazardous waste, for incineration	1.90	kg
	Heat, waste	15.30	MJ

Table A 9 Inventory for FAAc (C3H8N2O2), production (Zhang, Gao et al. 2017).

	Flow	Amount	Unit
Output	FAAc (C3H8N2O2), production	1	kg
Input	market for acetic acid, without water, in 98% solution state	8.85E-01	kg
	market for ammonia, liquid	3.65E-01	kg

	Flow	Amount	Unit
Input	market for hydrochloric acid, without water, in 30% solution state	4.17E-01	kg
	market for hydrogen cyanide	2.81E-01	kg
	market for nitrogen, liquid	2.88E-01	kg
	market for ethanol, without water, in 99.7% solution state, from ethylene	4.79E-01	kg
	market for steam, in chemical industry	4.45E+00	kg
	electricity, high voltage, production mix	7.92E-01	kWh
	market group for tap water	4E+02	kg
	Heat, waste	4.04E+01	MJ

Table A 10 Inventory for market for hidroidic acid (Gomez Trillos 2018).

	Flow	Amount	Unit
Output	market for hidroidic acid	1	kg
Input	market for hydrazine	1.15E-09	kg
	market for iodine	7.29E-11	kg

Table A 11 Inventory for market for lead iodide (Gong, Darling et al. 2015, Gomez Trillos 2018).

	Flow	Amount	Unit
Output	market for lead iodide	1	kg
Input	potassium nitrate production	-0.438	kg
	nitric oxide production	-0.0434	kg
	market for iodine	0.67	kg
	market for potassium hydroxide	0.291	kg
	market for lead	0.449	kg
	market for nitric acid, without water, in 50% solution state	0.729	kg
	market group for heat, district or industrial, natural gas	13.5	MJ
	market for electricity, low voltage	0.133	kWh

Table A 12 Inventory for hydrobromic acid (Zhang, Gao et al. 2017).

	Flow	Amount	Unit
Output	hydrobromic acid	1	kg
Input	bromine production	1.07E+00	kg
	market for hydrogen, gaseous	1.34E-02	kg
	air separation, cryogenic	2.88E-01	kg
	steam production, in chemical industry	4.45	kg
	electricity, high voltage, production mix	7.92E-01	kWh
	market for tap water	4.00E+02	kg
	Heat, waste	1.69E+01	MJ

Table A 13 Inventory for cesium bromide (Zhang, Gao et al. 2017).

	Flow	Amount	Unit
Output	Cesium bromide	1	kg
Input	market for lithium carbonate	8.32E-01	kg
	hydrobromic acid	0.41	kg
	air separation, cryogenic	2.88E-01	kg
	steam production, in chemical industry	4.45	kg
	electricity, high voltage, production mix	7.92E-01	kWh
	market for tap water	4.00E+02	kg
	market for water, deionised	4.50E+00	kg
	Heat, waste	1.53E+01	MJ

Table A 14 Inventory for perovskite layer adjusted from Gomez Trillos (Gomez Trillos 2018).

	Flow	Amount	Unit
Output	Perovskite layer	1	m^2
Input	market for methylammonium iodide	1.14E-04	kg
	market for formamidinium iodide	4.14E-04	kg
	market for lead iodide	1.52E-03	kg
	Cesium bromide	2.80E-05	kg
	market for dimethyl sulfoxide	5.00E-03	kg
	market for toluene, liquid	9.23E-03	kg
	market for N,N-dimethylformamide	2.09E-03	kg
	market for isopropanol	5.16E-03	kg
	market for heat, from steam, in chemical industry	7.16E-03	MJ
	market for electricity, low voltage	3.57E+00	kWh

Table A 15 Inventory for electron transporting layer, C60 (García-Valverde, Cherni et al. 2010).

	Flow	Amount	Unit
Output	Electron transporting Layer, C60	1	m^2
Input	market for cyclohexane	0.02924	kg
	market for ammonia, liquid	0.27107	kg
	market for sodium hypochlorite, without water, in 15% solution state	0.01183	kg
	market for hydrochloric acid, without water, in 30% solution state	0.0075	kg
	market for oxygen, liquid	0.0025	kg
	market for tap water	0.2112	kg
	market for toluene, liquid	0.00423	kg

Table A 16 Inventory for recombination layer (Louwen, Van Sark et al. 2015).

	Flow	Amount	Unit
Output	Recombination Layer	1	m^2
Input	market for sputtering, indium tin oxide, for liquid crystal display	2.00E-08	m^3
	market group for electricity, high voltage	1.5	kWh
	market for tap water	128	kg

Table A 17 Inventory for nitrogen trifluoride (Jungbluth, Stucki et al. 2012).

	Flow	Amount	Unit
Output	nitrogen trifluoride	1	kg
Input	ammonia production, partial oxidation, liquid	2.53E-01	kg
	chemical factory construction, organics	1.40E-09	unit
	heat production, natural gas, at boiler modulating >100kW	7.00E-02	MJ
	market for electricity, medium voltage	4.30E+01	kWh
	market for fluorine, liquid	1.69E+00	kg
	market group for transport, freight train	1.17E+00	tkm
	transport, freight, lorry 16-32 metric ton, EURO5	1.95E-01	tkm
	treatment of wastewater, average, capacity 1.6E8l/year	1.20E-02	m^3
	Fluorine	3.39E-03	kg
	Ammonia	5.06E-04	kg
	Water, cooling, unspecified natural origin	2.10E-02	m^3
	Water, turbine use, unspecified natural origin	1.20E-02	m^3

Table A 18 Inventory for hydrogenated nano-crystalline silicon oxide, PECVD (Lambertz, Grundler et al. 2011, Gomez Trillos 2018).

	Flow	Amount	Unit
Output	nc-SiOx:H(n), PECVD	1	m^2
Input	market for silicon tetrahydride	1.15E-05	kg
	phosphane production	2.30E-07	kg
	market for carbon dioxide, liquid	8.06E-06	kg
	market for hydrogen, gaseous	4.59E-03	kg
	market for tap water	183.60	kg
	market for oxygen, liquid	4.97E-04	kg
	market for electricity, medium voltage	1.71E-03	kWh
	nitrogen trifluoride	4.09E-03	kg

Table A 19 Inventory for intrinsic a-Si deposition, PECVD (Gomez Trillos 2018).

	Flow	Amount	Unit
Output	Intrinsic a-Si deposition, PECVD	1	m^2
Input	market for tap water	9.67	kg
	market for silicon tetrahydride	16E-04	kg
	market for hydrogen, liquid	24E-04	kg
	market for oxygen, liquid	2.62E-05	kg
	market for electricity, medium voltage	9E-05	kWh
	nitrogen trifluoride	3E-04	kg

Table A 20 Inventory for texturing/cleaning of mono-Si wafer (Gomez Trillos 2018).

	Flow	Amount	Unit
Output	Texturing/cleaning of mono-Si wafer	1	m^2
Input	market for water, deionised	33.43	kg
	market for hydrogen fluoride	0.10	kg
	market for sodium hydroxide, without water, in 50% solution state	0.16	kg
	market for hydrogen peroxide, without water, in 50% solution state	0.06	kg
	market for hydrochloric acid, without water, in 30% solution state	0.06	kg
	market for ammonia, liquid	0.01	kg
	market for compressed air, 1200 kPa gauge	0.25	m^3
	market for electricity, medium voltage	0.65	kWh

Table A 21 Inventory for mono-Si wafer for CZ wafer.

	Flow	Amount	Unit
Output	Mono-Si wafer	1	m^2
Input	market for single-Si wafer, photovoltaics	1	m^2
	Texturing/cleaning of mono-Si wafer	1	m^2

Table A 22 Inventory for metal contact layer, bottom, ZnO:Al (Wang, Li et al. 2011, Louwen, Van Sark et al. 2015).

	Flow	Amount	Unit
Output	Metal contact layer, bottom, ZnO:Al	1	m^2
Input	market for zinc oxide	0.0018	kg
	market for aluminium, wrought alloy	5.67E-05	kg
	market for tap water	895.68	kg
	market for electricity, medium voltage	11.03	kWh

Table A 23 Inventory for metal contact layer, bottom, Ag (Louwen, Van Sark et al. 2015).

	Flow	Amount	Unit
Output	Metal contact layer, bottom, Ag	1	m^2
Input	market for silver	0.0042	kg
	market for tap water	2559.08	kg
	market for electricity, medium voltage	31.50	kWh

Table A 24 Inventory for gas abatement (Louwen, Van Sark et al. 2015).

	Flow	Amount	Unit
Output	Gas abatement	1	m^2
Input	market for tap water	1.20	kg
	market for oxygen, liquid	5.1	kg
	market for nitrogen, liquid	4.30	kg
	market for propane	3.3	kg
	compressed air production, 1200 kPa gauge, <30kW, optimized generation	0.014	m^3

Table A 25 Inventory for Perovskite/c-Si tandem.

	Flow	Amount	Unit
Output	Perovskite/c-Si tandem	1	m^2
Input	Antireflective Coating	1	m^2
	Front Electrode	1	m^2
	Buffer Layer	1	m^2
	Hole Transport Layer	1	m^2
	Metal Contact Layer, Top	1	m^2
	Perovskite layer	1	m^2
	Recombination Layer	1	m^2
	Electron transporting Layer, C60	1	m^2
	nc-SiOx:H(n), PECVD	1	m^2
	Intrinsic a-Si deposition, PECVD	1	m^2
	Mono-Si wafer	1	m^2
	Intrinsic a-Si deposition, PECVD	1	m^2
	Intrinsic a-Si deposition, PECVD	1	m^2
	Metal contact layer, bottom, ZnO:Al	1	m^2
	Metal contact layer, bottom, Ag	1	m^2
	Gas abatement, tandem PSC/c-Si	1	m^2

Table A 26 Inventory for Perovskite/c-Si tandem, Photovoltaic panel production (Frischknecht, Itten et al. 2015).

	Flow	Amount	Unit
Output	Perovskite/c-Si tandem, Photovoltaic panel production	1	m^2
Input	c-Si/Perovskite tandem	1	m^2
	market for electricity, medium voltage	3.75	kWh
	market for diesel, burned in building machine	0.0087	MJ
	market for photovoltaic panel factory	4E-06	unit
	market for tap water	5.03	kg
	wire drawing, copper	0.103	kg
	tempering, flat glass	8.81	kg
	market for aluminium alloy, AlMg3	2.13	kg
	market for tin	0.013	kg
	market for lead	7.25E-04	kg
	market for diode, auxilliaries and energy use	0.0028	kg
	market for polyethylene, high density, granulate, recycled	0.0238	kg
	market for solar glass, low-iron	8.81	kg
	market for copper	0.103	kg
	glass fibre reinforced plastic production, polyamide, injection moulded	0.295	kg
	ethylvinylacetate production, foil	0.875	kg
	polyvinylfluoride production	0.112	kg
	polyethylene terephthalate production, granulate, amorphous	0.346	kg
	market for silicone product	0.122	kg
	corrugated board box production	0.763	kg
	1-propanol production	0.016	kg
	EUR-flat pallet production	0.05	unit
	hydrogen fluoride production	0.0624	kg
	isopropanol production	1.47E-04	kg
	potassium hydroxide production	0.0514	kg
	soap production	0.0116	kg
	transport, freight, lorry 7.5-16 metric ton, EURO5	5.85	tkm
	transport, freight train	42.5	tkm
	treatment of municipal solid waste, incineration	0.03	kg
	treatment of waste polyvinylfluoride, municipal incineration	0.112	kg
	treatment of waste plastic, mixture, municipal incineration	1.64	kg
	treatment of waste mineral oil, hazardous waste incineration	0.00161	kg
	treatment of spent solvent mixture, hazardous waste incineration	0.00503	kg
	Carbon dioxide, fossil	0.0218	kg

	Flow	Amount	Unit
	NMVOC, non-methane volatile organic compounds, unspecified origin	0.00806	kg
	Heat, waste	13.4	MJ

Table A 27 Inventory for BOS, open ground module (Jungbluth, Stucki et al. 2012, Gomez Trillos 2018).

	Flow	Amount	Unit
Output	BOS, open ground module	1	m^2
Input	market for photovoltaic mounting system production, for 570kWp open ground module	1	m^2
	market for inverter, 2.5kW	0.1	unit
	market for electricity, medium voltage	0.0164	kWh
	market for diesel, burned in building machine	3.50	MJ
	market for photovoltaics, electric installation for 3kWp module, at building	0.08	unit
	transport, freight, lorry 16-32 metric ton, EURO5	0.217	tkm
	market group for transport, freight train	5.41	tkm
	transport, freight, light commercial vehicle	1.14	tkm

Table A 28 Inventory for BOS, flat-roof installation (Jungbluth, Stucki et al. 2012, Gomez Trillos 2018).

	Flow	Amount	Unit
Output	BOS, flat-roof installation	1	m^2
Input	market for photovoltaic mounting system, for flat-roof installation	1	m^2
	market for inverter, 2.5kW	0.1	unit
	market for electricity, medium voltage	0.02	kWh
	market for photovoltaics, electric installation for 3kWp module, at building	0.08	unit
	transport, freight, lorry 16-32 metric ton, EURO5	0.256	tkm
	market group for transport, freight train	1.05	tkm
	transport, freight, light commercial vehicle	0.472	tkm

Table A 29 Inventory for BOS, slanted-roof installation (Jungbluth, Stucki et al. 2012, Gomez Trillos 2018).

	Flow	Amount	Unit
Output	BOS, slanted-roof installation	1	m^2
Input	market for photovoltaic mounting system, for slanted-roof installation	1	m^2
	market for inverter, 2.5kW	0.1	unit
	market for electricity, medium voltage	0.0203	kWh
	market for photovoltaics, electric installation for 3kWp module, at building	0.08	unit
	transport, freight, lorry 16-32 metric ton, EURO5	0.225	tkm

	Flow	Amount	Unit
	market group for transport, freight train	1.5	tkm
	transport, freight, light commercial vehicle	0.434	tkm

Table A 30 Inventory for BOS, facade installation (Jungbluth, Stucki et al. 2012, Gomez Trillos 2018)..

	Flow	Amount	Unit
Output	BOS, facade installation	1	m^2
Input	market for photovoltaic mounting system, for facade installation	1	m^2
	market for inverter, 2.5kW	0.1	unit
	market for electricity, medium voltage	0.02	kWh
	market for photovoltaics, electric installation for 3kWp module, at building	0.08	unit
	transport, freight, lorry 16-32 metric ton, EURO5	0.224	tkm
	market group for transport, freight train	1.61	tkm
	transport, freight, light commercial vehicle	0.444	tkm

Table A 31 Inventory for use phase, scenario 1 (Jungbluth, Stucki et al. 2012).

	Flow	Amount	Unit
Output	Use phase, scenario 1	1	m^2
Input	market for tap water	100	kg

Table A 32 Inventory for use phase, scenario 2 (Own Model).

	Flow	Amount	Unit
Output	Use phase, scenario 2	1	m^2
Input	market for tap water	100	kg
	Iodide	-0.00118	kg
	Lead	-0.0014	kg

Table A 33 Inventory for use phase, scenario 3 (Own Model).

	Flow	Amount	Unit
Output	Use phase, scenario 3	1	m^2
Input	market for tap water	100	kg
	Iodide	-0.00118	kg
	Lead	-0.0014	kg

Table A 34 Inventory for aluminium scrap, recovered from c-Si PV module treatment (Stolz, Frischknecht et al. 2016).

	Flow	Amount	Unit
Output	aluminium scrap, recovered from c-Si PV module treatment	-1	kg
Input	market for electricity, medium voltage	3.33E-01	kWh
	diesel, burned in building machine	5.40E-02	MJ

	Flow	Amount	Unit
	treatment of waste plastic, mixture, municipal incineration	-1.41E-01	kg
	treatment of waste plastic, mixture, sanitary landfill	-9.14E-03	kg
	transport, freight, lorry 3.5-7.5 metric ton, EURO5	6.01E-01	tkm

Table A 35 Inventory for glass cullets, recovered from c-Si PV module treatment (Stolz, Frischknecht et al. 2016).

	Flow	Amount	Unit
Output	glass cullets, recovered from c-Si PV module treatment	-1	kg
Input	market for electricity, medium voltage	9.51E-03	kWh
	diesel, burned in building machine	1.54E-03	MJ
	treatment of waste plastic, mixture, municipal incineration	-4.02E-03	kg
	treatment of waste plastic, mixture, sanitary landfill	-2.61E-04	kg
	transport, freight, lorry 3.5-7.5 metric ton, EURO5	1.72E-02	tkm

Table A 36 Inventory for copper scrap, recovered from c-Si PV module treatment (Stolz, Frischknecht et al. 2016).

	Flow	Amount	Unit
Output	copper scrap, recovered from c-Si PV module treatment	-1	kg
Input	market for electricity, medium voltage	1.90E+00	kWh
	diesel, burned in building machine	3.09E-01	MJ
	treatment of waste plastic, mixture, municipal incineration	-8.03E-01	kg
	treatment of waste plastic, mixture, sanitary landfill	-5.22E-02	kg
	transport, freight, lorry 3.5-7.5 metric ton, EURO5	3.43E+00	tkm

Table A 37 Inventory for recycling, PV waste (Latunussa, Ardente et al. 2016).

	Flow	Amount	Unit
Output	Recycling, PV waste	-1	m^2
Input	market for electricity, medium voltage	1.77E+00	kWh
	market for diesel, burned in building machine	6.38E-01	MJ
	market for water, completely softened	4.8315	kg
	market for nitric acid, without water, in 50% solution state	1.10E-01	kg
	market for lime, hydrated, packed	5.69E-01	kg
	glass cullets, recovered from c-Si PV module treatment	-10.70	kg
	copper scrap, recovered from c-Si PV module treatment	-6.83E-02	kg
	aluminium scrap, recovered from c-Si PV module treatment	-2.85E+00	kg
	silicon production, metallurgical grade	-5.41E-01	kg
	treatment of precious metal from electronics scrap, in anode slime, precious metal extraction	-7.80E-03	kg

	Flow	Amount	Unit
	treatment of waste wire plastic, municipal incineration	-0.36	kWh
	treatment of waste plastic, mixture, municipal incineration with fly ash extraction	-0.36	kWh
	treatment of waste polyvinylfluoride, municipal incineration	-0.36	kWh
	heat production, natural gas, at industrial furnace >100kW	-8	MJ
	treatment of waste glass, inert material landfill	-0.218	kg
	treatment of average incineration residue, residual material landfill	-0.0312	kg
	treatment of limestone residue, inert material landfill	-5	kg
	treatment of sludge, pig iron production, residual material landfill	-1	kg
	Nitrogen oxides	-0.0312	kg

Table A 38 Inventory for recycling, BOS waste (Rashedi and Khanam 2020).

	Flow	Amount	Unit
Output	Recycling, BOS waste	-1	m^2
Input	market for waste aluminium	-3.34E+00	kg
	market for waste reinforcement steel	-5.09E+00	kg

Table A 39 Inventory for residual landfill, PV waste (Rashedi and Khanam 2020).

	Flow	Amount	Unit
Output	Residual landfill, PV waste	1	m^2
Input	market for municipal solid waste	-3.00E-01	kg
	market for waste mineral oil	-3.64E+00	kg
	market for waste polyvinylfluoride	-1.10E-01	kg
	market group for waste glass	-1.01E+01	kg
	market group for waste paperboard	-1.1	kg
	glass fibre reinforced plastic production, polyamide, injection moulded	-1.90E-01	kg
	treatment of waste aluminium, sanitary landfill	-2.63E+00	kg
	Copper	1.13E-01	kg
	Nickel	1.63E-04	kg

Table A 40 Inventory for residual landfill, BOS waste (Rashedi and Khanam 2020).

	Flow	Amount	Unit
Output	Residual landfill, BOS waste	1	m^2
Input	market for reinforcement steel	-2,60E-01	kg
	marlet for waste electric wiring	-8,48E+00	kg
	market group for waste paperboard	-1,05E+00	kg

	Flow	Amount	Unit
	market for waste electric and electronic equipment	-6,24E-01	kg
	Copper	2,02214	kg
	Zinc	1,15E-02	kg

Table A 41 Inventory for incineration, PV waste (Rashedi and Khanam 2020).

	Flow	Amount	Unit
Output	Incineration, PV waste	-1	m^2
Input	treatment of waste plastic, mixture, municipal incineration	1.69E+00	kg

Table A 42 Inventory for incineration, BOS waste (Rashedi and Khanam 2020).

	Flow	Amount	Unit
Output	Incineration, BOS waste	-1	m^2
Input	treatment of waste polystyrene, municipal incineration with fly ash extraction	1.20E-01	kg
	treatment of waste polyvinylchloride, municipal incineration with fly ash extraction	6.16E-01	kg
	treatment of waste polyethylene, municipal incineration with fly ash extraction	4.17E+00	kg

Table A 43 Cradle-to-gate LCIA of the perovskite/Si tandem solar panel. Own table.

Impact Category	Unit per m^2	Perovskite/Si Tandem Solar Panel
Ecotoxicity, Freshwater 1,4-DCB eq.	1,4-DCB eq.	0.17
Ecotoxicity, Marine 1,4-DCB eq.	1,4-DCB eq.	1.47
Ecotoxicity, Terrestrial 1,4-DCB eq.	1,4-DCB eq.	7.80
Fossil Resource Scarcity kg oil-eq/unit of resource	kg oil-eq/unit of resource	80.46
Freshwater Eutrophication kg P-eq. /kg	kg P-eq. /kg	2×10^{-02}
Global Warming, 100 year timescale kg CO2eq/ kg GHG	kg CO2eq/ kg GHG	293.84
Ionizing Radiation kBq Co-60 to air eq/kBq	kBq Co-60 to air eq/kBq	31.10
Land Occupation m2·annual crop eq.	m2·annual crop eq.	8.42
Land Transformation m2·annual crop eq.	m2·annual crop eq.	8×10^{-02}
Marine Eutrophication kg N-eq. /kg	kg N-eq. /kg	8.17×10^{-03}
Mineral Resource Scarcity kg Cu-eq/kg ore	kg Cu-eq/kg ore	2.60
Ozone Formation, Damage to Ecosystems kg NOx-eq/kg	kg NOx-eq/kg	0.65
Ozone Formation, Damage to Humans kg NOx-eq/kg	kg NOx-eq/kg	0.63
Particulate Matter Formation kg PM2.5-eq/kg	kg PM2.5-eq/kg	0.54
Stratospheric Ozone Depletion, 100 year t. kg CFC11-eq/ kg ODS	kg CFC11-eq/ kg ODS	1.42×10^{-04}
Terrestrial Acidification kg SO2-eq/kg	kg SO2-eq/kg	1.02
Toxicity, Carcinogenic 1,4-DCB eq.	1,4-DCB eq.	2.75
Toxicity, Non-carcinogenic 1,4-DCB eq.	1,4-DCB eq.	21.13
Water Consumption m3-eq	m3-eq	12.30

Table A 44 Cradle-to-gate cumulative energy demand (CED) for the perovskite/Si tandem solar panel. Own table.

Cumulative Energy Demand	MJ-eq/m^2
Renewable Energy Resources, Biomass	139.87
Non-Renewable Energy Resources, Fossil	3686.9
Renewable Energy Resources, Geothermal	6.45
Non-Renewable Energy Resources, Nuclear	586.53
Non-Renewable Energy Resources, Primary Forest	0.13
Renewable Energy Resources, Kinetic (in Wind)	85.57
Renewable Energy Resources, Potential (in Barrage Water)	444.30
Renewable Energy Resources, Solar	1.70
Total	**4951.50**

Table A 45 Cradle-to-grave LCIA of installation, use and EoL phase of the perovskite/Si tandem solar panel. Own table.

Impact Categories Unit/m²	Installation and Supporting Structure				Use			End of Life		
	Open Ground Module	Flat-Roof	Facade	Slanted-Roof	Scenario 1	Scenario 2	Scenario 3	Scenario 1	Scenario 2	
					No Leakage	Leakage, Soil	Leakage, Water	Recycling	Landfill (91%)	Incineration (9%)
Ecotoxicity, Freshwater 1,4-DCB eq.	0.296	0.225	0.236	0.24	9.02×10^{-06}	9.02×10^{-06}	9.02×10^{-06}	0.0017	0.007	0.000505
Ecotoxicity, Marine 1,4-DCB eq.	0.861	0.75	0.762	0.763	1.55×10^{-05}	1.55×10^{-05}	1.55×10^{-05}	0.0042	0.011	0.00088
Ecotoxicity, Terrestrial 1,4-DCB eq.	53.88	51.31	51.76	51.72	1.5×10^{-04}	1.5×10^{-04}	1.5×10^{-04}	0.067	0.057	0.021
Fossil Resource Scarcity kg oil-eq/unit of resource	27.64	21.44	19.30	19.87	1.8×10^{-03}	1.8×10^{-03}	1.8×10^{-03}	1.78	0.4	0.0744
Freshwater Eutrophication kg P-eq. /kg	0.014	0.0121	0.0123	0.0124	5.5×10^{-07}	5.5×10^{-07}	5.5×10^{-07}	0.0002	4.85×10^{-05}	6.038×10^{-06}
Global Warming, 100 year timescale kg CO2eq/ kg GHG	116.11	81.23	79.89	82.46	6.8×10^{-03}	6.8×10^{-03}	6.8×10^{-03}	5.8	20.25	18.24
Ionizing Radiation kBq Co-60 to air eq/kBq	5.37	3.97	4.06	4.14	2.2×10^{-03}	2.2×10^{-03}	2.2×10^{-03}	0.43	0.06	0.015
Land Occupation m2·annual crop eq.	106.05	2.34	2.4	2.45	2.23×10^{-04}	2.23×10^{-04}	2.23×10^{-04}	0.44	0.092	0.0078
Land Transformation m2·annual crop eq.	0.03	0.014	0.016	0.015	1.43×10^{-06}	1.43×10^{-06}	1.43×10^{-06}	0.0019	0.00018	2.489×10^{-05}
Marine Eutrophication kg N-eq. /kg	0.0015	0.0011	0.0012	0.0011	7.03×10^{-08}	7.03×10^{-08}	7.03×10^{-08}	1.52×10^{-05}	0.0002	1.91×10^{-05}
Mineral Resource Scarcity kg Cu-eq/kg ore	6	3.6	3.75	3.76	9.17×10^{-05}	9.17×10^{-05}	9.17×10^{-05}	0.016	0.0123	0.002
Ozone Formation, Damage to Ecosystems kg NOx-eq/kg	0.42	0.31	0.312	0.319	1.69×10^{-05}	1.69×10^{-05}	1.69×10^{-05}	0.049	0.0074	0.0035
Ozone Formation, Damage to Humans kg NOx-eq/kg	0.4	0.3	0.3	0.31	1.65×10^{-05}	1.65×10^{-05}	1.65×10^{-05}	0.048	0.0073	0.00348
Particulate Matter Formation kg PM2.5-eq/kg	0.49	0.41	0.415	0.42	1.22×10^{-05}	1.22×10^{-05}	1.22×10^{-05}	0.017	0.0026	0.00067
Stratospheric Ozone Depletion, 100 years kg CFC11-eq/ kg ODS	6.53×10^{-05}	5.45×10^{-05}	5.47×10^{-05}	5.54×10^{-05}	3.53×10^{-09}	3.53×10^{-09}	3.53×10^{-09}	0	2.64×10^{-06}	2.95×10^{-06}

Impact Categories Unit/m²	Installation and Supporting Structure				Use			End of Life		
	Open Ground Module	Flat-Roof	Facade	Slanted-Roof	Scenario 1	Scenario 2	Scenario 3	Scenario 1	Scenario 2	
					No Leakage	Leakage, Soil	Leakage, Water	Recycling	Landfill (91%)	Incineration (9%)
Terrestrial Acidification kg SO2-eq/kg					2.71×10^{-05}	2.71×10^{-05}	2.71×10^{-05}	0.039	0.0059	0.0018
Toxicity, Carcinogenic 1,4-DCB eq.	6.4	3.46	4.1	4.11	5.15×10^{-04}	5.15×10^{-04}	5.15×10^{-04}	0	0.076	0.028
Toxicity, Non-carcinogenic 1,4-DCB eq.	162.84	159.5	159.7	159.74	3.97×10^{-04}	3.97×10^{-04}	3.97×10^{-04}	0.145	0.33	0.03
Water Consumption m3-eq	1.2	0.86	0.87	0.88	0.02	0.02	0.02	0.021	0.312	0.047

Table A 46 Cradle-to-grave cumulative energy demand (CED) for installation, use and EoL phase. Own table.

Cumulative Energy Demand MJ-eq/m²	Installation and Supporting Structure				Use			End of Life		
	Open Ground Module	Flat-Roof	Facade	Slanted -Roof	Scenario 1	Scenario 2	Scenario 3	Scenario 1	Scenario 2	
					No Leakage	Leakage, Soil	Leakage, Water	Recycling	Landfill (91%)	Incineration (9%)
Renewable Energy Resources, Biomass	29.03	21.73	22.18	23.15	0.004	0.004	0.004	11.18	0.4	0.08
Non-Renewable Energy Resources, Fossil	1270.69	984.3	887	913.34	0.083	0.083	0.083	81.83	18.27	3.4
Renewable Energy Resources, Geothermal	1.07	0.85	0.86	0.87	0.00028	0.00028	0.00028	0.15	0.016	0.0025
Non-Renewable Energy Resources, Nuclear	101.05	78.75	77.25	78.92	0.041	0.041	0.041	7.76	1.03	0.26
Non-Renewable Energy Resources, Primary Forest	0.07525	0.025	0.034	0.027	1.04×10^{-06}	1.04×10^{-06}	1.04×10^{-06}	0.003	0.000474	4.52×10^{-05}
Renewable Energy Resources, Kinetic, Wind	8.602	6.52	6.62	6.73	0.0039	0.0039	0.0039	0.38	0.1	0.021
Renewable Energy Resources, Potential, Water	114.48	82.38	85.29	88.19	0.0078	0.0078	0.0078	3.74	0.657	0.17
Renewable Energy Resources, Solar	0.0697	0.035	0.034	0.033	2.25×10^{-06}	2.25×10^{-06}	2.25×10^{-06}	0.004	0.0038	0.000135
Total	**1525.07**	**1174.58**	**1079.27**	**1111.3**	**0.14**	**0.14**	**0.14**	**105.05**	**20.48**	**3.35**

Testimony:

I herewith declare that I have written this paper on my own and that I have not used any other sources and materials than those indicated. I properly cited the materials I have relied upon. I have not submitted this document as a master thesis elsewhere.

23.09.2020, Oldenburg — Abeer

Date, Place — Signature